P080

UNIVERSITE DE LIEGE
FACULTE DES SCIENCES APPLIQUEES

Etude et modélisation de la réflexion lumineuse dans le cadre de l'éclairage prévisionnel

par

Jean-Jacques EMBRECHTS

Ingénieur Civil Electricien (Electronique),
Docteur en Sciences Appliquées
Chercheur Qualifié du Fonds National de la Recherche Scientifique

1995

Collection des Publications de la Faculté des Sciences appliquées n° 146
Direction : A. Germain, Institut de Chimie, Bât. B6, Sart Tilman, B-4000 LIEGE, BELGIQUE

Thèse défendue, avec succès, le 10 mai 1994, pour l'obtention du grade d'Agrégé de l'enseignement supérieur en Sciences appliquées de l'Université de Liège.

La commission de lecture était composée de :

G. CANTRAINE, Université de Liège, Président
J. DENDAL, Université de Liège
A. DUPAGNE, Université de Liège
H. VANDERSCHUREN, Université de Liège
C. EUGENE, Université Catholique de Louvain
M. FONTOYNONT, Ecole Nationale des Travaux Publics de l'Etat à Lyon

Le jury était composé des professeurs de la Faculté des Sciences appliquées de l'Université de Liège, ainsi que des membres de la commission de lecture; il était présidé par le Doyen G. L'HOMME.

Liège (Belgique) - Décembre 1995

Dépôt légal : D/1996/0480/01
ISSN 0075-9333

Foreword

A mathematical model of light reflection for lighting simulations : why ?

Since the early developments of Lighting Science, light reflection has always been assumed to be uniformly diffuse. Except in some situations.

Indeed, it must be recognized that the inaccuracies introduced by such a crude approximation could not be tolerated in some situations. In spite of this inconvenience, many years have passed before scientists really investigate other modelizations.

What is the reason of these new developments ? Is it the advent of the computer, which makes the complex phenomena more accessible ? Perhaps computer science played a significant role. But, more than other reasons, the evolution of the philosophy of lighting scientists has been the real detonator. Indeed, the illuminance is no more considered as the unique indicator of a good lighting installation : from now on, the luminance and the distribution of luminances in the visual field are also considered as fundamental parameters.

The reflection factor, as a global energetic factor, was sufficient to calculate the illuminances and flux transfers. This is not true anymore, if it is wanted to simulate a distribution of luminances, because the complex interaction between light and the objects of our environment cannot be accurately modelized by only one parameter.

It must be also precised that the present work is not intended to denigrate the Lambert law of diffuse reflection. It has indeed been (and will always be) very useful in lighting simulations. But we must not considered this law as a postulate anymore, pretending for example that : "anyway, a more realistic model will not change significantly the workplane illuminances". Interior lighting cannot be limited to simply illuminate the working plane : the imagination of the designer must be allowed to be developed in more complex directions.

Lighting is not only a technology. It is also a living science which, among others, has an urgent need in research, idea and theories. I will cite here the eminent James A. Worthey :

> *"Current methods of lighting design involve a mixture of theory and intuition. An important goal of research should be increasing the role of theory and decreasing that of intuition"*
>
> (Lighting Design & Application, July 1991, p.16)

On the 9th october 1992, the participants to the seminar "Computer Programs for Light and Lighting", organized in Vienna by the C.I.E. (Commission Internationale de l'Eclairage), have formally communicated their urgent need in research works, in the field of measurement and modelization of non-lambertian reflection.

Embrechts Jean-Jacques
Liège, the 3rd november 1993

CONTENTS

Chapter 1 : Introduction

Light penetrates into our world as electromagnetic waves or photon fluxes, illuminating the very large as well as the very small objects, the visible and invisible ones.

Our world is material : clusters of atoms, but also volumes, surfaces, static or moving objects, from the very small to the very large ones, from the microscopic to the macroscopic world.

Light reflection originates from the interaction between light and materials, from the vibration of the electrons on the rhythm of the electromagnetic field, when photons collide with the atoms of the material medium.

The illuminated material reveals its identity. The cluster of atoms becomes an object, the volumes and surfaces are viewed as spaces and colours. Our material world acquires all its significance and beauty thanks to light reflection : this is the complex reality.

To observe the macroscopic world in order to understand the microscopic one, trying to understand the "invisible" and predicting visible effets : this will be the aim of this work dedicated to light reflection.

To observe and understand will be the objectives of the two following chapters. The main physical results concerning the light reflection will be recalled in the second chapter. It will be seen that the discontinuity between air and another medium gives rise to what is called the *surface reflection*. The properties of this reflection will be analysed in terms of the nature of the medium (metal or dielectric), and in terms of the geometry of the surface (plane or rough). The heterogeneity of the medium will give rise to the volume or bulk reflection. Then, surface and volume contributions will be associated to give the spatial distribution of the reflected light intensity.

Observations are followed by measurements. The chapter 3 starts with the definition of the photometric quantities associated with light reflection and the methods currently in use to measure them. It will be shown that reflection goniophotometry (or gonioreflectometry) is not yet sufficiently developed, and that it will be necessary to conceive our own measurement system. This apparatus is also described in chapter 3, together with its requirements, options (plane of

incidence, spectral domain, ...), limitations and, finally, its accuracy. The measured quantity will be the radiance or the luminance factor, if the detector is a spectrophotometer or a luminance-meter, respectively.

The first results will show the spatial distribution of light, after reflection on several materials used in lighted interiors such as wood, glass, paper or pavements. They also reinforce the visual observations and lead to the conclusion that the Lambert law of uniform diffusion is not sufficient to describe all phenomena. The next step of the work is thus introduced : it will be assigned to modelization.

The modelization of light reflection is really the central part of this research. It is described in the fourth chapter. The model of surface reflection is an extension of the theory of P. Beckmann about the reflection of electromagnetic waves by rough surfaces. The extension consists in a vectorial approach and an expression of the theoretical results in terms of photometric quantities, such as the luminance factor. The vectorial approach of the scattered field will allow us to consider the dielectric materials and their optical properties.

This theory is compared with measurements results obtained with the apparatus described in chapter 3. The comparison shows that it is necessary to include in the model, a mathematical function to take into account the shadowing effects between surface elements. This study is mainly based on measurements carried out on frosted clear glass samples. This material has the two following interesting properties : first, it only reflects light with its surface (no volume scattering) and, secondly, its optical characteristics are well-known.

The model describing the volume reflection will derive from an experimental study of light reflected by an opaline glass sample. The plane surface of this sample insures that the surface and the volume components can be separated during the measurements.

Finally, both models of light reflection are associated in a general expression, described by the equation (4.52). Five parameters are necessary to define each material : the refraction index, a surface roughness parameter, the amplitude of coherent surface reflection (the contribution which gives the image of the source) and the amplitudes of the incoherent surface and volume reflections. A mathematical procedure has been developed to determine the parameters of any material, from reflection measurements in the plane of incidence.

This general model has been compared with other models, including the Lambert law and some more sophisticated ones. The comparison shows the benefits afforded by our five parameters expression.

The problem of computing illuminances and luminances in an interior is approached in chapter 5. The difficulty here is to modelize obstructions and walls reflection by a non-lambertian model. Therefore, a calculation procedure, based on the radiosity technique, is introduced.

This procedure will then be developed in a lighting software called LUXCALC. Several tests of this software have been carried out, including a comparison with in-situ illuminances and luminances measurements. Finally, the general model of light reflection described in chapter 4 will be introduced in LUXCALC. Its influence on the calculated values, on their accuracy and on the computing time will also be analysed.

Chapter 2 : Physical properties of light reflection

2.1. Light reflection on a plane surface

Consider a parallel beam of light propagating along a straight line in the air. It could have been produced, for example, by a small source placed at the focus of a converging lens.

If the light beam falls on another medium, the following phenomena are observed :
- one part of the beam is reflected in the original medium (air);
- the other part of the beam penetrates into the second medium, and is finally absorbed if this medium is sufficiently thick.

Let us analyse the case where the interface between both media is perfectly plane.

2.1.1. Interface between air and another dielectric, homogeneous, transparent and isotropic medium

In this case, the reflected beam remains parallel and propagates along a direction which is symmetrical from the direction of incidence, with respect to the vector normal to the surface (fig.2.1). The reflected light rays belong to the plane of incidence, defined by that normal and the direction of incidence. This reflection is called the **specular** or **regular reflection**. Typical examples of it are the reflection of light on a glass sample, or on a quiet surface of water.

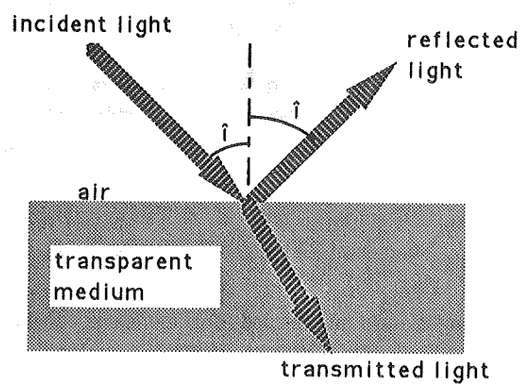

Figure 2.1 : Specular reflection on a transparent medium.

The other part of the light beam propagates again along a straight, but different line, in the transparent medium : this phenomenon is called the **refraction**.

Some useful expressions are recalled hereafter.

Plane wave polarized in a direction perpendicular to the plane of incidence[1]

The incident light is here considered as a monochromatic electromagnetic wave of angular frequency ω. The incident electric vector $\vec{E_i}$ is perpendicular to the plane of incidence, and θ_i is the angle between the direction of incidence of the plane wave and the normal to the surface. Then, it follows [1, p.39] :

$$\vec{E_i}\ (x,y,z,t) = e^{j(k\ x\ \sin\theta_i\ -\ k\ z\ \cos\theta_i\ -\ \omega t)}\ \vec{1_y}$$

$$k = \frac{\omega}{c} = \frac{2\ \pi}{\lambda} \qquad (2.1)$$

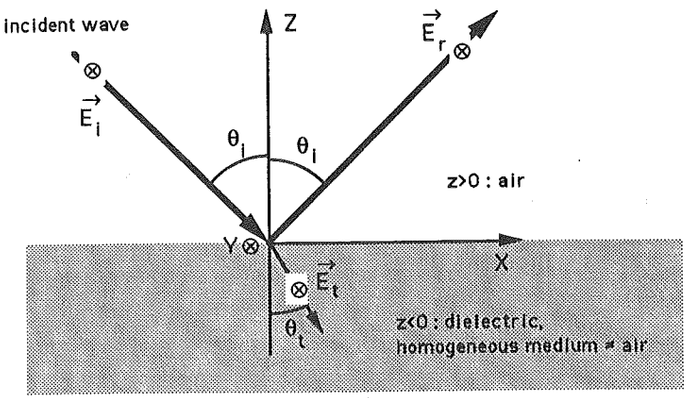

Figure 2.2 : Reflection of a plane wave $\vec{E_i}$, polarized in a direction perpendicular to the plane of incidence, by the plane surface z=0 (symbols : see text).

"λ" is the wavelength, "k" is the wave number and "c" is the speed of light in the medium (z>0).

[1] We use the convention here that the term "perpendicular polarization" refers to an electric vector perpendicular to the plane of incidence.

When the plane wave reaches the plane interface (XY) between both media[2] , a reflected plane wave $\vec{E_r}$ is created, which propagates in the original medium (z>0). Also, a transmitted plane wave $\vec{E_t}$ is created, which penetrates into the second medium (z<0), such that :

$$\vec{E_r}\ (x,y,z,t) = R_s\ e^{j(k\ x\ \sin\theta_i\ +\ k\ z\ \cos\theta_i\ -\ \omega t)}\ \vec{1_y}$$

$$\vec{E_t}\ (x,y,z,t) = T_s\ e^{j(k\ x\ \sin\theta_t\ -\ k\ z\ \cos\theta_t\ -\ \omega t)}\ \vec{1_y} \qquad (2.2)$$

The reflection and transmission coefficients (R_s and T_s, respectively) of the perpendicularly polarized wave are given by the **Fresnel** expressions [1, p.40] :

$$R_s = \frac{\cos\theta_i\ -\ n\ \cos\theta_t}{\cos\theta_i\ +\ n\ \cos\theta_t}$$

$$T_s = \frac{2\ \cos\theta_i}{\cos\theta_i\ +\ n\ \cos\theta_t} \qquad (2.3)$$

"n" is the refractive index of the second medium, i.e. the ratio between the speed of light in the first (z>0) and the second (z<0) media. Introducing **Snell** law ($\sin\theta_i = n\ \sin\theta_t$) , we have :

$$R_s = \frac{\cos\theta_i\ -\ \sqrt{n^2\ -\ \sin^2\theta_i}}{\cos\theta_i\ +\ \sqrt{n^2\ -\ \sin^2\theta_i}}$$

$$T_s = \frac{2\ \cos\theta_i}{\cos\theta_i\ +\ \sqrt{n^2\ -\ \sin^2\theta_i}} \qquad (2.4)$$

Plane wave polarized in a direction parallel to the plane of incidence

The electric vector $\vec{E_i}$ now lies in the plane of incidence, in a direction perpendicular to the direction of propagation (fig. 2.3). In this case, we have [1, p.39] :

[2] In theory, this sentence is only correct, if the dimensions of the plane are infinite. The influence of finite dimensions will be examined later.

$$\vec{E_i}\ (x,y,z,t) = (\cos\theta_i\ \vec{1_x} + \sin\theta_i\ \vec{1_z})\ e^{j(k\ x\ \sin\theta_i\ -\ k\ z\ \cos\theta_i\ -\ \omega t)}$$

$$\vec{E_r}\ (x,y,z,t) = R_p\ (-\cos\theta_i\ \vec{1_x} + \sin\theta_i\ \vec{1_z})\ e^{j(k\ x\ \sin\theta_i\ +\ k\ z\ \cos\theta_i\ -\ \omega t)}$$

$$\vec{E_t}\ (x,y,z,t) = T_p\ (\cos\theta_t\ \vec{1_x} + \sin\theta_t\ \vec{1_z})\ e^{j(k\ x\ \sin\theta_t\ -\ k\ z\ \cos\theta_t\ -\ \omega t)} \qquad (2.5)$$

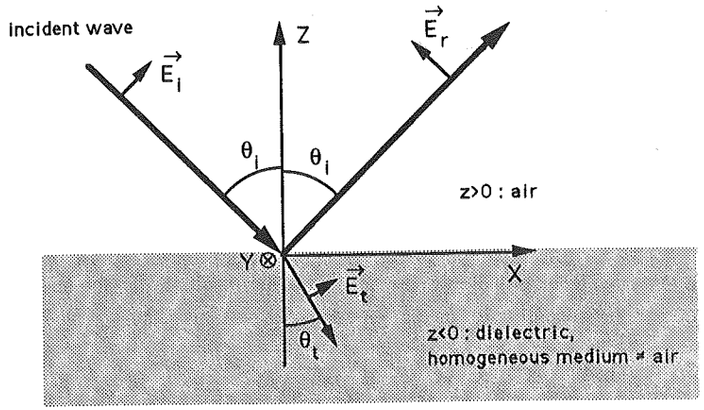

Figure 2.3 : Reflection of a plane wave $\vec{E_i}$ polarized in the plane of incidence, by the plane surface z=0 (symbols : see text).

The Snell law can again be applied, which gives the following Fresnel expressions for the reflection and transmission coefficients :

$$R_p = \frac{n^2 \cos\theta_i - \sqrt{n^2 - \sin^2\theta_i}}{n^2 \cos\theta_i + \sqrt{n^2 - \sin^2\theta_i}}$$

$$T_p = \frac{2\ n \cos\theta_i}{n^2 \cos\theta_i + \sqrt{n^2 - \sin^2\theta_i}} \qquad (2.6)$$

Plane wave with any polarization.

The incident electric vector lies along any direction perpendicular to the direction of propagation. It has a parallel component (A_p) and a perpendicular component (A_s).

The reflected energy is proportional to the square of the reflected wave amplitude [1, p.41], that is to[3] ($|A_p R_p|^2 + |A_s R_s|^2$). The reflection factor R^2 is the ratio between the reflected and incident intensities :

$$R^2 = \frac{|A_p R_p|^2 + |A_s R_s|^2}{|A_p|^2 + |A_s|^2} \qquad (2.7)$$

Figure 2.4 shows the dependance of this reflection factor on the angle of incidence θ_i, in the case of an air/glass interface (n=1.52). Note that this factor tends to 1, if the angle θ_i tends to 90° : under grazing incidence, all the energy is reflected by the interface.

If the plane wave is polarized in a direction parallel to the plane of incidence, there exists an angle θ_{iB} for which the reflected energy vanishes : this is the Brewster angle. In the case of an air/glass interface, this angle is arctang(n)=56°40' (see fig. 2.4).

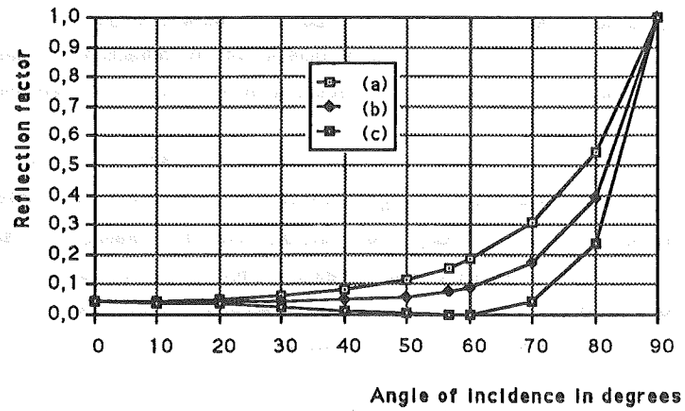

Figure 2.4 : Reflection factor of an air/glass interface (R^2) as a function of the angle of incidence of light (in degrees) :
a) wave polarized in a direction perpendicular to the plane of incidence
b) natural light : average value of (a) and (c)
c) wave polarized in the plane of incidence.

[3] The amplitudes A are generally complex numbers and their modulus is noted |A|.

The natural light [1, p.44] is characterized by an electric vector with a constant amplitude (at a fixed point), but polarized along a rapidly changing random direction. Yeh [11] gives the following information : the periods of light oscillations are less than 2.6 10^{-15} seconds (corresponding to 780 nm in vacuum), whereas the period of polarization variations is about 10^{-8} seconds for natural light. If the average value of the reflection factor (2.7) is taken over a period greater than 10^{-8} seconds, we obtain the reflection factor for natural light represented by curve (b) in figure 2.4.

The colour of reflected light

The question here is to determine if the spectral distribution of the reflected light is the same as the incident light spectrum. In other words, does the reflection factor depend on the wavelength ?

The analysis of expressions (2.4) and (2.6) indicates that only the refractive index "n" is able to introduce a wavelength dependence. In fact, it is easy to show that this index effectively depends on the wavelength : when light travels from air to glass, it can be observed that the deviation of the light beam, expressed by the angle θ_t (see 2.3), depends on the wavelength. This is the well-known phenomenon of the dispersion of light, associated with the refraction. It necessarily implies that the refractive index "n" changes with the frequency of light oscillations (see Snell law).

This spectral dependence originates from the interaction of light (and particularly the incident electric vector $\vec{E_i}$) with the atoms of the refractive medium. These atoms are polarized under the influence of the field $\vec{E_i}$ and their charges (ions and electrons) are vibrating at the same frequency. This motion of the electric charges creates electromagnetic waves which radiate outside the body. In liquids and solids where the interactions between atoms are important, the waves radiated by all electrons are in phase and create the specular reflection.

Sommerfeld [9, p.26] and Jenkins and White [6, p. 455] state that only a thin atomic surface layer is responsible for this specular reflection, since the waves created in the bulk of the medium are cancelled by interferences. Thus, the specular or regular reflection will also be called the "surface reflection".

The intensity of the reflected wave depends on the amplitude of the vibrating charges' oscillations. If the frequency of the incident electromagnetic wave is one of the resonance frequencies of the charges bounded to the atoms of the medium, then the vibrating amplitude will be amplified and the incident energy will be partly re-emitted (as a specularly reflected wave) and partly

transformed into heat : the medium does not transmit the electomagnetic waves at this frequency [6, p. 455], and this phenomenon is called selective absorption.

It follows that an important regular reflection generally coincides with selective absorption. For most dielectric homogeneous media, a charecteristic resonance is observed in the ultraviolet domain (it is caused by the electrons vibrations) and another one in the infrared region (caused by the heavier ions) : see figure 2.5. Glass, for example, has a selective absorption band for wavelengths lower than 380 nm and greater than 2.5 µm.

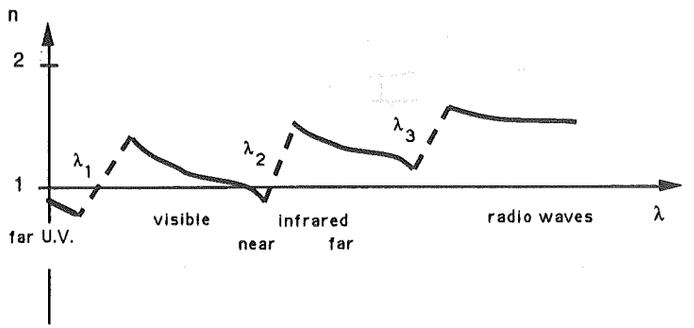

Figure 2.5 : Typical variation of the refractive index "n" of a dielectric homogeneous medium, as a function of wavelength. The resonance frequencies are noted λ_1, λ_2 and λ_3.
(From Jenkins et White [6])

So, it can be concluded that the specular reflection on a dielectric homogeneous medium generally depends on the wavelength. However, this dependence is not very accentuated in the visible region, except for a few material[4], and this reflection will be considered as non-selective [9, p. 39, and 18]. Therefore, the light source and its image in the medium have the same colour.

This assumption has also been adopted by Rombauts [8], who futhermore attributes the representative value n=1.5 to all dielectric materials. However, it can be seen on figure 2.6, that this second assumption is too restrictive. In the following, the value of the refractive index will be kept as general as possible.

[4] For example, the fuchsine pigment selectively absorbs the yellowish-green radiations and transmits a saturated red coloured light.

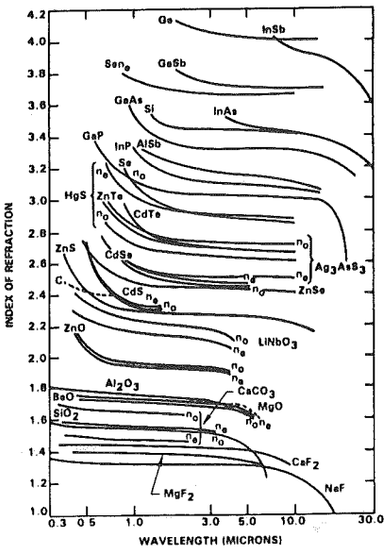

Figure 2.6 : Refractive index of some materials, as a function of wavelength (μm). For birefringent crystals, n_o is the ordinary refractive index and n_e, the extraordinary refractive index. From Yeh [11]

2.1.2. Interface between air and a conducting medium (metal)

Light reflection is again specular. However, the following differences are observed :

- light which penetrates into the metal is immediately absorbed : the penetration depth is very thin, only a small fractional part of the wavelength [6]. Metals can be considered as opaque materials;
- the reflected intensity is much more important than the intensity reflected by a dielectric medium, even at non-grazing incidences;
- light reflection by metals is often colored : the image of a white source is yellow in gold, red in copper, and so on... (see fig. 2.7).

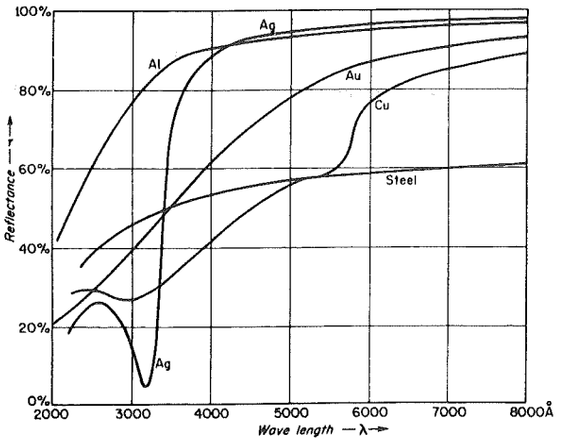

Figure 2.7 : Reflection factor (percents) of some metals at normal incidence, as a function of wavelength (Å). From Jenkins et White [6]

The origin of this different behaviour is to be found in the existence of free electrons which create surface electric currents. These currents transform the incident energy into heat dissipation, but also into specularly reflected waves. Therefore, the high absorption due to free electrons corresponds to a strong reflection : this coincidence has already been observed for dielectrics at the resonance frequency.

In the wave propagation equations, and in the Fresnel formula (eqs. 2.1, 2.3, 2.4, 2.6 et 2.7), the real quantities (k, n and even θ_t) are replaced by complex quantities containing the conductivity of the medium. It follows that the Fresnel reflection coefficients are no longer real, but complex values. Also, the polarization of the reflected wave is generally different from the polarization of the incident wave : see references [1,6,7] for further details.

The spectral dependence of the metallic reflection is more accentuated than the dependence observed for dielectrics : see, for example, figure 2.7. Note that the first observation of this section, concerning the opacity of metals, must be precised : in fact, metals can be transparents at some specific wavelengths. This is the case for silver at 320 nm (fig. 2.7), and for sodium at 200 nm.

The colour of the image of the light source in the metal tends to be less saturated, as the angle of incidence approaches 90° (grazing incidence). Indeed, for $\theta_i = 90°$, the equations (2.4) and (2.6) are still valid for metals and give $R_s = R_p = -1$, at all frequencies (see fig. 2.8). It follows that the wavelength dependence of the reflection factor vanishes, and that the reflected light rays have the same colour as the incident light rays. This can be observed, for example, with a copper plate illuminated by an incandescent light source : at grazing incidence, the image of source is not reddish, but white.

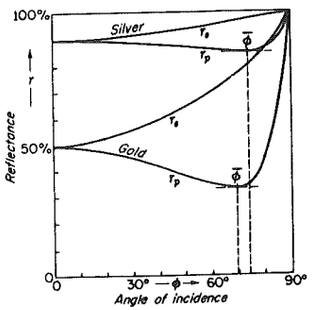

Figure 2.8 : Reflection factor (percents) of gold and silver, as a function of the angle of incidence (in degrees). The incident light is either polarized in a direction perpendicular to the plane of incidence (r_s) , or in the plane of incidence (r_p).
From Jenkins et White [6]

Some authors [8] attribute this phenomenon to the existence of two kinds of reflections for metals: one is a typical dielectric surface reflection (spectrally neutral), and the other is a typical colored metallic reflection. Both reflections would be specular and, therefore, both reflected beams would be superposed in the same direction. At normal incidence, the colored metallic reflection would be the more important, whereas the dielectric surface reflection would prevail at grazing incidence.

It is difficult to corroborate these assumptions with the electromagnetic theory, since two different contributions can hardly be observed in the expression of the reflection factor [1]. In this work, the following interpretation is preferred : light reflection on a plane conducting surface is specular, and the reflection factor depends on the angle of incidence and on the wavelength. Both dependences are combined to give the metallic reflection.

2.1.3. Interface between air and a heterogeneous dielectric medium

In real situations, most objects and materials are heterogeneous media : a celling covered with glossy oil-painting, a varnished table, a colored glass, polished plastic objects, these are several examples of plane surfaces belonging to this category.

The following phenomena can be observed for these materials :

- a specular reflection, which is generally not colored, as it is the case for transparent dielectrics. The reflected intensity increases with the angle of incidence;
- a diffuse reflection (light is spread in all directions), which is generally colored (fig. 2.9). The reflected intensity is less dependent on the angle of incidence. It follows that the viewing direction seems to have no influence on the lighness and on the colour appearance of the illuminated surface, except in the specular diretion.

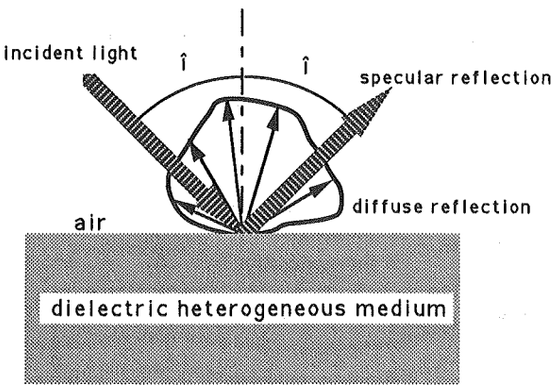

Figure 2.9 : Reflection and scattering of light on a dielectric heterogeneous medium (plane interface).

Both reflections overlap in the specular direction. As the angle of incidence tends to 90°, the achromatic surface reflection is more and more important. At grazing incidence, the image of the source (which has the same colour as the real source) is even masking the view of the medium itself.

Again, the origin of the diffuse reflection is to be found in the interaction of light with the particles of the medium.

Carniglia [3] and Croce[5] mention defects of homogeneity in the bulk of thin dielectric films, which are different from surface irregularities. These defects induce a spatial dependence of the refractive index, and light scattering in the medium ("volume scattering" [2,18,64]). This scattered light is partly re-emitted out of the medium : this re-emission is called the diffuse reflection[5].

Light scattering in the medium is not due to the molecules : molecular scattering also exists in homogeneous media and determines the speed of light in liquids and solids. Moreover, it is only significant in a single direction : the direction of refraction [6].

Light scattering in the medium must rather be attributed to bigger particles : we can imagine them as "micro-media" randomly spread in the inclusive medium (see figure 2.10).

The light scattering phenomenon does not explain all observations. Indeed, light scattering is a special case of light reflection, when the size of the reflecting surface has the same magnitude as the wavelength [6, p.456]. So, the scattered light is generally not colored for a non-conducting particle. Therefore, how can we explain the colour of diffuse reflection ? Sommerfeld [9] does explain the green colour of foliage as the following : chlorophyl is a plant-pigment which only transmits green light, and absorbs all other radiations. White light which penetrates into the foliage goes through the chlorophyl particles and becomes green by transmission. Then, this green light is scattered in the bulk of the medium, without spectral transformation. The same phenomena are observed with the pigments used in oil-painting.

The conclusion is [6, p.446, and 64] that diffuse reflection is due to the combined effects of light transmission by selectively absorbing particles (the pigments) and multiple reflections or multiple scattering on defects of homogeneity in the bulk of the medium. The complexity of all this process, and the random distribution of the scattering particles inside the medium, lead to a "re-emission" of light in all directions, which seems to be nearly isotropic : see also the measurements performed by Uetani and Matsuura [64].

[5] see also the C.I.E. (Commission Internationale de l'Eclairage) definition of light reflection in references [4] and [15].

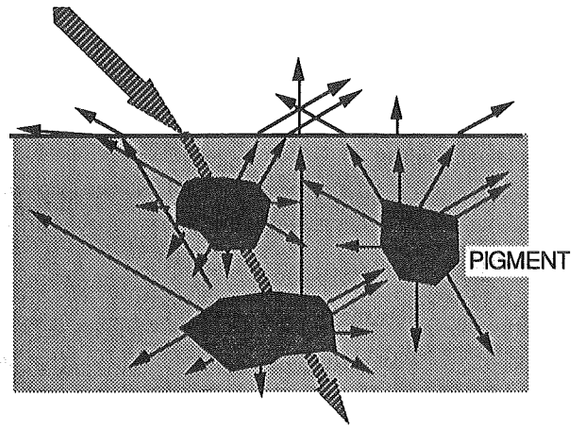

Figure 2.10 : Simplified scheme of diffuse reflection

The simplified scheme shown in figure 2.10 also illustrates why plane metallic interfaces do not diffuse light. Even if some impurities are present in the metal, light does not penetrate enough to reach them and, therefore, diffuse reflection is not created.

2.1.4. Note

Some materials have not been examined here, since they are seldom used in a lighting problem.

For example, the reflection of light on crystals or anisotropic media gives rise to a reflected light beam and two refracted light beams [1,6,7,9].

Also, the layered media will not be analysed here. These materials are made of several dielectric films, with different optical properties. Light reflection on these media depends on the ratio between the layers' thickness and the wavelength (filtering properties) : see reference [11].

2.2. Light reflection on a rough surface

2.2.1. First observations

A surface is called a "rough surface", if the corrugations (i.e. the height variations with respect to the mean plane of the interface) are large enough to significantly modify the light scattering indicatrix of this surface. It will be shown later that the roughness of a surface depends on the wavelength of the incident light.

It is supposed here that only the surface reflection is considered, i.e. the reflected light waves created by the vibrations of the electric charges, which are bounded to the atoms located in the vicinity of the interface.

Whatever the medium under the rough surface, the following phenomena are observed : the intensity of light reflection which is high and specular for a plane surface, is significantly reduced in the case of a rough surface. Moreover, the reflected light is spread around the specular direction, and this leads to a fuzzy image of the luminous source appearing on the surface. This unsharpness becomes more important as the roughness of the surface increases. If the surface is very rough, the image of the source is masked by the "volume" reflection.

It will also be shown that the roughness properties of a surface depend on the angle of incidence of light. At grazing incidence, the image of the source mentioned above becomes sharper, though the roughness of the surface is kept constant. This can be observed for a road surface which seems to reflect the sky when it is viewed under a grazing direction.

Finally, the roughness of a surface does not introduce significant colour modifications in the reflected light : as for a plane surface, light reflection by a rough surface is generally non-selective in the case of dielectrics, and selective in the case of metals. However, this observation will be precised in the following chapters (§ 2.2.3).

2.2.2. The Rayleigh's criterion

The theory of electromagnetic waves reflected by a rough surface will be developed in the fourth chapter . Here is only presented the theory of **Rayleigh**, which is able to simply explain the influence of the wavelength and the angle of incidence.

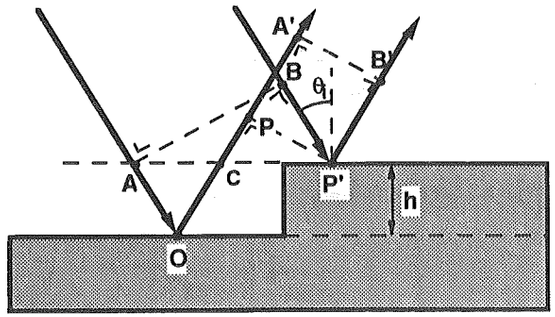

Figure 2.11 : Reflection of a plane wave on a surface gradient; development of the Rayleigh's criterion (symbols are defined in the text).

Figure 2.11 illustrates the influence of a step of height "h" in a plane surface. The incident waves are in phase at points A and B. They are no more in phase at A' and B', since the path AOA' is longer than the path BP'B' . The path difference is expressed as :

$$\Delta = |\vec{AO}| + |\vec{OC}| + |\vec{CP}| - |\vec{BP'}| = \frac{2\,h}{\cos\theta_i} + |\vec{CP}| - |\vec{BP'}|$$

Since $|\vec{CP}| = |\vec{CP'}| \sin\theta_i$ and $|\vec{BP'}| = (|\vec{AC}| + |\vec{CP'}|) \sin\theta_i$, we can write :

$$|\vec{CP}| - |\vec{BP'}| = - |\vec{AC}| \sin\theta_i = - 2\,h\,\mathrm{tg}\theta_i \sin\theta_i$$

and $$\Delta = 2\,h\cos\theta_i \qquad (2.8)$$

Remember that the phase of the reflected wave (see eq. 2.2) is proportional to $k\Delta = \left(\frac{2\,\pi\,\Delta}{\lambda}\right)$.

So, the reflected wave is coherent, only if $k\Delta << 1$. However, if $k\Delta = \pi$, the phases corresponding to both reflected light rays are opposite and their contributions vanish. Rayleigh considered that a surface is rough if $k\Delta > \frac{\pi}{2}$, that is :

$$h > \frac{\lambda}{8\cos\theta_i} \qquad (2.9)$$

The choice of $\left(\frac{\pi}{2}\right)$ as lower bound is somewhat arbitrary, and some authors rather prefer $\frac{\pi}{4}$ or $\frac{\pi}{8}$. An interesting discussion of this problem can be found in Beckmann and Spizzichino [38].

The influence of the wavelength is well described by the equation (2.9). As the wavelength increases, the surface reflects light more and more like a plane interface, for a given step "h" and a given angle of incidence θ_i.

The same specular behaviour is observed at grazing incidence (as θ_i approaches $\frac{\pi}{2}$), for a given wavelength. This can explain the behaviour of the road surface mentioned previously.

2.2.3. Evidence of two contributions in the surface reflection

The following experiment illustrates again the criterion of Rayleigh : observe, at grazing incidence, the image of a "white" (colour temperature = 4000°K) tubular fluorescent lamp on a frosted glass surface (figure 2.12). The reverse side of the sample has been painted in black, to minimize the influence of transmitted light reflection on it.

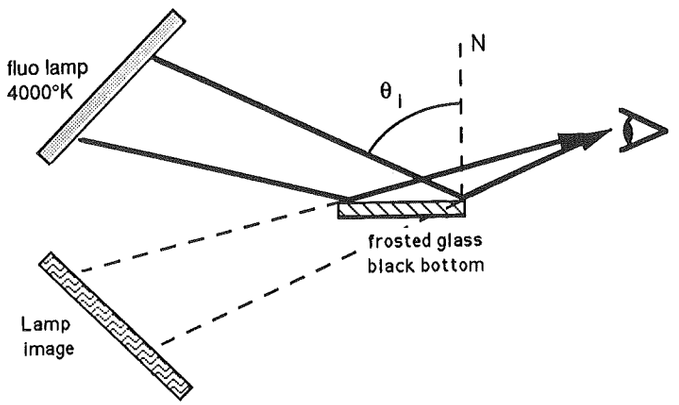

Figure 2.12 : Experiment showing two contributions in surface reflection.

If the viewing angle and the angle of incidence are close to 90° with respect to the normal N, the image of the fluorescent lamp is white and sharp. Its colour is identical with the real lamp's colour. As the viewing direction deviates from the grazing direction, the image of the lamp gradually vanishes and is surrounded by a halo. Moreover, the colour of the image becomes yellow, and then rapidly moves towards red, as the viewing angle decreases.

Below a given value of this angle, the image of the lamp disappears, leaving only the white halo.

This experiment can be explained as follows : at grazing incidence ($\cos\theta_i \approx 0$ in 2.9), all wavelengths are specularly reflected. As θ_i decreases, the corrugations of the surface create light scattering (leading to the halo) and the intensity of light reflected in the specular direction is gradually reduced. However, this reduction depends on the wavelength : indeed, following the Rayleigh's criterion, the first radiations vanishing in the specular direction are the blue ones (short wavelengths) and, therefore, the colour of the image moves towards the complementary colour (yellow). As θ_i still decreases, only the longer wavelengths are specularly reflected, giving a reddish image.

The volume reflection cannot be incriminated here, since the body of the glass sample is transparent. Thus, there would be two simultaneous contributions to surface reflection :

- a very directional one, which is identical to the contribution of a plane interface. The intensity associated with this component is reduced, as the amplitude of the surface's corrugations increases. This reflection creates a sharp image of the source : one point source creates one point of the image;
- the other contribution is generally less directional and spread around the specular direction, creating the halo : here, one point source creates several points in the image.

It will be seen in the fourth chapter that the model of Beckmann can take these two components into account, since the expression of the reflected intensity will be composed of two terms : one for the coherent specular reflection, and the other for the incoherent reflected light.

2.3. Summary : spatial distribution of the reflected light

To sum up, light reflection on a plane surface is illustrated by the diagrams of figure 2.13.

The incident light intensity I_i creates the specularly reflected intensity I_s : it is generally achromatic (except for metals), and generates the image of the light source.

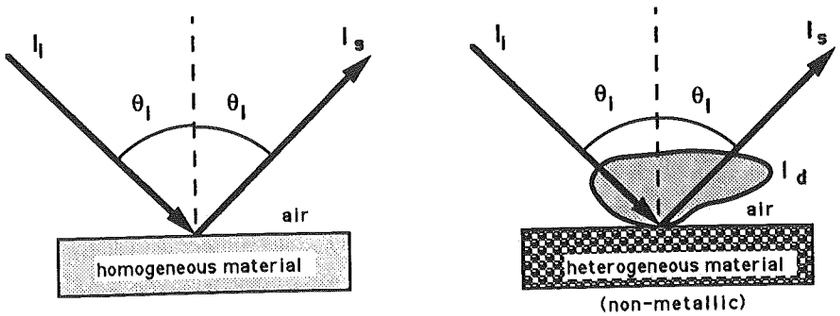

Figure 2.13 : Schematic illustration of the reflection on a plane surface.

If the medium is not homogeneous, a part of the transmitted intensity is re-emitted as scattered light (I_d), spread in all directions. This scattered light has interacted with the bulk of the material, and it is generally colored. There is no scattering in the case of metals, since light does not penetrate enough into the material.

If the surface is rough (fig. 2.14), the following modifications are observed :

- the specularly reflected intensity I_s is reduced, as the amplitude of the surface's corrugations increases. An image of the source is still visible on the surface, if this attenuation is limited;

- part of the reflected light is transformed into surface scattering intensity (I_{sc}). The angular spread around the specular direction increases with the amplitude of the corrugations. The source is still imaged in the surface of the material, but the image is not sharp anymore : it rather appears as a halo.

Furthermore, the influence of roughness depends on the wavelength and on the angle of incidence.

The light beams represented by I_s and I_{sc} are generally achromatic for non-metallic materials. Sometimes, it can be observed that the reflected component I_s rapidly turns to yellow, and then to red, within a very short interval of angles of incidence. However, this behaviour is rather exceptional.

Finally, it must be noted that some materials don't have a well-defined surface [8] : for example, a woollen carpet or any material with very rough surface. They will be considered here as a limiting case of figure 2.14, for which I_s and I_{sc} vanish.

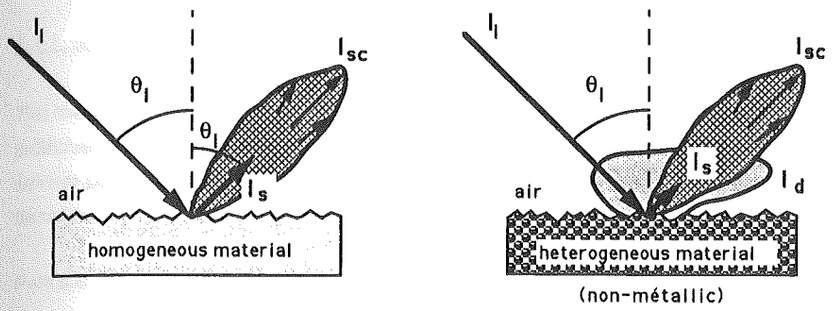

Figure 2.14 : Schematic illustration of the reflection on a rough surface.

Chapter 3 : Measurement of light reflection

3.1. State of the art

3.1.1. Measured quantities

The measured quantities associated with light reflection on a material are defined in a report published by the C.I.E. (Commission Internationale de l'Eclairage) in 1977 [15]. In this report, several possible geometrical configurations to measure these quantities are listed : they will be described later.

Perhaps the more usual quantity is the reflectance. It is defined as the ratio of the flux reflected by a material to the incident flux : see the International Lighting Vocabulary [4] I.L.V., § 845-04-58. It depends on the spectral distribution of the incident radiation, on its polarization state and on its spatial distribution.

In the case of an isotropic diffuse reflection, the reflectance is sufficient to completely describe the luminous reflection properties of the material. Indeed, the isotropic diffuse reflection is characterized by the **Lambert** law, which states that the intensity I_r reflected in a direction θ (figure 3.1) is given by :

$$I_r(\theta) = I_{r0} \cos \theta \qquad (3.1)$$

where I_{r0} is the intensity reflected in the direction perpendicular to the macroscopic plane surface.

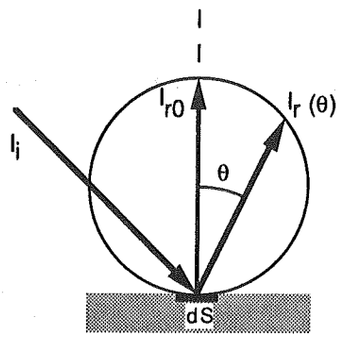

Figure 3.1 : Lambert law

The figure 3.1 illustrates that the element of surface dS receives the element of flux $d\Phi_i = E\ dS$, where "E" is the illuminance at dS. The reflected luminous flux can be obtained by integration of (3.1) over all possible directions of reflection : $d\Phi_r = \pi\ I_{r0}$. Applying the definition of the reflectance ρ , we have :

$$\rho = \frac{d\Phi_r}{d\Phi_i} = \frac{\pi\ I_{r0}}{E\ dS} \qquad (3.2)$$

Introducing (3.2) in (3.1) gives :

$$I_r(\theta) = \frac{\rho\ E}{\pi} \cos\theta\ dS \qquad (3.3)$$

Whatever the origin of the illuminance may be or, in other words, whatever the incidence of light in figure 3.1, the reflectance completely defines the spatial distribution of the reflected intensity[1].

Obviously, no material exactly follows the theoretical behaviour expressed by the Lambert law (cfr. chapter 2). Therefore, other quantities must be defined to describe the reflection on real materials.

In general, the luminance factor is introduced : it is defined [4] as the ratio of the luminance of a surface in a given direction to that of a perfect reflecting diffuser identically illuminated.

The equation (3.3) states that the luminance of the perfect reflecting diffuser (ρ=1) is equal to $\frac{E}{\pi}$.

It follows that the luminance factor β_V[2] is given by :

$$\beta_V(\theta_i, \phi_i, \theta_r, \phi_r) = \frac{\pi\ L(\theta_i, \phi_i, \theta_r, \phi_r)}{E(\theta_i, \phi_i)} \qquad (3.4)$$

See figure 3.2 for the definition of the angles of incidence (θ_i, ϕ_i) and the angles of viewing (θ_r, ϕ_r).

---

[1] The isotropic diffuser characterized by ρ=1 is called the perfect reflecting diffuser (I.L.V. 845-04-54)

[2] The symbol "β" is more common, but "β_V" is rather used here to distinguish the luminance factor from the radiance factor "β_e", which is the same quantity not corrected by the spectral luminous efficiency. "β_V" is also used here to avoid confusion with an angle β which will be introduced later.

A surface with a symmetrical texture is characterized by a luminance factor which only depends on three angles, since the geometrical configuration is not influenced by ϕ_i .

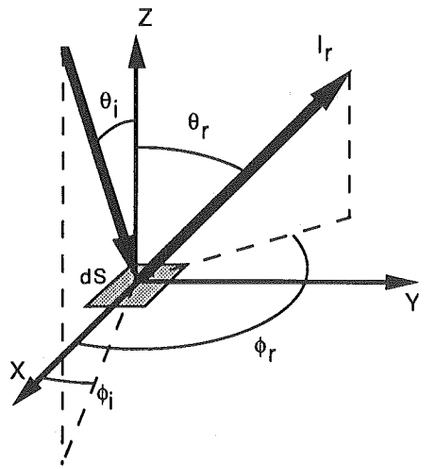

Figure 3.2 : Definition of the angles $(\theta_i, \phi_i, \theta_r, \phi_r)$ in a system with axis XYZ attached to the element of surface dS.

The luminance coefficient "q" (I.L.V. 845-04-70 and 845-04-71) is the quotient of the luminance of the surface element dS in the direction (θ_r, ϕ_r) by its illuminance. It is directly related to the luminance factor since, by (3.4), $\beta_V = \pi\ q$. This luminance coefficient is mainly used in the U.S.A., where it is called the "bi-directional reflectance distribution function (BRDF)", if the illuminance is produced by a directional incident radiation.

During light reflection measurements, the reflected radiation analysed by the detector has an angular extent which is never zero. So, the "luminance factor" and the "luminance coefficient" are only theoretical concepts. In practice, what is measured is the "reflectance factor" [3] (R). This is the ratio of the flux reflected in the directions delimited by a given cone with apex at the surface element and centered on the direction (θ_r, ϕ_r) to the flux reflected in the same directions by a perfect reflecting diffuser identically illuminated.

If the solid angle associated with the given cone is close to zero, R is similar to the luminance factor. If the solid angle is 2π, R is similar to the reflectance.

---

[3] No standard french translation : see the I.L.V. [4], definition n° 845-04-64

3.1.2. Geometrical configurations for the measurements

The publication C.I.E. n° 38 [15] describes nine modes of reflection measurement. Among them, only four are widely used :

- the hemispherical/hemispherical mode : the incidence of light is diffuse (illumination by an hemisphere with an isotropic luminance) and the reflected flux is encompassing the entire hemisphere. The measured quantity is the reflectance at diffuse incidence (ρ_{dif}).
- the hemispherical/conical mode : the incidence of light is diffuse and the reflected flux is only encompassing a given cone (g'), the solid angle of which is to be defined. The measured quantity is the reflectance factor $R_{dif/g'}$.
- the conical/hemispherical mode : the measured quantity is ρ_g, where (g) identifies the cone containing the incident flux.
- the conical/conical mode : the measured quantity is the reflectance factor $R_{g/g'}$.

The measurement of reflectances (ρ_g or ρ_{dif}) is generally carried out with the use of an integrating "Ulbricht" sphere, collecting the reflected flux. Only in particular cases (for example in the study of standard diffusors [19,29]) is the reflected flux calculated by mathematically integrating the reflectance factor over all possible directions of reflection.

To measure ρ_g, the sample should be illuminated perpendicularly, and the aperture angle of the light beam should be less than 10° [15].

The measurements in the conical/conical mode are often carried out in the specular direction, to measure the regular reflection [15,30]. Otherwise, the angles of incidence and viewing are often 45° and 0°, or 0° and 45° respectively. An example of such a measurement is the determination of spectral reflection in colorimetry [13].

To sum up, the following geometrical configurations are the most widely used [16] :

45°/normal (noted 45/0)
normal/45° (0/45)
diffuse/normal(d/0)
normal/diffuse(0/d)
diffuse/diffuse(d/d)

The first three configurations give a reflectance factor . If the incident and reflected beams are sufficiently thin (10° following [15]) , the reflectance factor can be considered as a luminance factor. The last two configurations give a reflectance.

It must also be noted that the directions of incidence and viewing can be inverted without changing the value of the measured factor (Helmholtz principle of reciprocity). So, the following equalities hold : $\beta_{v,0/45} = \beta_{v,45/0}$ and $\beta_{v,d/0} = \rho_0$.

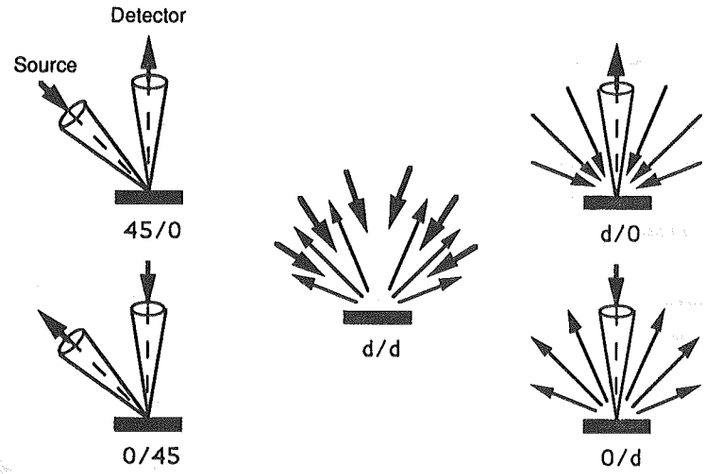

Figure 3.3 : The most widely used geometrical configurations in the study of light reflection.

3.1.3. Relative character of the measurements

In general, the measurements of reflection properties are carried out in comparison with a primary or secondary standard of reflection, for which the measured quantity is known. Since 1969, the C.I.E. has defined the primary standard of reflection as the perfect reflecting diffuser, that is an ideal surface which would reflect all the incident flux. This perfect reflecting diffusor cannot be realized in practice.

Therefore, the calibration of secondary standards cannot be performed as relative measurements, but rather in an absolute way. More precisely, the simultaneous measurements of the luminance of the sample and its illuminance are necessary : see eq. (3.4). The reader who is interested by this problem should consult references [16,23,29] for more details.

3.1.4. Measurement of the spatial distribution of the reflected flux

The quantities measured by the configurations illustrated in figure 3.3 do not completely describe the spatial distribution of flux reflected by any material. Therefore, the approximation of an isotropic diffuser is often used, in order to simplify the problem or to allow an easy standardization of the reflection properies. With this approximation, it is sufficient to measure only one or two quantities of fig. 3.3.

For example, the reflectance of paper is measured under diffuse incidence, in a viewing direction perpendicular to the sample [15]. Kok and Monard [27] use the same geometry for the measurements of building materials. Erb [23] is measuring $\beta_{v,45/0}$ and $\beta_{v,d/0}$ for several reflection standards.

However, several applications require a more accurate description of the diffusion indicatrix, i.e. the spatial distribution of the reflected intensity or the luminance factor.

The study of reflection standards [19,25] has already been mentioned above. Also in road lighting, the international publications have recommended, several years ago, the measurement of the luminance coefficient of the road, for an angle of viewing of 89° from the normal [12,14]. The standardized representation of this measurement is illustrated in figure 3.4.

Figure 3.4 : Luminance factor or luminance coefficient (q) of a road sample. The standardized representation shows the"iso-r" curves ($r=10^4\ q\ \cos^3\gamma$). The sample is placed at (0,0) in the diagram. The source is placed at (x,y,H) and illuminates the sample under an angle of incidence γ. The angle of viewing is 89° from the normal. (C.I.E. Publication n° 30-2 [14]).

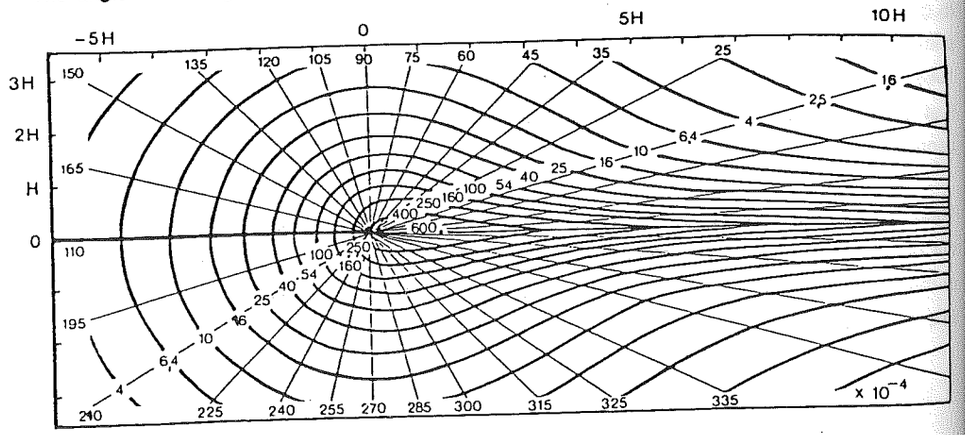

Since the development of computers, the conception of lighting softwares results in more and more finished and sophisticated products. Also in this field, an increasing demand for more general indicatrices of diffusion is formulated. Indeed, this could lead to better simulations, since the performances of the softwares are now strongly influenced by the accuracy of the data, more than by the calculation procedure itself.

Everywhere around the world, goniophotometers are now developed to measure the spatial distribution of the flux reflected by several materials [8, 19, 21,22,24,28,31]. However, no "standardized" apparatus has still been adopted : each of them are conceived and adjusted for a particular application : the study of reflection standards, metallic materials for luminaires reflectors and semi-diffusing materials are some examples of treated applications.

This measurement technique is still very new : not only the apparatus, but also the measurement procedures are not standardized. Nothing else than the general principles of C.I.E. publication n°38 [15] is recommended, concerning the specification of angular steps, aperture angles for the incident and reflected beams, distance between the source and the sample ...

3.2. Measurement of the luminance factor in the plane of incidence : principle

3.2.1. Aim of the study

Our study of mixed reflection started in 1987. At that time, only a few laboratories were equipped with an apparatus which could measure the spatial distribution of the luminance factor. Moreover, we needed an instrument that would be flexible and easily available. So, it was decided to set up our own experimental apparatus, in the dark chamber of the Acoustics and Lighting Department of the University of Liège [21].

The measurement apparatus should be simple and classical, at the expense of the number of possible applications. However, the measurements have been considered accurate enough to support the modelization of mixed reflection, which was and still is the main objective of our research.

In particular, the measurements are limited to the plane of incidence. It will be shown in the following chapter that this already allows an interesting analysis of the reflection properties of any material.

From the beginning, we have introduced the spectral dimension, in order to take into account the influence of the wavelength of the incident light.

3.2.2. Foreword

It has been explained in §3.1.2 that the luminance factor itself will not be measured, but rather the corresponding reflectance factor .

However, both factors can be considered as equal, since the aperture angles associated with the incident and viewing beams are small enough (their value will be precised later). So, the expression "luminance factor" will be kept in the following.

3.2.3. Description of the measurement procedure

The goniophotometric method is fundamental if the spatial distribution of the luminance factor is to be determined [16]. So, this method has been adopted and developed.

The following elements are common to all goniophotometric equipments (fig. 3.5) :
- the light source (S), associated with a possible converging optical system (L);
- the sample of material, the luminance factor of which has to be measured;
- the detector of radiation (R), with its own optical system;
- an instrument to measure the angles of incidence (θ_i, ϕ_i) and viewing (θ_r, ϕ_r).

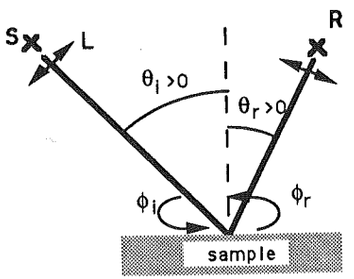

Figure 3.5 : Principle of the goniophotometric method.

The surface of the sample is considered as macroscopically plane, if the surface roughness is much smaller than the dimensions of the sample, the distance between the source and the material and also the distance between the sample and the detector.

The light rays illuminating the sample should be as parallel as possible (same angle of incidence θ_i). This condition is not met in practice, but it is well approximated by :
- enlarging the distance between the source and the sample and/or
- placing a converging lens in front of the source.

The same observations can be formulated for the light beam analysed by the detector.

The light wave reflected by the sample is measured in a direction defined by the angle θ_r, which is itself measured from the perpendicular to the macroscopically plane surface. In our measurement system, the three directions (incidence, perpendicular to the sample, viewing) are situated in the same plane, which is called the plane of incidence. Therefore, the determination of the angle ϕ_r is not necessary.

The measurements are limited to the plane of incidence, for the following reasons :
- first of all, to make the practical realization of the goniophotometer easier and to reduce the measurement time for a given sample. This is important, since the instrument is not self-acting : for example, the angles θ_i and θ_r must be changed manually.

Figure 3.6 : Definition of the aperture angles of the incident (1) and viewing (2) beams. (C.I.E. Publication n° 38 [15])

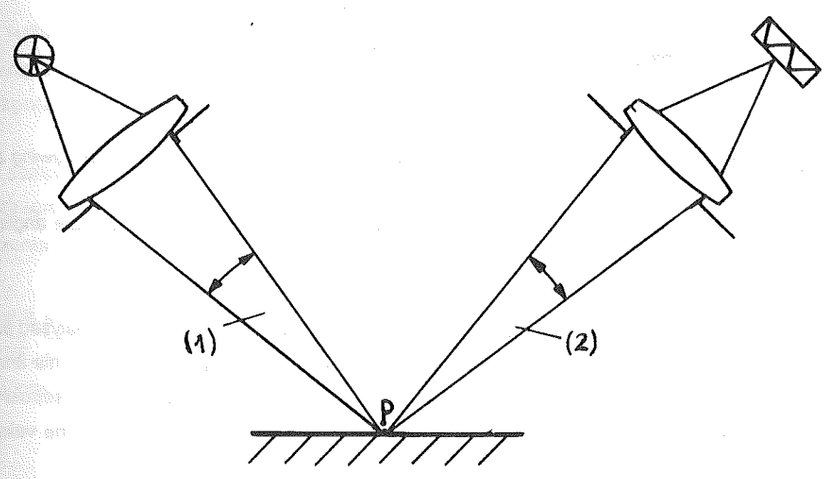

- secondly, the study of light reflection phenomena (see chapter 2) and their mathematical modelization (see chapter 4) show that most behaviours have their maximum intensity in the plane of incidence. This is particularly the case for the specular reflection[4].

The figure 3.5 describes the goniophotometer equipped with a point source and a punctual detector. This is not realized in practice : the geometrical extents of the source and the detector imply that there are several possible paths from a point P of the sample to the source or the detector (figure 3.6). These different paths are situated in a cone with an extent characterized by the aperture angle [15] (defined by the angle or half-angle at the apex).

Also, the surface analysed on the sample is not punctual. The detector can be situated at the apex of a cone with a finite aperture, which includes all the "visible" directions and which is generally delimited by a diaphragm. This cone defines on the sample a finite area, which is the analysed surface (fig. 3.7).

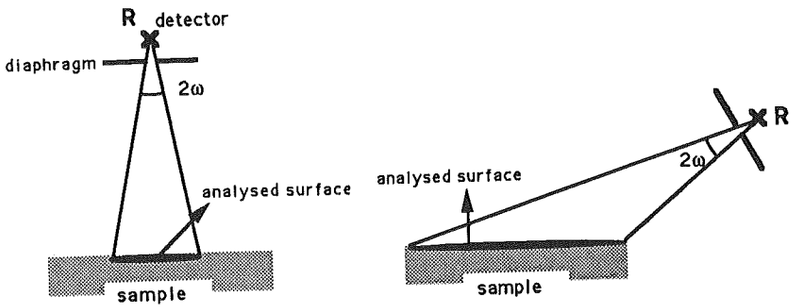

Figure 3.7 : Modification of the analysed surface on the sample as a function of the viewing angle.

The geometrical extent of this surface grows with the viewing angle θ_r , if the aperture angle of the cone ω is kept constant : see figure 3.7.

We have decided to work with a constant aperture angle ω , instead of keeping the analysed surface constant : indeed, this option leads to more simple goniophotometers [26]. However, this also implies that the sample must be homogeneous. In particular, the illuminated surface should completely include the analysed surface. This condition will introduce limitations in the values of the angles of incidence and viewing.

---

[4] Of course, this observation is true for materials which have a symmetrical texture, i.e. materials with reflection properties which do not depend on the azimutal angle ϕ_i .

The theoretical variations of the angles θ_i and θ_r described in figure 3.5 are given here for a sample with a symmetrical texture :

- from 0° to 90° for the angle of incidence θ_i ,
- from -90° to +90° for the angle of viewing θ_r.

However, the angle of incidence is practically limited at 80° by the condition of a constant illumination on the analysed area. Also, the viewing angle will be limited at 70° or 80°, since the analysed surface must be included in the real surface of the sample : it depends in fact on the size of the sample and the aperture angle of the detector. Finally, it must be noted that it is impossible to measure in the configuration $\theta_i = -\theta_r$, when the sample is hidden from the source by the detector.

3.2.4. Calculation of the flux reaching the detector

The figure 3.8.a is a plane view of the path followed by the light rays between the sample and the detector F. The surface analysed on the sample is located in a plane perpendicular to the figure. At the beginning of the study, the detector was the monochromator of a spectrophotometer (see §3.3) and "F" stands for the entrance slit of the monochromator. The maximum dimension of the slit is 1.4 cm : this is much smaller than the distance between the sample and the slit (about 1 m).

The surface of the sample can be rotated around the vertical axis $\vec{z}$, in order to change the viewing direction. The point E on the sample belongs to this axis and the direction $\vec{EF}$ is horizontal.

The sample is seen from the slit F through a cone with aperture 2ω , determined by a circular diaphragm D. The plane of the macroscopic surface of the sample is defined by two axis : the horizontal axis $\vec{u}$ and the vertical axis $\vec{v}$.

There is another axis system which is fixed and centered in E : the axis $\vec{x}$ is parallel to the optical axis $\vec{EF}$, $\vec{z}$ is vertical and $\vec{y}$ is the third axis of the system. The axis $\vec{u}$ can be rotated in the horizontal plane (xy) : the angle of rotation is noted α.

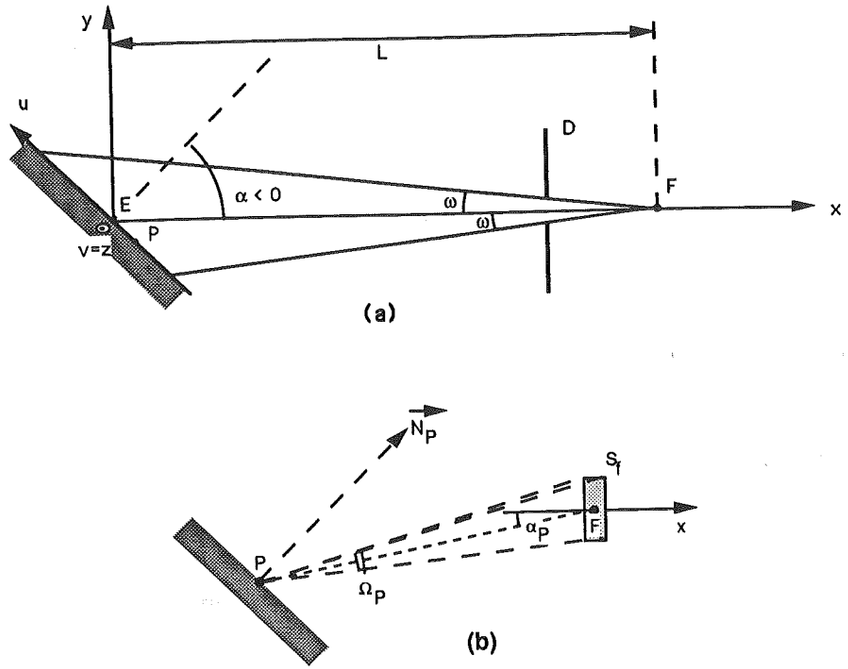

Figure 3.8

a) Path followed by the light rays between the sample (hatched surface) and the entrance slit F of the monochromator : plane view and axis system

b) Detail of the entrance slit and the solid angle under which it is viewed by the point P of the sample surface

The figure 3.8.b is a more detailed view of the slit F (area S_f) situated in a plane perpendicular to $\vec{x}$. S_f determines a solid angle Ω_P with apex at a point P of the sample surface. The luminous flux $d\Phi_P$, leaving P and collected by the slit, can be approximated by the product of the solid angle Ω_P and the intensity reflected at the center of the beam (eq. 3.5).

Such an approximation supposes that the variation of the intensity and the luminance factor inside the solid angle Ω_P can be neglected. Now, the corresponding aperture angle measured at the apex of the cone is smaller than 1°, if we consider the dimensions mentioned above. Therefore, the following mathematical developments are correct, if the variation of the luminance factor around the viewing direction (± 0.5°) is not significant. It can be already noted that the procedure is not valid for highly specular materials !

$$d\Phi_P \approx I(\theta_P, \phi_P, \hat{\imath}_P)\,\Omega_P$$

$$\Omega_P = \frac{S_f \cos\alpha_P}{d_P^2} \qquad (3.5)$$

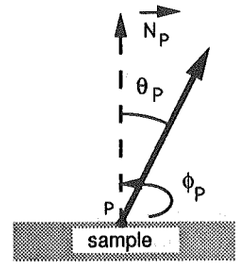

Figure 3.9 : A viewing direction is defined by the angles θ_P and ϕ_P. $\vec{N_P}$ is the normal to the sample at P.

In (3.5), the angles θ_P and ϕ_P define the direction $\vec{PF}$ from the point P (figure 3.9) and $\hat{\imath}_P$ symbolizes the influence of the angle of incidence of light at P or, more generally, the spatial distribution of the incident light. d_P is the distance between P and F.

In the coordinates system (x,y,z), we have :

$$P(u,v) = (u \sin\alpha,\ u \cos\alpha,\ v)$$

$$\vec{N_P} = (\cos\alpha,\ -\sin\alpha,\ 0)$$

$$F = (L, 0, 0) \text{ et } \quad \vec{PF} = (L - u\sin\alpha,\ -u\cos\alpha,\ -v) \qquad (3.6)$$

which give :

$$d_P^2 = L^2 - 2\,u\,L\sin\alpha + u^2 + v^2$$

$$\cos\theta_P = \frac{\vec{PF}.\vec{N_P}}{|\vec{PF}|\,|\vec{N_P}|} = \frac{L\cos\alpha}{d_P}$$

$$\cos\alpha_P = \frac{\vec{PF}.\vec{x}}{|\vec{PF}|} = \frac{L - u\sin\alpha}{d_P} \qquad (3.7)$$

The definition of the luminance factor[5] can now be applied and the equations (3.5) to (3.7) lead to:

$$d\Phi_P \approx \beta_e(\theta_P, \phi_P, \hat{i}_P)\, I_0 \cos\theta_P \frac{S_f \cos\alpha_P}{d_P^2}$$

$$d\Phi_P \approx \beta_e(\theta_P, \phi_P, \hat{i}_P)\, I_0\, S_f \frac{L\cos\alpha\,(L - u\sin\alpha)}{d_P^4} \qquad (3.8)$$

I_0 is the intensity reflected by the perfect diffuser in the direction perpendicular to its surface.

The total flux entering the slit of the monochromator encompasses the contributions of all elements of flux $d\Phi_P$, coming from the analysed surface of the sample determined by the cone of aperture 2ω (emitting surface S_E) :

$$\Phi = \iint_{S_E} d\Phi_P \qquad (3.9)$$

Doing this, it is assumed that the contribution of every point of the surface S_E to the total flux entering the slit of the monochromator can be expressed by the equation (3.5). This is justified by the fact that the distance d_P is much greater that the dimensions of the slit. Applying the definition of the perfect diffuser gives :

$$I_0 = L_0\, dS_P = \frac{E_P}{\pi} dS_P \qquad (3.10)$$

where L_0 and E_P are the luminance and the illuminance of a perfect diffuser located at point P and covering the surface dS_P. The element of surface (dS_P) can be expressed in polar coordinates by $dS_P = \rho\, d\rho\, d\psi$ (see figure 3.10) .

Finally, using (3.9) and (3.10) :

$$\Phi \approx \int_0^{2\pi} d\psi \int_0^{R(\psi)} \beta_e(\theta_P,\phi_P,\hat{i}_P) \frac{E(\rho,\psi)}{\pi} S_f \frac{\rho\, L\cos\alpha\,(L - \rho\cos\psi\sin\alpha)}{(L^2 - 2\rho L\cos\psi\sin\alpha + \rho^2)^2} d\rho \qquad (3.11)$$

[5] the spectral dependence of the luminance factor is here obvious, since the detector is a spectrophotometer. However, this dependence will not be explicitely stated, in order to keep the symbolization clear (otherwise, we should have noted $\beta_e(\lambda)$).

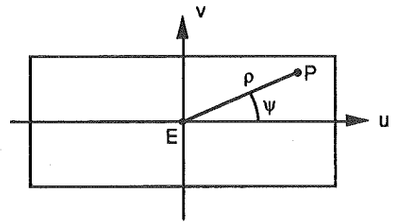

Figure 3.10 : Polar coordinates system defining the location of a point P on the sample, from the reference point E.

The emitting surface S_E on the sample is bounded by the curve containing the points P such that the angle between $\vec{PF}$ and $\vec{x}$ must be ω (figure 3.8.a) :

$$\frac{\vec{PF}.\,\vec{x}}{|\vec{PF}|} = \cos\omega \qquad (3.12)$$

and, using (3.7) :

$$\frac{L - R(\psi)\cos\psi\sin\alpha}{\sqrt{L^2 - 2L\,R(\psi)\cos\psi\sin\alpha + R^2(\psi)}} = \cos\omega$$

$$\Rightarrow R(\psi) = \frac{L\,tg\omega}{\cos\psi\sin\alpha\,tg\omega \pm \sqrt{1 - \cos^2\psi\sin^2\alpha}} \qquad (3.13)$$

The solution $-\sqrt{\ }$ has no physical sense, because there is only one unique positive value $R(\psi)$, for ψ comprised between 0 et 2π, in our experimental procedure.

Going on further with the analysis of (3.11), it is assumed that β_e is constant in every point P of the emitting surface. This implies that the sample should be as homogeneous as possible, but also that the luminance factor should not depend too much on the incidence and viewing directions belonging to the same incident or measured light bundle. The practical angular extents (in degrees) of both bundles will be precised later. However, we can already mention that the experimental procedure defined here is not suitable for highly specular materials.

In (3.11), $\beta_e(\theta_P, \phi_P, \hat{i}_P)$ is then approximated by $\beta_e(\hat{o}, \hat{i})$, where $\hat{o}$ is the mean viewing angle defined by the direction $\vec{EF}$ (figure 3.8) and $\hat{i}$ is the mean angle of d'incidence defined by the

direction $\vec{SE}$ (S is the location of the source which is supposed to be punctual). So, the following expression can be written :

$$\Phi \approx \bar{\beta}_e(\hat{o}\ ,\ \hat{i})\ \frac{S_f\ L\ \cos\alpha}{\pi} \int_0^{2\pi} d\psi \int_0^{R(\psi)} \frac{E(\rho,\psi)\ \rho\ (L - \rho\ \cos\psi\ \sin\alpha)}{(L^2 - 2\ \rho\ L\ \cos\psi\ \sin\alpha + \rho^2)^{\ 2}}\ d\rho \qquad (3.14)$$

$\bar{\beta}_e(\hat{o}\ ,\ \hat{i})$ is not the accurate value of the luminance factor of the sample, for the given angles $\hat{o}$ and $\hat{i}$, but rather a mean value which effectively approaches the true value $\beta_e(\hat{o}\ ,\ \hat{i})$ only if the second condition expressed above is verified.

The expression (3.14) can be integrated analytically in the case of a uniform illuminance of the sample :

$$\int_0^{2\pi} d\psi \int_0^{R(\psi)} \frac{\rho\ (L - \rho\ \cos\psi\ \sin\alpha)}{(L^2 - 2\ \rho\ L\ \cos\psi\ \sin\alpha + \rho^2)^{\ 2}}\ d\rho \ = \frac{\pi\ \sin^2\omega}{L\ \cos\alpha} \qquad (3.15)$$

and, finally :

$$\Phi \approx \bar{\beta}_e(\hat{o}\ ,\ \hat{i})\ E\ S_f\ \sin^2\omega \qquad (3.16)$$

If the sample is illuminated by a point source located at distance D, with an intensity I, and under the angle of incidence $\hat{i}$, we have :

$$\Phi \approx \bar{\beta}_e(\hat{o}\ ,\ \hat{i})\ \cos\hat{i} \left(\frac{I\ S_f\ \sin^2\omega}{D^2}\right) \qquad (3.17)$$

3.2.5. Uncertainty on the viewing angle

The angle $\delta \geq 0$, between the direction of the reflected light ray $\vec{EF}$ (figure 3.8) and the direction of the ray $\vec{PF}$, where P belongs to the visible surface S_E, can be written :

$$\cos\delta = \frac{\vec{PF}.\ \vec{x}}{|\vec{PF}|} = \frac{L - \rho\ \cos\psi\ \sin\alpha}{\sqrt{L^2 - 2\ L\ \rho\ \cos\psi\ \sin\alpha + \rho^2}} \qquad (3.18)$$

It will be shown in the following that :

$$0 \leq \delta \leq \omega = 2.4° \qquad (3.19)$$

Indeed, figure 3.11 represents the dependence of cos δ on the coordinate ρ, for a given value of the angle ψ. It is shown that the angle δ reaches its maximum value for the maximum value of ρ, that is $\rho = R(\psi)$. Applying the definition (3.13) of $R(\psi)$ in the expression (3.18) gives :

$$(\cos\delta)_{min} = \cos\omega \qquad (3.20)$$

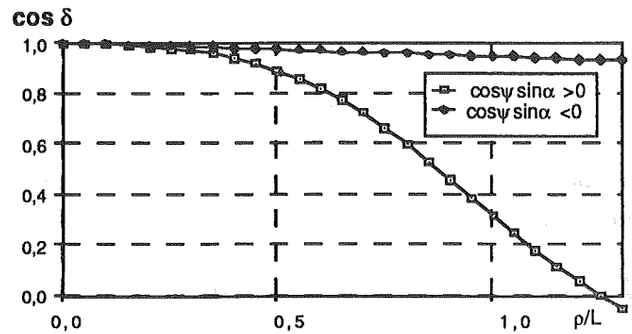

Figure 3.11 : Cosinus of the angle δ (see text) as a function of the polar coordinates (ρ,ψ) of the point P belonging to the sample

It must be remembered that the angle ω is determined by the circular aperture of a diaphragm, placed between the slit of the monochromator and the sample. An approximate value for ω is given by the following (see figure 3.8) :

$$\text{tg}\ \omega = \frac{\text{diaphragm radius}}{\text{distance diaphragm-slit}} = \frac{1.25\ \text{cm}}{30\ \text{cm}} \quad \Rightarrow\ \omega = 2.4° \qquad (3.21)$$

Note : if the size of the slit is taken into account, about 0.5° must be added to this value (cfr.§3.2.4).

3.2.6. Uncertainty on the angle of incidence

The description of figure 3.8 is recalled in figure 3.12, which also includes the light source S.

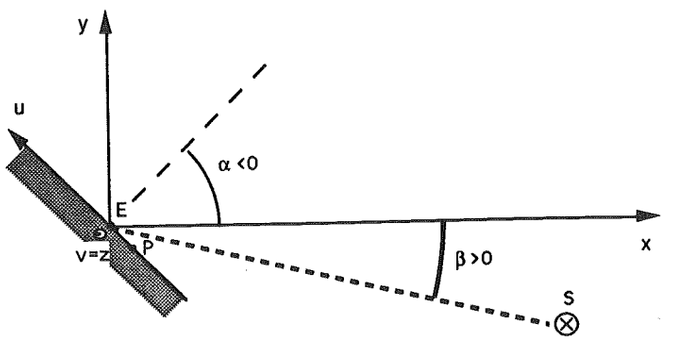

Figure 3.12 : Plane view of the source, the sample and the axis system

We must now calculate the angle $\tau \geq 0$ between the principal direction of incidence $\vec{SE}$ and any direction of incidence $\vec{SP}$, with P belonging to the visible surface S_E :

$$\vec{SP} = (u \sin\alpha - D \cos\beta \, , \, u \cos\alpha + D \sin\beta \, , \, v)$$

$$\vec{SE} = (- D \cos\beta \, , \, D \sin\beta \, , \, 0)$$

$$\cos\tau = \frac{\vec{SP}.\vec{SE}}{|\vec{SP}| \; D} = \frac{D + u \sin(\beta-\alpha)}{\sqrt{D^2 + 2\,u\,D \sin(\beta-\alpha) + u^2 + v^2}} \qquad (3.22)$$

It is remembered that D is the distance between the source S and the point E on the sample.

The minimum value of this function for P(u,v) belonging to the visible surface S_E can be calculated, which gives[6] :

$$0 \leq \tau \leq 5.3° \qquad (3.23)$$

[6] The upper bound of (3.23) corresponds to the worse situation when there is no lens between the light source and the sample. Indeed, it can be understood that a converging lens reduces the divergence of the incident light bundle.

Detailed calculations are presented in appendix 3.1.

3.3. Description of the equipment

It was first intended to measure the spectral radiance factor and to analyse the influence of the wavelength on the reflection properties of a material. Therefore, the detector must be a spectrophotometer, i.e. a monochromator followed by a photomultiplier and a measuring instrument. We used the spectrophotometer Zeiss PMQII, equipped with the monochromator M4QIII.

The light source is an incandescent lamp (Philips "cinema",110V, 500W, E27, TYP-375E). It is supplied with stabilized 220V, followed by a 220V/110V transformer . The stabilization guarantees the constancy of the luminous intensity I, emitted by the source in the direction of the sample (see eq. 3.17). The power supply of the source itself can be adjusted by a potentiometer, between 0 and 110V.

Such a powerful source is necessary, since the minimum luminous intensity required to carry out the spectral measurements is high. Indeed, the radiant fluxes measured by the spectrophotometer in narrow wavelength bands (5nm) are very weak. This requires a high amplification of the photoelectric current. However, a too high electric amplification leads to the instability of the measured value [34]. So, it is interesting to provide enough light from the source in order to keep the measured flux within reasonable limits.

A plano-convex lens can be added to the lamp, in order to enhance its luminous intensity in the direction of the sample, and also to enhance the parallelism of the incident light rays. However, this last property of the lens is difficult to obtain, because the light source is not punctual. Its dimensions cannot be neglected, if they are compared with the focal distance of the lens (9 cm, aperture 6 cm).

The lens is also interesting, since it reduces the unwanted radiations created by the light reflections on objects situated in the vicinity of the sample : see figure 3.13.

It must finally be mentioned that the measurements are carried out in a dark room, again to reduce the influence of unwanted radiations.

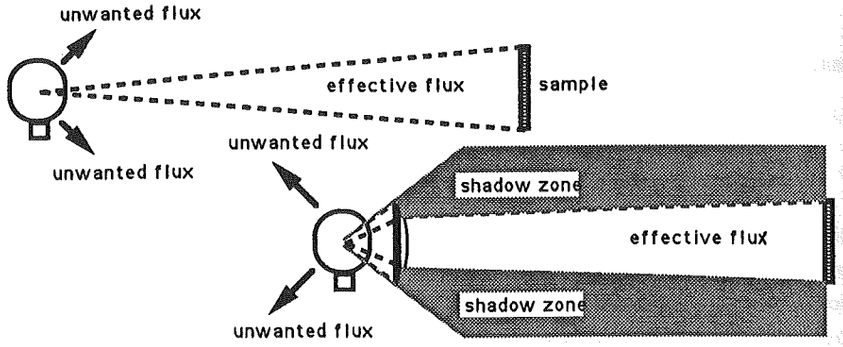

Figure 3.13 : Comparison of the incident light beam without and with lens.

The figure 3.14 shows the arrangement of the measuring apparatus. The viewing direction has been fixed, since the detector (R) is composed of a heavy and clumsy equipment. On the contrary, the sample (E) and the source (S) can be rotated around the same vertical axis passing through point E.

The light source (S) and its lens (L) are located at the end of a rotating arm of 1.47 m (fig.3.15). The rotation of this arm around the vertical axis passing through E is represented by the angle β which can be practically adjusted between 5 and 180 degrees.

The sample is fixed on a carriage of the optical bench, at the same height than the source, that is 1.295 m above the floor (height of the filament). The bench is associated with the viewing direction. Therefore, the surface of the sample is vertical and the plane of incidence is horizontal.

The luminous radiation reflected by the sample in the horizontal direction parallel to the optical bench is deviated at right angle by a mirror M (6 cm X 4 cm) and sent to the monochromator R.

This compact arrangement allows the operator to easily access the sample and the measuring display of the spectrophotometer (fig. 3.14), without making useless movements. The operator is also able to move around the sample without influencing the measured radiation.

The circular aperture of the diaphragm D (diameter 25 mm) is placed in the path of the light rays and limits the reflected light bundle analysed by the monochromator. The rotation of the sample around the vertical axis in E is represented by the angle α. The area of the sample viewed by the monochromator through the aperture D is circular and centered in E, if the sample is perpendicular to the optical bench ($\alpha = 0$ in figure 3.14). If $\alpha \neq 0$, this area becomes nearly

elliptical (see equation 3.13), the more stretched as $|\alpha|$ grows. This is illustrated by the picture 3.3, which is obtained by lighting the exit slit of the monochromator and, so, forcing the light rays to follow the opposite path, from the detector R to the sample E.

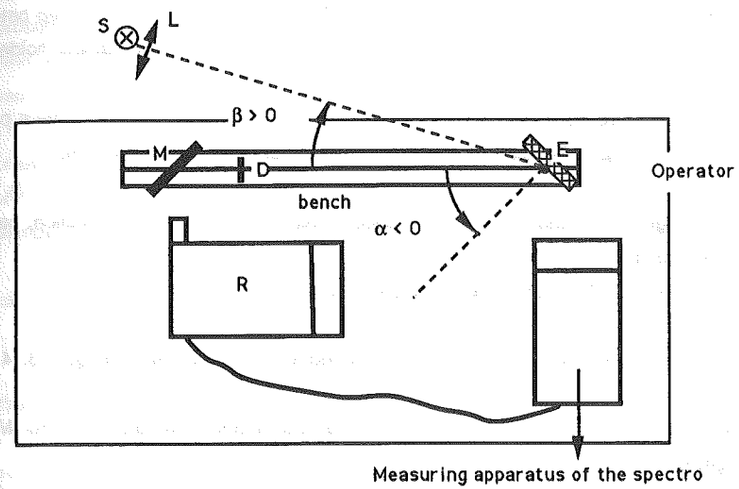

Figure 3.14 : Arrangement of the measuring instruments : plane view

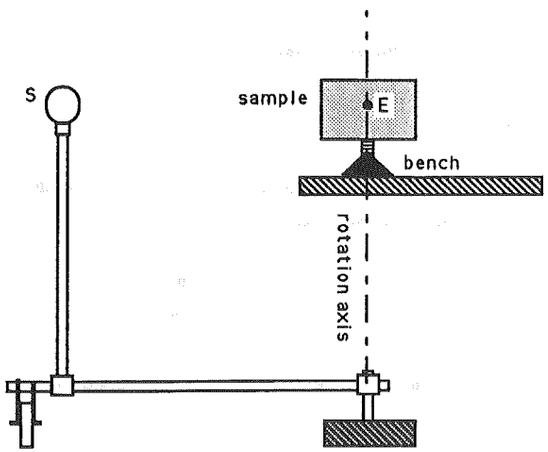

Figure 3.15 : Illustration of the source S on its rotating arm and of the sample on its carriage.

The distance between the diaphragm D and the entrance slit of the monochromator (passing through the mirror) is approximately 30 cm. Therefore, the length of the light path between the sample and the entrance slit was comprised between 92 and 99 cm during the experiments.

A pointer attached to the sample holder directly indicates the value of the angle α on a protractor. To measure the angle β, several discrete locations of the rotating arm (every 10° step between β =10° and β =160°) have been marked on the floor, using a mirror on the sample holder [21].

Several adjustments were necessary before starting the measurements. The adjustment procedure is detailed in reference [21]. To sum up, the two following operations must be done :

- to guide the light beam analysed by the monochromator in an horizontal direction, parallel to the optical bench;
- to adjust the zero position for the α and β graduations.

It is also noted that some opaque screens must be added to the arrangement of figure 3.14, in order to :

- avoid the direct illumination of the entrance slit of the monochromator, the mirror M or the diaphragm D.
- reduce the unwanted radiations reaching the surfaces located around the sample : such surfaces are the monochromator box and the measuring instrument of the spectrophotometer.

3.4. Determination of the luminance factor[7]

3.4.1. Substitution method

A reference sample with known luminance factor is used in the same conditions as the tested sample (same angles $\hat{\imath}$ and $\hat{o}$). It follows, from (3.14), that :

$$\bar{\beta}_e(\hat{o}\ ,\ \hat{\imath}) = \beta_{e,ref}(\hat{o}\ ,\ \hat{\imath})\ \frac{\Phi}{\Phi_{ref}} \qquad (3.24)$$

The quotient of both readings, multiplied by the reference luminance factor, gives $\bar{\beta}_e$.

[7] More precisely, we should talk about the spectral radiance factor, since the detector is a spectrophotometer. The reader can easily distinguish both quantities by the context. See also footnotes 2 and 5 of this chapter.

advantages :

- the illuminance of the sample must not be uniform;
- the abolute value of the luminance factor $\bar{\beta}_e$ is derived;

drawbacks :

- the procedure is too tedious : indeed, to insure the stability of the light source and the detector, both measurements of Φ and Φ_{ref} must be made within a short interval of time. So, for each configuration ($\hat{o}$,$\hat{\imath}$), substitution of both samples would be necessary;
- but, most of all, this procedure requires a reference sample for which the luminance factor $\beta_{e,ref}(\hat{o},\hat{\imath})$ is known, for each angle of incidence $\hat{\imath}$, each angle of viewing $\hat{o}$, and each wavelength if the measurements are to be carried out in the spectral domain.

Since such a reference sample is not available, the following method has been preferred.

3.4.2. Relative method of comparison

The reference is here the luminance factor of the tested sample itself, at specific values of the angles of viewing and incidence, respectively $\hat{o}_{ref}$ and $\hat{\imath}_{ref}$.

The measured flux has been expressed as (3.17) :

$$\Phi \propto \bar{\beta}_e(\hat{o}\ ,\ \hat{\imath})\ \cos\hat{\imath}$$

$$\Phi_{ref} \propto \bar{\beta}_e(\hat{o}_{ref}\ ,\ \hat{\imath}_{ref})\ \cos\hat{\imath}_{ref}$$

$$\bar{\beta}_e(\hat{o}\ ,\ \hat{\imath}) = \bar{\beta}_e(\hat{o}_{ref}\ ,\ \hat{\imath}_{ref})\ \frac{\cos\hat{\imath}_{ref}}{\cos\hat{\imath}}\left(\frac{\Phi}{\Phi_{ref}}\right) \qquad (3.25)$$

The value of the luminance factor is again obtained with two flux measurements (Φ and Φ_{ref}). The relative distribution of the luminance factor is now determined in the plane of incidence. This distribution is relative because the factor $\bar{\beta}_e(\hat{o}_{ref}\ ,\ \hat{\imath}_{ref})$ is of course unknown. However, this factor can be measured by the comparison with a reference sample, in one of the standard geometrical configurations described in figure 3.3. For example, the configuration $\hat{\imath}_{ref}$ = 45° and $\hat{o}_{ref}$ = 0° can be chosen.

Another requirement is that the illuminance of the sample has to be uniformly distributed on its surface, if the expression of the flux (3.17) is to be used.

Moreover, the proportional relation (3.25) is valid if the light source intensity (I) is kept constant during the procedure, a condition which is not rigorously met in practice. This is also true for the detector stability. Therefore, it is preferable to write the following expression, where "K" is the "stability factor" :

$$\bar{\beta}_e(\hat{o}\ ,\ \hat{i}) = K\ \bar{\beta}_e(\hat{o}_{ref}\ ,\ \hat{i}_{ref})\ \frac{\cos \hat{i}_{ref}}{\cos \hat{i}} \left(\frac{\Phi}{\Phi_{ref}}\right) \qquad (3.26)$$

The error of taking K=1 will be analysed later.

3.4.3. Summary of the formulated hypothesis

1) It is assumed that the contribution of every point of the visible surface S_E to the total flux entering the slit of the monochromator can be expressed by the equation (3.5).

2) The luminance factor is approximately constant in the vicinity of the given viewing direction and of the specified direction of incidence. The angular interval to be considered is 2.4 degrees around the viewing direction and less than 5.3 degrees around the direction of incidence. Moreover, the sample must be quite homogeneous, meaning that $\bar{\beta}_e$ is approximately constant on its surface.

3) The sample is uniformly illuminated for the relative method of comparison.

4) The light source and the photoelectric detector are stable during all the measurement procedure corresponding to the method of comparison.

3.4.4. Measurement procedure in practice

•) starting configuration parameters : these are the electric power supply of the source (V), the wavelength adjusted at the monochromator and the width of the entrance slit. In most situations, the entrance slit is fixed at 0.15mm. Therefore, the resulting bandwiths are the following : 3 nm at 400 nm, 6 nm at 500 nm, 10 nm at 600 nm and 14 nm at 700 nm [34].

•) adjusting the value 100% of the flux on the measuring apparatus : this value corresponds to a given reference position of the source and the detector;

•) placing the light source at the desired location : the angle β (figure 3.14) is fixed between 10° and 150°, by 10° steps;

•) orienting the sample: at each angle β , the value of the reflected flux is determined (in percents), for the angle α varying between -70° and +70°, by 10° steps. Remember that this angle is limited, by the condition that the visible surface must be kept included in the real surface of the sample;

•) if an absolute measurement is wanted, the factor $\bar{\beta}_e(\hat{o}_{ref}\ ,\ \hat{i}_{ref})$ must be determined (see 3.25);

•) end of measurement.

The lower and upper bounds of the angle α must now be precised, for a given value of the angle β. First, the incident light should always come from the same side of the normal. This is illustrated in figure 3.12 : it has been decided that the light should always come from the negative values of "u", which implies that $\beta \geq \alpha$.

Moreover, the light source must always illuminate the same face of the sample, which leads to $(\beta - \alpha) < 90°$. So, the lower and upper bounds for the angle α are :

$$\beta - 80° \leq \alpha \leq \min(\beta, 70°)$$

$$10° \leq \beta \leq 150° \qquad (3.27)$$

The figure 3.16 illustratres the domain of the possible values of the viewing angle ô (also noted θ_r at the beginning of this chapter) and incidence angle î (= θ_i). Respecting the sign conventions introduced in figures 3.5 and 3.12, the following relations have been applied to derive fig. 3.16 :

$$\hat{o} = \theta_r = \alpha$$

$$\hat{i} = \theta_i = \beta - \alpha \qquad (3.28)$$

The hatched domain corresponds in practice to the configurations where the sample is obscured by the detector. Within the greyish zone, the luminance factor is obtained by applying the Helmholtz principle of reciprocity:

$$\bar{\beta}_e(\hat{o} = \theta_r, \hat{i} = \theta_i) = \bar{\beta}_e(\hat{o} = -\theta_i, \hat{i} = -\theta_r) \qquad (3.29)$$

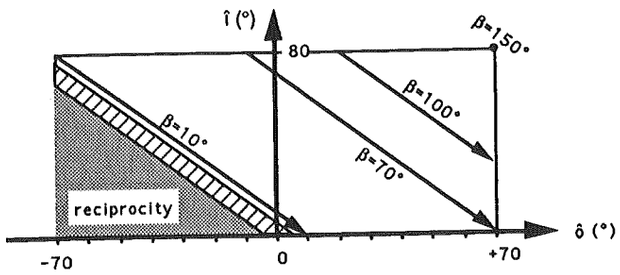

Figure 3.16 : Domain of the possible values of the viewing angle ô and the angle of incidence î (degrees) in the plane of incidence (see text).

3.4.5. Application : measurement of a sample of agglomerated wood panel

The sample has the following dimensions : 25.3 cm X 19 cm. Its spectral radiance factor has been determined by the procedure described above. The results at five wavelengths are illustrated in figure 3.17.

For an angle of incidence of 10°, it can be seen that the measured spectral radiance factor is approximately constant at all viewing angles (deviation : ± 20% at 450 nm and ± 10% at 650 nm). However, a specular behaviour clearly appears for an angle of incidence of 80°.

Under 10° incidence, the relative spectral distribution of the radiance factor $\bar{\beta}_e$ is approximately the same at all viewing angles. This is illustrated in table 3.1, where the arbitrary value 100 has been attributed to the radiance factor $\bar{\beta}_e$ at 550 nm. So, the hue and saturation of the material colour do not depend on the viewing direction, since both colour attributes are related to the relative spectrum of the reflected light. However, the luminance, which represents the third dimension of colour, is somewhat greater at positive viewing angles (forward scattering) than at negative angles.

Figure 3.17 : Spectral radiance factor $\bar{\beta}_e$ (%) of a sample of agglomerated wood, as a function of the viewing angle ô (in degrees). The relative intensity ($I = \bar{\beta}_e \cos\hat{o}$) is represented on the right. The curves correspond to measurements at the following wavelengths : 450 nm (–––), 500 nm (---), 550 nm (– · – · –), 600 nm (·····), 650 nm (–––).

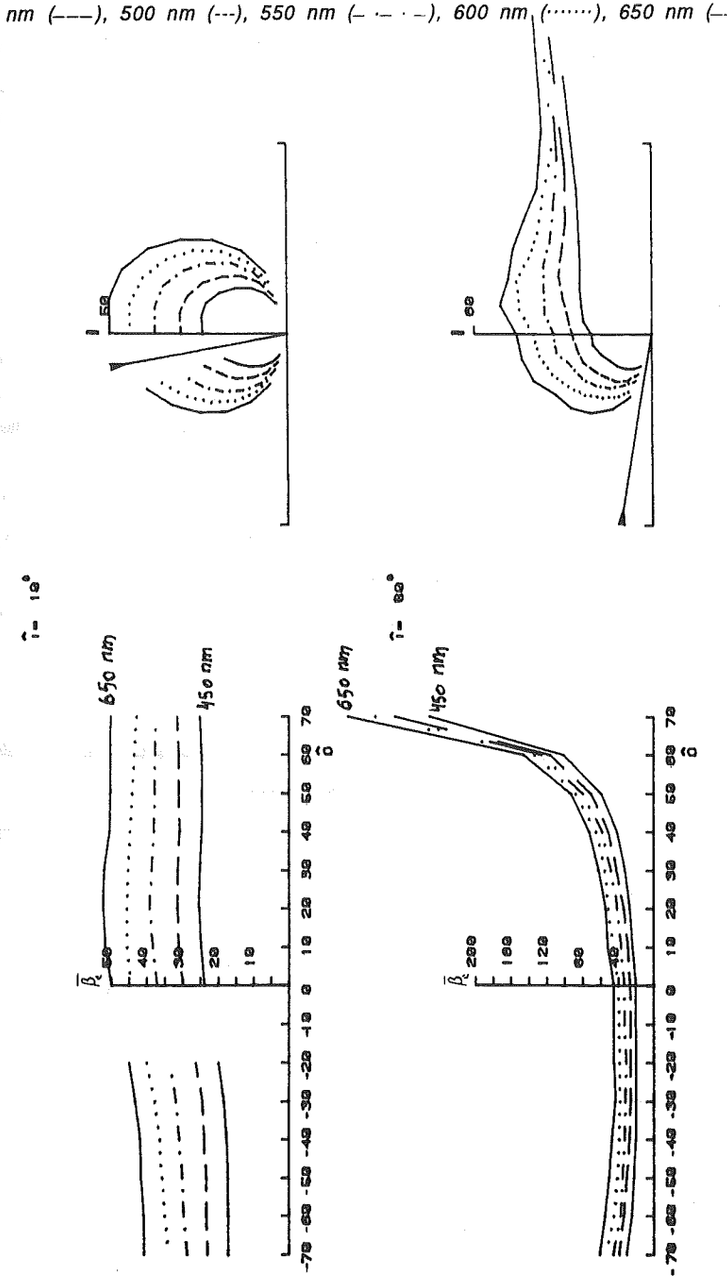

Table 3.1 : Relative spectral radiance factor, measured for the sample of agglomerated wood ; incidence 10 degrees

ô (degrees)	wavelength λ(nm) 450	500	550	600	650
-70	60	80	100	118	142
-40	57	78	100	118	136
0	64	80	100	119	134
+10	65	81	100	119	134
+40	65	81	100	117	133
+70	68	85	100	115	134

Under 80° incidence, a strong tendency to the equalization of the reflection spectrum clearly appears in the specular direction (see ô=70° in table 3.2). Indeed, the surface reflection predominates in this case. So, the reflection tends to be achromatic for a non-metallic material.

Note : the reference value which has been used to transform relative measurements into absolute measurements (see. § 3.4.2) is the spectral radiance factor $\beta_{e,d/0}(\lambda)$. This factor has been determined in a previous study [20] with the apparatus RA3 of the Zeiss spectrophotometer [34], by comparison with a white reference sample of diffuse reflection (Zeiss n°20011).

Table 3.2 : Relative spectral radiance factor, measured for the sample of agglomerated wood ; incidence 80 degrees

ô (degrees)	wavelength λ(nm) 450	500	550	600	650
-70	67	84	100	118	133
-40	61	83	100	118	143
0	62	81	100	120	137
+30	67	86	100	113	128
+50	74	88	100	110	117
+70	84	97	100	104	114

3.4.6. Influence of the lens

Two measurements have been performed on the same sample of agglomerated wood : the first measurement with a lens placed in front of the source, and the second measurement without lens. The relative deviations between the results of both measurements hardly exceed 2 percents. It is shown in reference [21] that the deviations greater than 2 percents are probably due to unwanted radiations, which are significant in the measurements without lens (reflections on the surfaces located around the sample).

Note : The lens must be so oriented that the sample (or, at least, its visible surface) is illuminated as uniformly as possible.

3.4.7. Influence of the polarization of the detected light

The monochromator can introduce an influence of the polarization of the detected light on the measurement results. This influence can be comprised between 10 and 40 percents [17,30]. Of course, the light emitted by the incandescent lamp in our apparatus is not significantly polarized. But, polarization may appear after "surface" reflection (see figure 2.4). Therefore, the polarization state of the reflected light will depend on the angles of incidence and viewing. As a consequence, the total transmittance of the monochromator will also depend on both angles.

In order to analyse this influence of polarization, a polarization filter (fig. 3.18) has been introduced in the detected light beam, after reflection on the wood sample. The filter is perpendicular to the analysed light rays. The monochromator is tuned on the wavelength 600 nm.

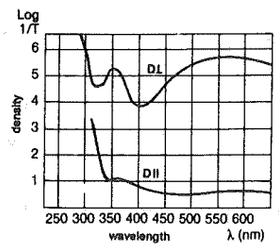

Polarization Filter Type 10 K **03 6320**
Suitable for Stress/Strain Optics, for laboratory and/or teaching purposes.
Middle range transmission for white light ≈ 33%.
Total transmission for 2 filters with axes of polarization parallel > 20%.
Total transmission for 2 filters with axes of polarization perpendicular, 0.002%.
Damping power: less than 1:10,000.
Polarization, more than 99.99%.
Thermal Load max. ≈ 70°C at continuous service.
Polarization axis is marked at the rim.
Mounted in rotational holder with scale in 1° divisions, Ø 78 mm aperture.

Figure 3.18 : Polarization filter used for the test.

The measured fluxes corresponding to β=110° and several polarization filter orientations are presented in table 3.3. The amplification of the spectrophotometer is kept constant for all measurements[8]. The polarization filter is circular and can be rotated in its plane, around the optical axis. Its orientation is indicated by the angle δ , between a reference direction drawn on the filter and the direction perpendicular to the plane of incidence (fig. 3.19).

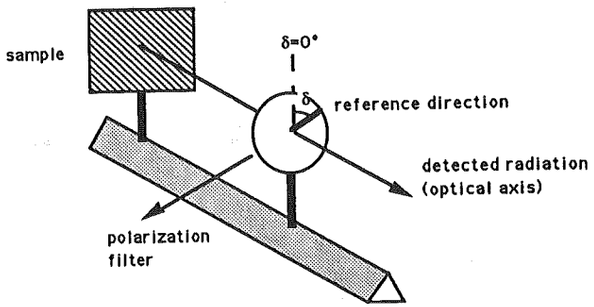

Figure 3.19 : Definition of the angle δ describing the orientation of the polarization filter.

Table 3.3 : Relative values of flux reflected by the agglomerated wood sample (β=110°), for several viewing angles α and several orientations of the polarization filter. The angle δ is defined in the text.

Filter orientation δ (degrees)	Viewing angle α (degrees) 70	60	50	40	30
0	100	95	71	43	20
45	137	154	111	56	25
90	127	137	98	52	23
135	97	90	67	42	20
225	137	152	108	56	25
270	124	134	97	52	24
315	97	88	66	41	20
WITHOUT FILTER	117	121	87	49	22

[8]Except for the results obtained "without filter", for which the relative values have been adjusted to match the average flux, calculated for all filter orientations, and corresponding to α=30° and 40°. Indeed, it is at these angles that the influence of polarization must be minimum.

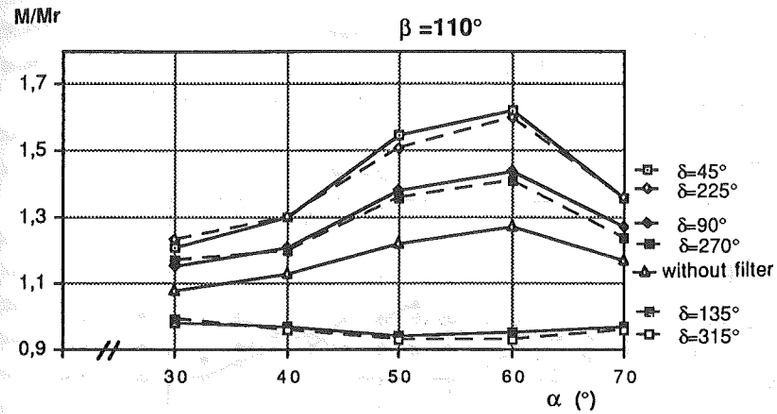

Figure 3.20 : Ratio between the flux M reflected by the sample and measured with polarization filter, and the reference flux M_r, corresponding to an orientation of the filter δ=0° (all other parameters of the measurement being the same).

The ratios between the detected fluxes and their reference flux, corresponding to an orientation of the polarization filter δ=0°, are shown in figure 3.20. The following observations can be made :

- the influence of the polarization filter orientation on the measured flux can be significant : deviations up to 50% are observed in the detected flux values, for a given value of the viewing angle α;
- this influence is particularly important between 50° and 60° (β=110°) : these geometrical conditions correspond to the direction of specular reflection;
- two symmetrical orientations of the polarization filter (δ shifted by 180°) lead approximately to the same results. The small differences can be attributed to the measurements errors;
- the measurement results obtained "without filter" are very close to the average value of two fluxes, measured for two filter orientations shifted by 90° from one another.

This last observation is very important. Indeed, it is known that the average value obtained for two perpendicular directions of vibration gives the luminance factor for natural incident light [19,30]. In the above example, this means that the measurements executed "without filter" can approximate this luminance factor with an error less than 5%. The maximum deviation is obtained in the direction of specular reflection, where the influence of polarization is the most significant.

At non-grazing incidences, the surface reflection of the agglomerated wood sample is weaker and the influence of polarization vanishes (fig. 3.21, β=10°) : in this figure, it is seen that the deviations induced by the orientation of the polarization filter are less than 3%.

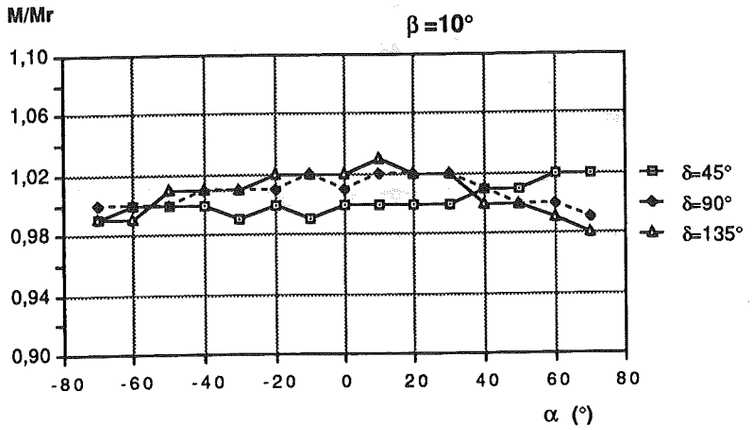

Figure 3.21: Ratio between the flux M reflected by the sample and measured with polarization filter, and the reference flux M_r, corresponding to an orientation of the filter δ=0° (all other parameters of the measurement being the same).

Comment : these arguments are based on flux measurements. However, the equation (3.26) shows that the luminance factor is proportional to the quotient of two detected fluxes, namely the one corresponding to the given angles of incidence and viewing, and a reference flux. It would be wise to define this reference flux for incidence and viewing directions not corresponding to specular reflection, in order to avoid polarization influence on this reference value. Once this decision has been adopted, the above arguments directly apply to the luminance factor measurements.

3.4.8. Measurements errors

The main sources of errors are the following :

•) lamp and detector instabilities

The lamp must reach its stable working conditions. Then, it has been observed that the luminous intensity slightly fluctuates (±0.5)% during a complete measurement of all reflected fluxes in the plane of incidence. In the same manner, the instability of the spectrophotometer can be expressed by an uncertainty of 0.5%. Better results are obtained if the detector is periodically calibrated during a complete measurement of the diffusion indicatrix.

It is concluded that the total instability error (lamp+detector) is about 1% on the measurement of flux.

•) error due to unwanted radiations

If the incident light beam is focused by a lens during the measurements, the unwanted radiations (reflections,...) have a negligible influence (< 0.5% detected for 100% incident light, α=0°, λ=550nm, entrance slit= 0.15mm). Without lens, their influence becomes significant, even if screening is used outside the optical axis : up to 3% are detected for 100% incident light in α=0°. Light reflections on the walls and the light grey floor of the dark chamber are amplified with an unfocused light beam and are mainly responsible for this error.

•) polarization errors

About 1% for most measurement configurations. This error can reach 5% in the specular viewing direction, when the surface reflection contribution is significant. This is particularly the case at grazing incidences, i.e. for β > 110° (see §3.4.7).

The polarization errors can be avoided by taking two measurements at each angle of incidence and each angle of viewing : these two measurements must be performed with a polarization filter oriented in two perpendicular directions of polarization. However, this increases the duration of the total measurement procedure.

•) reading errors[9] on the angles α and β

Assume that the graduation 0° has been accurately determined on each angular scale.

The value of the angle α is read with an uncertainty of about 0.2°. This implies a relative error on the measured flux comprised between 0.3% and 1%, for the wood sample and β=10°. The greatest errors (1%) are observed for the less significant values of flux, corresponding to a "negative" (backward) grazing viewing direction which is close to the direction of incidence.

For β = 110°, this error can reach 3%, if the angle of incidence is greater than 60°, and 4% if β =140°.

---

[9] These errors must be distinguished from the uncertainties on the angles δ and $\hat{\imath}$ (§3.2.5 and 3.2.6) .

The angular graduation for β has been built from the graduation for α, replacing the sample by a plane mirror [21]. So, the above-mentioned errors must be doubled to take into account the uncertainty on the angle β.

To sum up, the uncertainty on the readings of α and β leads to errors of about 0.6% on the measured flux, if the angle of incidence is less than 60°. Otherwise, the same error can reach 2% outside the specular viewing direction, and 8% in the vicinity of this direction[10]. Of course, these conclusions depend on the type of material analysed , and particularly on its specular behaviour.

Therefore, the measurement procedure proposed here is not convenient for the determination of the regular reflection, but well for the mixed luminous reflection.

•) spectrophotometer error

Only few information on this error can be obtained from the constructor of the PMQII [34]. An error of about 0.3% is mentioned for a transmission measurement. Moreover, errors due to stray light inside the monochromator are less than 0.2%. An error of 0.5% has been adopted here (the polarization errors are not included in this contribution : see above).

In conclusion, the total uncertainty on the measured flux is less than 2.6%, if the angle of incidence is less than 60°. Otherwise, this error can reach 14% in the specular direction of viewing.

We can now evaluate the maximum error on the luminance (radiance) factor. First remember its expression (3.26) :

$$\bar{\beta}_e(\hat{o} , \hat{i}) = K \; \bar{\beta}_e(\hat{o}_{ref} , \hat{i}_{ref}) \; \frac{\cos \hat{i}_{ref}}{\cos \hat{i}} \left(\frac{\Phi}{\Phi_{ref}}\right)$$

$$K \approx 1 \qquad (3.26)$$

The uncertainty on the angle of incidence $\hat{i} = \beta - \alpha$ (eq. 3.28) is about 0.4° (0.2° on α and β). This leads to an error on the factor $\left(\frac{1}{\cos \hat{i}}\right)$ of 0% in $\hat{i}$=0 , 1% in $\hat{i}$=60° and 4% in $\hat{i}$=80°.

[10] These evaluations have been confirmed by the analysis of the reproducibility of the measured values on the agglomerated wood sample [21].

Therefore, the following estimations are obtained, by adding the instabilities errors (1% on K), the error on $\left(\frac{1}{\cos \hat{i}}\right)$ and the errors on the fluxes Φ and Φ_{ref} (2.6% because $\hat{i}$<60°) [11] :

7% for $\hat{i} < 60°$
10% for $\hat{i} \geq 60°$, outside the specular direction
20% for $\hat{i} \geq 60°$, in the specular direction

These are of course upper bounds for the measurement errors, which are hardly encountered in practical situations. However, they clearly point out the interest of measuring the angles as accurately as possible.

3.5. Measurements with a luminancemeter

3.51. Principle of the measurement

In figure 3.14, the spectrophotometer is replaced by a luminancemeter which is situated directly along the axis of the optical bench (no deviation of the reflected light beam by a mirror in this case). The luminancemeter is a Photo Research Spectra Spotmeter 1500-01.

The measurement with the luminancemeter, equipped with a photopic V(λ) filter, gives the distribution of the luminance L(ô,î). The light intensity emitted by the source is again kept constant. This luminance represents in fact the mean value taken on the visible surface S_E of the sample, which is seen through the optical aperture of the apparatus (1°). As the illuminance of the sample is proportional to the cosine of the angle of incidence î, an expression similar to (3.17) is obtained :

$$L(\hat{o},\hat{i}) \; + \; \bar{\beta}_v(\hat{o} , \hat{i}) \cos \hat{i} \qquad (3.30)$$

The measurement of a reference value $\bar{\beta}_v(\hat{o}_{ref} , \hat{i}_{ref})$ is necessary to determine the proportion factor in (3.30), which gives :

$$\bar{\beta}_v(\hat{o} , \hat{i}) = \bar{\beta}_v(\hat{o}_{ref} , \hat{i}_{ref}) \; \frac{\cos \hat{i}_{ref}}{\cos \hat{i}} \left(\frac{L(\hat{o},\hat{i})}{L_{ref}}\right) \qquad (3.31)$$

[11] The uncertainty on $\left(\bar{\beta}_e(\hat{o}_{ref} , \hat{i}_{ref}) \cos \hat{i}_{ref}\right)$ should also be added : it depends on the measuring instrument used to determine this value.

The determination of $\bar{\beta}_V(\hat{o}_{ref}, \hat{i}_{ref})$ is carried out by an illuminance measurement $E(\hat{i}_{ref})$ in the reference direction of incidence $\hat{i}_{ref}$ (the illuminance meter is a "Spectra® Photometer /Radiometer, Model 301"). So, (3.31) becomes :

$$\bar{\beta}_V(\hat{o}, \hat{i}) = \pi \frac{\cos \hat{i}_{ref}}{\cos \hat{i}} \left(\frac{L(\hat{o},\hat{i})}{E(\hat{i}_{ref})} \right) \qquad (3.32)$$

The uncertainty on the viewing angle is now ω=1° (instead of 2.4° in § 3.2.5) and the uncertainty on the incidence angle is only 2°, instead of 5.3° (Appendix 3.1).

The following amendments must be made to the study of § 3.4.8 , concerning the measurement errors :

- the detector is not influenced by the polarization of the incident light [32];
- the accuracy of the illuminance measurement influences the error on the luminance factor (see eq. 3.32);
- the most important errors coming from the angular readings are unchanged.

3.5.2. Application : measurement on a tunnel wall sample

This measurement has been undertaken within the activities of the C.I.E. Technical Committee TC 4-24. It should be examined if a keramics wall tile could be considered as a uniform diffusor, verifying the Lambert law, or not.

The keramics sample is not a favourable one for our measurement procedure, since it already shows a specular behaviour from an angle of incidence of 20°.

The measurement results in the plane of incidence are presented in figure 3.22. A (nearly) lambertian behaviour (constant luminance factor) is observed outside an angular zone of about 20° around the specular direction. Within this zone, the luminance factor reaches very high values. However, two additional deviations from the Lambert law can be found :

- firstly, the mean luminance factor in the "diffuse" zone decreases at grazing incidences. It is nearly constant until an incidence of 60° ($\bar{\beta}_V \approx 0.75$), and then continuously decreases until ($\bar{\beta}_V \approx 0.6$) at 80°;

- secondly, if the angle of incidence is kept constant, the luminance factor decreases at grazing viewing directions.

Both phenomena are furthermore bound by the Helmholtz principle of reciprocity.

It is therefore not accurate to simply modelize this keramics sample by a uniform diffusor outside the specular zone of reflection. This problem will be analysed more intensively in the next chapter. In particular, it will be seen that the increase of the surface reflection intensities at grazing incidences implies an attenuation of the light "re-emitted" by the bulk heterogeneities of the material.

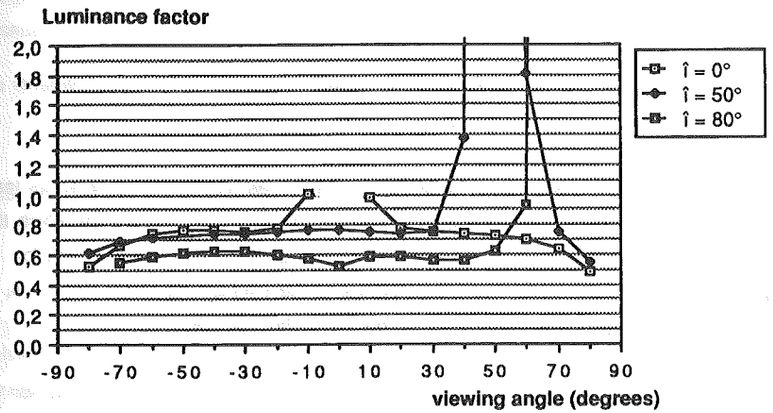

Figure 3.22 : Luminance factor of a tunnel wall keramics. The measurement results are presented here for three angles of incidence : î= 0°, 50° et 80°.

The measurements performed on this keramics sample can inform us about the reproducibility of the results obtained. In the following are compared two luminance factors measurements of the same surface aimed on the sample, the second measurement being operated four hours after the first one. The deviations observed between both measurements only come from the instability of the light source and from the angular errors (see § 3.4.8).

Outside the specular viewing direction, the mean deviation between both measurements is 1.8% for an angle of incidence $\hat{i}$ = 0° and 4.3% for $\hat{i}$ = 80° : see figure 3.23.

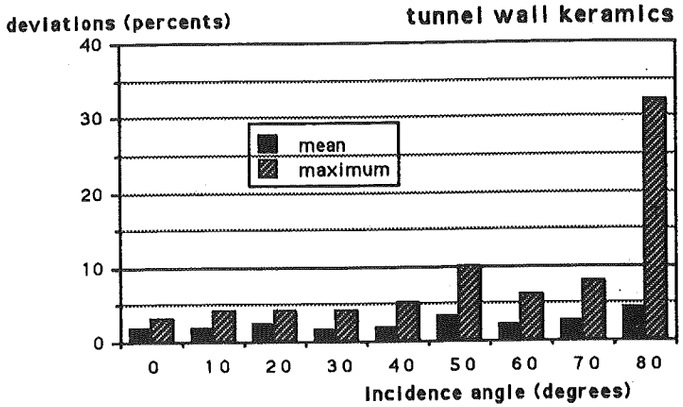

Figure 3.23 : Relative deviations observed between two luminance factor measurements of the same keramics sample.

This observation confirms the conclusion of § 3.4.8 which states that the angular errors tend to increase with the angle of incidence. Besides the configuration (î=80°, δ=70°) for which the deviation is 32%, all other deviations are less than 10%. They are even less than 5% for incidences up to 40° (see fig. 3.23) : this corresponds to the estimations given in § 3.4.8, if we take into account the unfavourable character of this particular sample.

This unfavourable character is also illustrated by the deviations observed in the specular direction, which are comprised between 5% and 18%. Remember that these deviations are mainly due to the steep gradient of the luminance factor and its significant influence on the angular errors.

Another measurement has been performed to test the influence of the situation of the surface aimed on the sample. The mean deviations then rise to 3% (for î=0°) and 6.5% (î=80°), outside the specular direction. If these values are compared with those illustrated in figure 3.23 (from 1.8% to 4.3%), it is concluded that a difference of about 2% can be attributed to the non-uniformity of the surface of the sample.

Appendix 3.1. Uncertainty on the angle of incidence

The minimum of the following function must be found (see eq. 3.22) :

$$\cos\tau = \frac{D + u\sin(\beta-\alpha)}{\sqrt{D^2 + 2uD\sin(\beta-\alpha) + u^2 + v^2}} \qquad (3.A1)$$

among all points P(u,v) belonging to the visible surface S_E of the sample, which is seen through the slit of the monochromator.

If u is kept constant, ($\cos\tau$) is minimum for the maximum value of v (cfr. 3.A1), i.e. for the point P situated at the periphery of the surface S_E :

$$\cos\tau \geq \frac{D + u\sin(\beta-\alpha)}{\sqrt{D^2 + 2uD\sin(\beta-\alpha) + R^2(\psi)}} \qquad (3.A2)$$

$R(\psi)$ must then be expressed as a function of u. Equation (3.13) gives :

$$u = R(\psi)\cos\psi = \frac{L\,tg\,\omega}{\sin\alpha\,tg\,\omega \pm \sqrt{\cos^2\alpha + tg^2\psi}} \qquad (3.A3)$$

The positive sign (just before the square root) corresponds to ($\cos\psi > 0$), whereas the negative sign corresponds to ($\cos\psi < 0$). Applying (3.A3) gives:

$$\pm u\sqrt{\cos^2\alpha + tg^2\psi} = L\,tg\,\omega - u\sin\alpha\,tg\,\omega$$

$$\cos^2\psi = \frac{1}{1 + tg^2\psi} = \frac{1}{1 + \frac{tg^2\omega\,(L - u\sin\alpha)^2}{u^2} - \cos^2\alpha}$$

$$R^2(\psi) = \frac{u^2}{\cos^2\psi} = u^2\sin^2\alpha + tg^2\omega\,(L - u\sin\alpha)^2 \qquad (3.A4)$$

Applying (3.A4) in (3.A2) leads to a function of one variable (u). The roots of the first derivative are given by :

$$u\left(D\left(\sin^2(\beta-\alpha) - \sin^2\alpha\right) - \sin\alpha\,tg^2\omega\,(L\sin(\beta-\alpha) + D\sin\alpha)\right)$$

$$+ L\,tg^2\omega\,(L\sin(\beta-\alpha) + D\sin\alpha) = 0 \qquad (3.A5)$$

If the factor of u (within brackets) is positive, the minimum value of (cos τ) corresponds to the solution of (3.A 5). Otherwise, the minimum of (cos τ) is, either in $\left(u=R_{\psi=0}\right)$, or in $\left(u=-R_{\psi=\pi}\right)$.

With D = 1.5m, L = 1m and ω = 2.4° (see §3.3), we have :

$(\cos\tau)_{min}$ = 0.996 , i.e. τ_{max} = **5.3°**, for α=70° and β=80°, if $|\alpha| \leq 70°$;
$(\cos\tau)_{min}$ = 0.978 , i.e. τ_{max} = **12.2°**, for α=80° and β=90°, if $|\alpha| \leq 80°$.

The aperture angle ω is 1° instead 2.4° in the case of a luminancemeter (see §3.5). So, the minimum values become :

$(\cos\tau)_{min}$ = 0.999 , i.e. τ_{max} = **2.0°**, for α=70° and β=70°, if $|\alpha| \leq 70°$;
$(\cos\tau)_{min}$ = 0.997 , i.e. τ_{max} = **4.3°**, for α=80° and β=80°, if $|\alpha| \leq 80°$.

Appendix 3.2. Measurement results for several material samples

These measurements have been performed with the luminancemeter as detector. The results are presented below as luminance factor relative values (in comparison with the luminance factor $\beta_{v,40/0}$, corresponding to the angle of incidence "inc"=40° and to the angle of viewing "obs"=0°). The reference value for this factor has been fixed arbitrarily to $\beta_{v,40/0}$ = 100.

The absolute value of the luminance factor $\beta_{v,40/0}$ has been indicated within the caption of each table.

An exception is the keramics sample, for which the absolute luminance factors are directly given, in percents. Moreover, the angle of viewing is extended up to 80° for this sample.

The symbols " ***** " indicate that the measurement is not possible in this configuration of source and receptor : this is the case in the direction of retroreflection, or when the luminance of the image source in the specular direction is too high.

Table 3.A.1 :

Plywood sample. The reference value 100 corresponds to $\beta_{v,40/0}$ =0.391.

LUMINANCE FACTOR

obs/inc	0	10	20	30	40	50	60	70	80
-70.0	98.1	93.1	90.1	90.3	92.7	97.2	106.0*******		138.1
-60.0	99.6	92.6	88.7	90.0	91.1	94.7*******		106.0	117.7
-50.0	98.9	92.3	89.7	89.2	90.9*******		94.7	97.2	107.1
-40.0	100.0	95.1	90.4	90.4*******		90.9	91.1	92.7	100.7
-30.0	105.4	97.0	93.9*******		90.4	89.2	90.0	90.3	96.9
-20.0	112.4	105.3*******		93.9	90.4	89.7	88.7	90.1	96.3
-10.0	128.3*******		105.3	97.0	95.1	92.3	92.6	93.1	96.3
.0	*******	128.3	112.4	105.4	100.0	98.9	99.6	98.1	100.7
10.0	122.3	136.1	127.0	116.1	111.3	109.9	108.2	106.9	114.3
20.0	107.4	122.3	137.6	133.9	127.8	124.4	123.1	125.0	131.3
30.0	100.7	109.8	128.8	151.4	150.2	146.1	149.3	149.0	150.0
40.0	94.4	104.7	120.8	144.6	173.5	179.8	180.7	181.0	186.4
50.0	92.7	102.4	118.0	139.8	171.9	218.7	224.8	233.1	245.9
60.0	91.8	101.5	117.0	137.0	171.2	220.9	305.0	332.9	375.5
70.0	91.0	100.7	113.7	136.4	169.6	219.6	321.3	569.9	744.9

Table 3.A.2 :

White sheet of paper on agglomerated wood. The reference value 100 corresponds to $\beta_{v,40/0}$ =0.887.

LUMINANCE FACTOR

obs/inc	0	10	20	30	40	50	60	70	80
-70.0	93.9	93.8	92.6	91.4	92.2	93.1	93.3*******		101.9
-60.0	97.4	95.9	93.7	94.5	93.3	92.7*******		93.3	98.7
-50.0	99.4	96.6	97.0	94.1	94.1*******		92.7	93.1	95.8
-40.0	100.0	99.3	96.9	96.6*******		94.1	93.3	92.2	93.9
-30.0	104.3	101.6	99.7*******		96.6	94.1	94.5	91.4	94.9
-20.0	106.3	103.7*******		99.7	96.9	97.0	93.7	92.6	90.2
-10.0	108.9*******		103.7	101.6	99.3	96.6	95.9	93.8	91.9
.0	*******	108.9	106.3	104.3	100.0	99.4	97.4	93.9	88.4
10.0	109.1	111.9	110.2	105.2	104.5	103.1	99.0	96.1	104.2
20.0	105.4	110.8	111.9	111.9	109.7	106.4	103.3	109.2	107.9
30.0	102.8	103.5	111.9	117.1	115.2	113.8	117.8	117.8	119.4
40.0	97.5	103.0	108.8	114.7	125.5	132.3	131.5	134.1	139.0
50.0	96.4	101.1	104.6	113.2	131.0	151.6	159.0	165.3	182.7
60.0	94.3	96.6	102.9	115.3	129.7	158.6	209.7	244.8	291.3
70.0	89.5	93.9	101.5	111.6	129.7	161.5	241.4	447.2	698.2

Table 3.A.3 :

Opaline glass sample. The reference value 100 corresponds to $\beta_{v,40/0}$ =0.415.

LUMINANCE FACTOR

obs/inc	0	10	20	30	40	50	60	70	80
-70.0	85.6	90.8	89.0	83.8	89.0	89.4	86.4*******		58.2
-60.0	99.2	96.8	95.3	96.6	98.7	97.8*******		86.4	64.0
-50.0	100.6	98.4	99.7	100.9	101.5*******		97.8	89.4	68.8
-40.0	100.0	100.1	101.0	101.8*******		101.5	98.7	89.0	62.3
-30.0	100.4	101.0	102.1*******		101.8	100.9	96.6	83.8	67.8
-20.0	101.8	101.5*******		102.1	101.0	99.7	95.3	89.0	69.2
-10.0	102.7*******		101.5	101.0	100.1	98.4	96.8	90.8	61.0
.0*******		102.7	101.8	100.4	100.0	100.6	99.2	85.6	66.8
10.0	103.0*******		101.7	101.6	102.3	102.7	95.5	89.4	59.9
20.0	102.2	101.9*******		104.0	104.5	102.0	99.4	86.3	64.4
30.0	101.3	102.5	104.4*******		104.9	105.3	98.1	90.8	66.4
40.0	102.5	103.2	105.0	105.2*******		103.9	102.8	92.3	68.8
50.0	101.8	102.7	103.0	105.6	105.2*******		105.4	94.4	70.2
60.0	99.8	99.2	100.8	101.3	104.3	106.4*******		97.6	74.0
70.0	91.0	91.4	92.0	94.2	96.5	98.0	99.0*******		59.9

Table 3.A.4 :

Opaline plastic sample. The reference value 100 corresponds to $\beta_{v,40/0}$ =0.519.

LUMINANCE FACTOR

obs/inc	0	10	20	30	40	50	60	70	80
-70.0	85.8	90.9	86.2	82.6	91.6	90.9	96.1*******		69.5
-60.0	98.2	95.0	93.2	98.0	100.3	103.9*******		96.1	68.6
-50.0	99.2	97.6	101.1	103.4	107.3*******		103.9	90.9	73.3
-40.0	100.0	102.3	103.9	106.7*******		107.3	100.3	91.6	59.4
-30.0	104.1	104.3	106.5*******		106.7	103.4	98.0	82.6	64.0
-20.0	109.3	108.3*******		106.5	103.9	101.1	93.2	86.2	71.4
-10.0	118.2*******		108.3	104.3	102.3	97.6	95.0	90.9	60.0
.0*******		118.2	109.3	104.1	100.0	99.2	98.2	85.8	62.1
10.0	125.3*******		114.3	103.9	102.2	102.4	95.4	86.4	53.7
20.0	111.7	126.3*******		113.7	108.1	103.3	98.1	82.8	59.7
30.0	105.5	109.6	127.3*******		114.9	106.0	97.1	87.2	61.3
40.0	101.8	104.8	110.8	129.5*******		114.2	104.6	89.0	62.7
50.0	100.8	102.4	105.8	113.2	150.1*******		119.9	99.2	64.0
60.0	98.5	99.0	100.8	104.3	115.4	162.7*******		149.3	91.7
70.0	89.5	89.9	90.4	93.0	97.7	111.6	204.5*******		141.4

Table 3.A.5 :

White panel of laminated wood. The reference value 100 corresponds to $\beta_{v,40/0}$ =0.934.

LUMINANCE FACTOR

obs/inc	0	10	20	30	40	50	60	70	80
-70.0	84.1	88.7	86.5	89.1	89.5	91.1	90.1*******		79.0
-60.0	93.8	92.8	93.3	93.3	96.0	97.4*******		90.1	85.1
-50.0	95.7	95.0	95.3	98.2	98.9*******		97.4	91.1	80.1
-40.0	100.0	97.3	99.4	100.9*******		98.9	96.0	89.5	78.1
-30.0	106.4	102.4	101.7*******		100.9	98.2	93.3	89.1	76.9
-20.0	119.5	110.2*******		101.7	99.4	95.3	93.3	86.5	80.3
-10.0	131.9*******		110.2	102.4	97.3	95.0	92.8	88.7	71.5
.0*******		131.9	119.5	106.4	100.0	95.7	93.8	84.1	70.8
10.0	132.6	137.0	130.9	118.3	108.4	100.0	90.0	84.5	67.6
20.0	118.5	131.4	139.7	135.7	120.9	105.3	95.6	84.4	62.8
30.0	106.8	119.1	137.0	148.4	142.7	127.4	107.0	89.0	79.9
40.0	100.2	108.4	123.1	147.1	168.4	166.5	145.9	126.1	94.4
50.0	96.3	98.9	109.7	133.6	177.3	222.3	245.1	236.7	204.1
60.0	91.9	93.1	97.6	117.2	166.3	255.4	439.5	641.8	546.5
70.0	86.4	86.6	89.1	99.5	133.4	275.3	675.5	2460.4	2080.6

Table 3.A.6 :

White wall pavement. The reference value 100 corresponds to $\beta_{v,40/0}$ =0.790.

LUMINANCE FACTOR

obs/inc	0	10	20	30	40	50	60	70	80
-70.0	81.5	86.6	85.7	82.8	85.3	85.7	89.5*******		67.9
-60.0	94.9	93.7	92.6	96.0	96.3	98.6*******		89.5	60.4
-50.0	97.5	97.5	99.1	99.7	103.5*******		98.6	85.7	60.4
-40.0	100.0	100.8	100.9	104.3*******		103.5	96.3	85.3	57.9
-30.0	101.2	101.4	105.4*******		104.3	99.7	96.0	82.8	62.9
-20.0	102.3	105.4*******		105.4	100.9	99.1	92.6	85.7	64.6
-10.0	106.5*******		105.4	101.4	100.8	97.5	93.7	86.6	61.2
.0*******		106.5	102.3	101.2	100.0	97.5	94.9	81.5	60.4
10.0	108.1*******		102.3	100.9	99.6	98.6	91.4	84.9	52.1
20.0	103.8	103.3*******		101.1	100.4	97.0	94.0	81.9	57.9
30.0	102.6	102.5	102.5*******		99.6	97.7	92.6	81.5	54.6
40.0	102.6	101.0	100.8	101.1*******		96.4	91.4	80.7	58.8
50.0	100.5	99.4	99.4	98.6	97.9*******		92.3	80.7	57.1
60.0	96.7	96.0	95.1	94.1	94.6	94.6*******		82.8	56.3
70.0	88.0	86.8	85.8	86.3	85.9	85.6	88.5*******		50.5

Table 3.A.7 :

Concrete block. The reference value 100 corresponds to $\beta_{v,40/0}$ =0.285.

LUMINANCE FACTOR

obs/inc	0	10	20	30	40	50	60	70	80
-70.0	99.8	107.0	114.4	123.0	132.7	148.7	179.0*******		262.8
-60.0	100.0	104.9	110.7	116.3	128.5	144.7*******		179.0	195.7
-50.0	100.3	103.3	107.0	114.2	126.4*******		144.7	148.7	163.8
-40.0	100.0	103.1	107.1	116.4*******		126.4	128.5	132.7	150.5
-30.0	100.1	103.5	110.3*******		116.4	114.2	116.3	123.0	134.6
-20.0	102.0	107.1*******		110.3	107.1	107.0	110.7	114.4	121.3
-10.0	105.8*******		107.1	103.5	103.1	103.3	104.9	107.0	113.6
.0*******		105.8	102.0	100.1	100.0	100.3	100.0	99.8	102.2
10.0	105.0	100.8	98.6	97.7	97.3	95.9	96.6	94.3	107.2
20.0	100.9	98.4	96.9	96.0	94.1	94.2	91.9	95.9	105.8
30.0	98.6	96.5	95.1	92.9	93.1	90.3	91.1	94.7	104.5
40.0	98.3	95.6	93.1	92.1	90.3	90.5	91.7	96.4	108.1
50.0	98.2	93.7	91.0	90.2	89.3	91.8	94.0	100.8	118.6
60.0	96.6	93.3	92.1	89.8	91.1	92.1	99.0	111.6	140.5
70.0	97.8	94.9	91.4	91.7	93.3	98.6	108.4	132.7	195.3

Table 3.A.8 :

Tunnel wall keramics. The luminance factor is directly indicated in percents.

LUMINANCE FACTOR

obs/inc	0	10	20	30	40	50	60	70	80
-80.0	51.6	57.3	59.3	62.5	62.6	60.8	58.5	55.0*******	
-70.0	66.7	68.4	71.2	70.6	70.6	68.3	66.9*******		55.0
-60.0	73.3	74.1	74.1	74.0	72.8	71.9*******		66.9	58.5
-50.0	75.8	75.8	75.1	74.5	73.8*******		71.9	68.3	60.8
-40.0	76.7	75.0	75.3	74.4*******		73.8	72.8	70.6	62.6
-30.0	75.6	75.6	74.1*******		74.4	74.5	74.0	70.6	62.5
-20.0	77.6	74.6*******		74.1	75.3	75.1	74.1	71.2	59.3
-10.0	100.1*******		74.6	75.6	75.0	75.8	74.1	68.4	57.3
.0*******		100.1	77.6	75.6	76.7	75.8	73.3	66.7	51.6
10.0	98.3	718.0	109.7	78.6	76.4	75.1	71.7	64.7	59.1
20.0	77.2	98.8	789.5	110.8	77.2	74.5	70.5	68.9	58.0
30.0	75.5	77.3	102.1	939.6	111.6	75.5	74.0	68.7	56.3
40.0	74.4	74.7	77.6	113.3	1258.2	137.8	78.0	69.5	56.6
50.0	72.7	74.0	73.6	75.9	117.6	2301.6	179.7	79.1	63.0
60.0	70.7	69.6	69.9	72.1	76.1	180.4	5600.0	354.3	92.5
70.0	63.5	63.6	64.1	64.8	66.7	74.8	304.62	0610.0	1648.8
80.0	48.3	47.9	48.4	49.3	50.6	55.3	80.0	729.67	1410.0

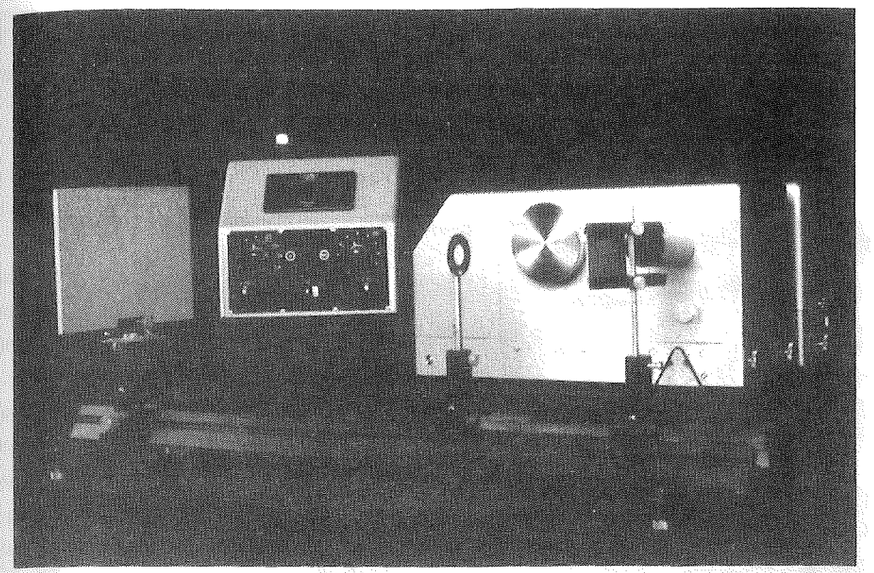

Picture 3.1 : View of the experimental equipment set up to measure the luminance factor. From left to right : the sample on its carriage, the measuring apparatus of the spectro and the monochromator. In the foreground are the diaphragm and the deviation mirror. (picture by G. VERDIN).

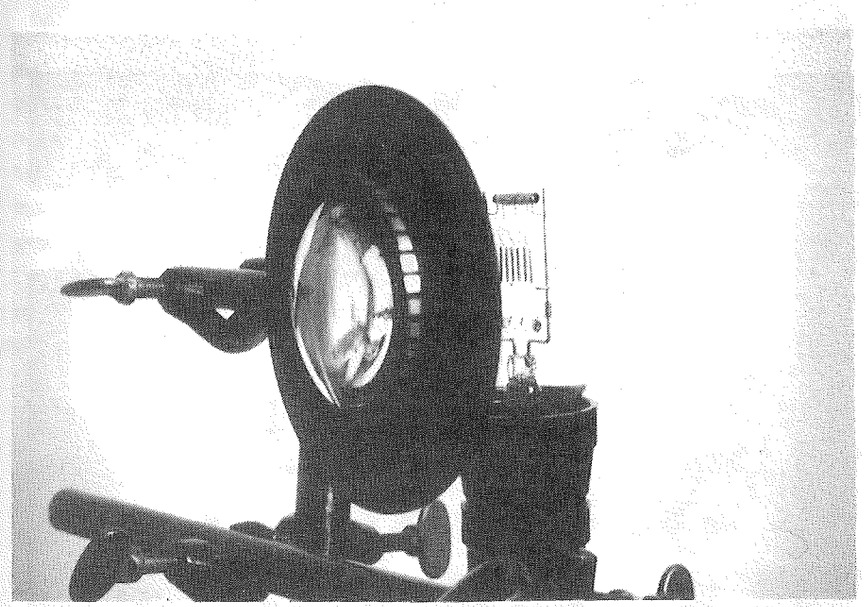

Picture 3.2 : Light source and converging lens (picture by G. VERDIN).

Pictures 3.3.

Visible surface of the sample, obtained by illuminating the exit slit of the monochromator :
top : this surface is circular for $\alpha=0°$;
below : it is nearly elliptical for $\alpha=70°$.
(pictures by G. VERDIN)

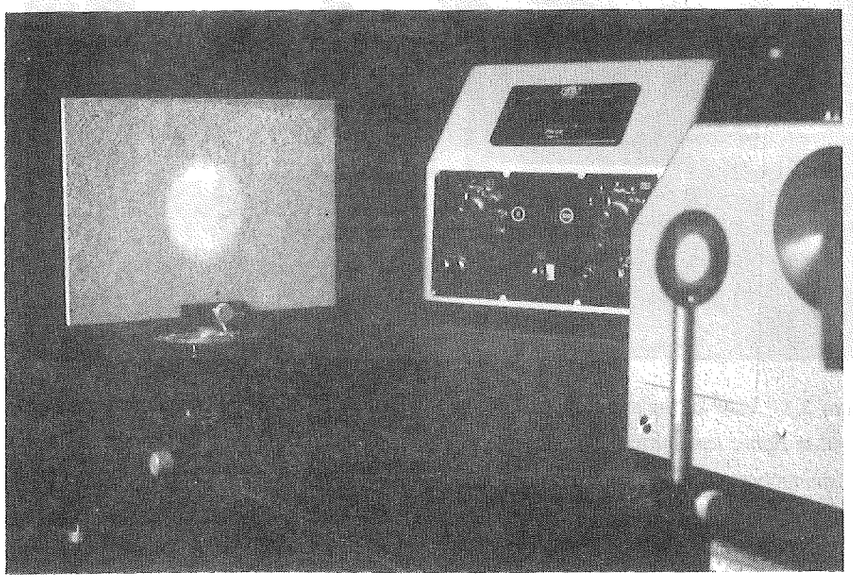

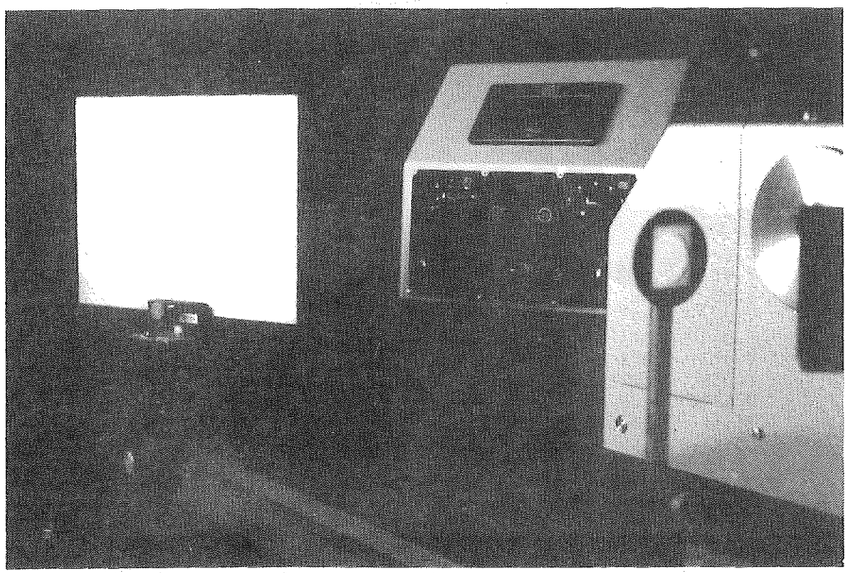

Chapter 4 : Modelization of light reflection

4.1. Introduction

The analysis performed in the second chapter and the first measurements results described in the third chapter have shown that the Lambert model of diffuse reflection is not sufficient to correctly represent the behaviour of most materials encountered in Interior Lighting situations.

The fact that this model is still widely used today in calculation methods can be explained by its very simple formulation. Now, some new calculation techniques can take into account non-lambertian diffusion indicatrices. But this possibility is still underestimated, because there exists no general model for light reflection. So, it is now time for lighting engineers to develop and test reflection models which are closer to the real behaviour of materials.

In this chapter, it is intended to derive a macroscopic model for light reflection, taking into account the following requirements :

- to give the intensity reflected by a material, for all directions of incidence and viewing;
- this model should be sufficiently general, and its applications should not be limited to some particular surfaces : for example, to slightly rough surfaces, for which the mean amplitude of the corrugations is lower than the wavelength;
- the model should only contain a small number of parameters to represent a given sample of material;
- finally, it should not be too intricate, in order to allow fast calculations by computer. Indeed, the determination of the luminous field in a complex situation can require many repeated evaluations of the model.

The problem of light reflection by a rough surface will be first analysed. Volume scattering will be treated in a subsequent section.

4.2. Scattering by a rough surface

4.2.1. Overview

The scattering[1] of electromagnetic waves by rough surfaces has been analysed in three main directions.

Firstly, through the small perturbation method (S.P.M.), also referred as the Rayleigh-Fano theory. This method assumes that the scattered electomagnetic fields can be expressed as power series of the surface corrugations. These series are limited to the first, second or even fourth order [35,55,56,59]. The phase of the electromagnetic fields can also be expressed as power series : this method belongs to the phase perturbation techniques [41,42]. In practice, their application is limited to the slightly rough surfaces.

The perturbation theory has been widely used to analyse the scattering of luminous or X-ray waves by multi-layered dielectric mirrors, with slightly rough interfaces. Vector theories has been developed [2,43,44,45,49]. Some of them were able to derive the scattered energy in all viewing directions, but the amplitude of the corrugations was always supposed to be lower than the incident wavelength. This condition is difficult to meet when X-rays are considered : so, Vidal and Vincent [65] proposed a new vector theory which is also valid for very rough surfaces, but which has only been developed in the specular direction.

Secondly, the solution of the generalized telegraphists' equations [36,37] has led to the so-called "full wave solution". The boundary conditions on the rough surface are expressed without any approximation, such that they can lead to general solutions. However, their formulation contains power series of the wavelength and it is generally too intricate for our purpose.

Finally, a third approach is the Kirchhoff approximation [38,50] which uses particular boundary conditions. It is assumed here that the rough surface can be locally replaced (at each point) by the local tangent plane. Therefore, this method is theoretically limited to surfaces for which the local radius of curvature is greater than the wavelength.

This last approach will be used in this chapter. Perturbation methods are too restrictive in their applications, whereas full wave solutions are too complex. Moreover, the Kirchhoff approximation has already been developed, mainly for one-dimensional surfaces, by Beckmann [38] who already found very interesting results. This method will be hereafter reformulated, including a vector

[1] In french, the term " **diffusion**" has been used in the original text

representation : this will allow us to take into account the reflection coefficients at each point of the surface.

Two other experimental approaches can also be found in the litterature. The first one is the model of reflection described by Hori et al [47], which was intended to represent surface reflection by the materials used in luminaire reflector design :

$$I_r(\theta) = I_r(\theta_s)\,(1 - \sin X)^{\alpha} \qquad (4.1)$$

$I_r(\theta_s)$ is the intensity of light reflected in the specular direction, "X" is a linear expression of θ and non-linear expression of θ_s , whereas "α" is the "specularity factor", depending on the surface roughness. However, how this model has been established is not clearly formulated.

The second one is based on an empirical equation (type Pearson V) and was proposed by Moon and Spencer [53,54] :

$$\xi = A\,x^{-p}\,e^{-\gamma/x} \qquad (4.2)$$

where ξ is the quotient of the radiance of the sample in the viewing direction θ to the intensity of the incident light (W/m^2). The quantities ($x=90°-\theta$) and (A,p,γ) are experimental parameters. The three last ones are determined by fitting the model with the diffusion indicatrices measured in the plane of incidence. The model has been particularly tested with slightly rough metallic surfaces. It is also able to take into account an "off-specular" reflection peak, which can be observed under some well-defined conditions.

4.2.2. Expression of the electromagnetic field scattered by a rough surface

The model of light reflection which is proposed in this chapter is based on a fundamental research carried out by P. Beckmann [38]. Some refinements will be necessary, concerning for example the preliminary assumptions or the introduction of the local reflection properties of the surface. Indeed, Beckmann has developed his theory for perfectly conducting surfaces, which allowed him to consider only a scalar electromagnetic field. We rather propose here a vector formulation which will be more adapted to describe non-conducting surfaces, and we will also extent the theory to the photometric quantities which are more common in lighting science.

So, both formulations (the scalar and vectorial ones) will obviously present common features. The option has been taken to reproduce Beckmann's developments where they will be necessary to the general understanding of the present formulation.

Let a volume V be bound by the closed surface S. E is a scalar function which satisfies the wave equation[2] :

$$\nabla^2 E + k^2 E = 0 \qquad (4.3)$$

Let **M** be a given point[3] somewhere in the volume and G, the Green function of any other point **M'** :

$$G(M') = \frac{e^{jkr}}{r} \qquad (4.4)$$

where r is the distance between the points **M** and **M'**. The Green function also satisfies the equation (4.3), except if **M'≡M**.

The Helmholtz integral theorem [38] states that the function E at **M** can be derived from the values of E and its first derivatives on the closed surface S :

$$E(M) = \frac{1}{4\pi} \iint_S \left[E \frac{\partial G}{\partial n} - G \frac{\partial E}{\partial n}\right] dS \qquad (4.5)$$

where the symbol $\frac{\partial}{\partial n}$ represents the derivative along the normal directed towards the interior of the surface S in dS.

Obviously, E could be one of the three components of the electric vector of the electromagnetic field. In figure 4.1, the rough surface is illuminated by the incident plane wave $\vec{E}_1$. The reference volume V (belonging to the propagating medium) is bounded by the infinite sphere Σ , by the rough surface S^+ illuminated by the incident radiation and by the reverse side S^- which is not directly illuminated.

Applying the Helmholtz-integral theorem (4.5) leads to a surface integral on the sphere Σ which gives the incident electromagnetic field at **M**, a surface integral on S^+ which gives the scattered

---

2 "k" is the wave number.

3 A great number of symbols will be used throughout this section. Bold characters will represent points in the three-dimensional space.

field, and a third surface integral on S^- which vanishes, since the electromagnetic field and its derivatives are supposed to be negligible in this shadow zone. The scattered electric vector is finally obtained :

$$\vec{E}_s(M) = \frac{1}{4\pi} \iint_{S^+} \left[\vec{E} \frac{\partial G}{\partial n} - G \frac{\partial \vec{E}}{\partial n}\right] dS \qquad (4.6)$$

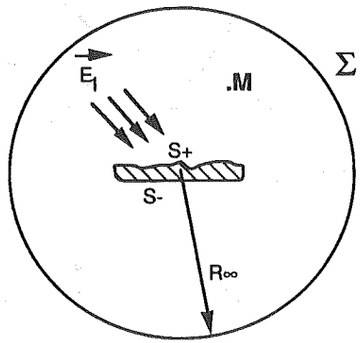

Figure 4.1: Incident plane wave $\vec{E}_1$ on a rough surface and application of the Helmholtz-integral theorem : see text.

This last expression is not exact in a theoretical sense, since the assumption of the vanishing field on S^- is only an approximation. Furthermore, this assumption implies that the electric field $\vec{E}$ is not continuous on the whole surface S, a condition which would be required to apply the equation (4.5). Therefore, the electromagnetic field described by (4.6) does not satisfy the Maxwell equations. The exact solution can be found in Thourel [62] or in De Broglie [40] : it is referred as the Kottler's formula. Two extra terms are added to the expression (4.6), but it is shown that these terms become negligible if the point **M** is sufficiently far away from the surface [4].

The figure 4.2 shows a rectangular rough surface extending from (x=-X) to (x=+X) and (y=-Y) to (y=+Y). The roughness amplitude is described by the function z= ξ(x,y). The altitude z=0 has been attributed to the mean amplitude of the corrugations.

The medium below the surface is homogeneous.

---

4 This condition is always relative to the wavelength, which is about one micron for light waves. Therefore, this condition is not restrictive in Lighting Science.

Consider a monochromatic plane wave incident upon the surface. The direction of propagation $\vec{k_1}$ lies in the plane of incidence XZ and is characterized by the angle θ_1 between $\vec{k_1}$ and the vector $\vec{1}_z$, which is perpendicular to the mean plane of the corrugations.

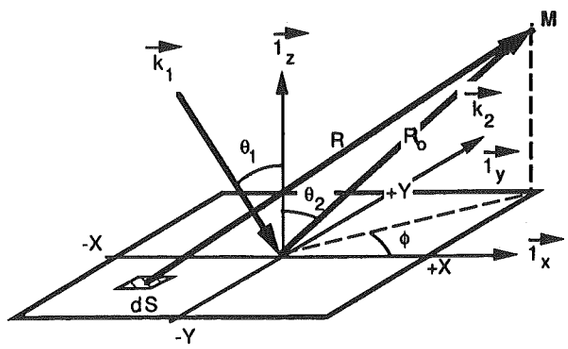

Figure 4.2 : Geometrical parameters describing the rough surface scattering (the symbols are defined in the text).

The incident electric vector $\vec{E_1}$ lies in a plane perpendicular to $\vec{k_1}$. It is parallel to the polarization vector $\vec{P}$ which is described below :

$$\vec{k_1} = k\,[\sin\theta_1\ ,\ 0\ ,\ -\cos\theta_1\ ]$$

$$\vec{P} = [\ A^+ \cos\theta_1,\ A^-\ ,\ A^+ \sin\theta_1\ ]$$

$$\vec{E_1}(\vec{r}) = \vec{P}\ e^{\,j(\vec{k_1}.\vec{r}\ -\ \omega t)}$$

$$\vec{r} = [\ x, y, z\ ] \qquad \text{and} \qquad k = \frac{2\pi}{\lambda} \qquad (4.7)$$

A^+ and A^- are the amplitudes of the incident electric vector, respectively in the plane of incidence and perpendicular to this plane. The radiation detector is located at distance R_o from the centre of the surface, in the scattering direction $\vec{k_2}$ defined by the angles θ_2 and ϕ.

To calculate the Helmholtz integral (4.6), the field $\vec{E}$ and its first derivatives must be determined on the rough surface. With the Kirchhoff approximation , it is assumed that the field and its derivatives are given by their value which would be obtained if the surface was replaced by the local tangent plane. This assumption is only valid, if the local radius of curvature of the surface's corrugations are much greater than the wavelength.

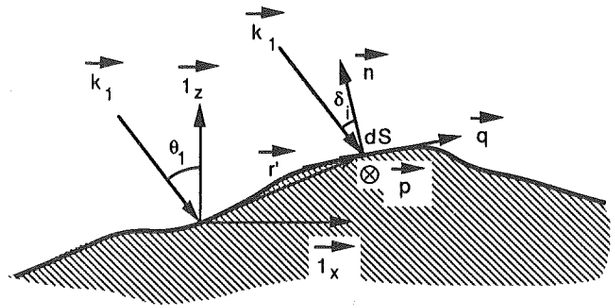

Figure 4.3 : Local axis system ($\vec{q}$, $\vec{p}$,$\vec{n}$) which has been defined to determine the electromagnetic field on the surface element dS ($\vec{r}'$).

A local axis system has been created in dS to determine $\vec{E}$ and its derivatives : see figure 4.3. Let $\vec{n}$ be the local unitary vector perpendicular to the surface element dS. The two other axis of the system ($\vec{p}$ and $\vec{q}$) are located in the tangent plane : $\vec{p}$ is parallel to[5] $\vec{n} \times \vec{k_1}$ and $\vec{q}$ is parallel to $\vec{p} \times \vec{n}$. The incident electric vector (on the surface element dS specified by the position vector $\vec{r}'$) and the specularly reflected electric vector ($\vec{E_{1s}}$) can be expressed in this local system by :

$$\vec{E_1}(\vec{r}') = e^{\,j(\vec{k_1}.\vec{r}'\ -\ \omega t)}\ [\ P_p\,\vec{p} + P_n\,\vec{n} + P_q\,\vec{q}\ ]$$

$$\vec{E_{1s}}(\vec{r}') = e^{\,j(\vec{k_1}.\vec{r}'\ -\ \omega t)}\ [\ R_s\,P_p\,\vec{p} + R_p\,(P_n\,\vec{n} - P_q\,\vec{q}\ )]$$

$$= e^{\,j(\vec{k_1}.\vec{r}'\ -\ \omega t)}\ \vec{P_s}(\vec{r}')$$

$$P_p = \vec{P}.\vec{p}\ \ ;\ P_q = \vec{P}.\vec{q}\ \ ;\ P_n = \vec{P}.\vec{n} \qquad (4.8)$$

---

[5] $\vec{p} \times \vec{n}$ represents the cross product of two vectors $\vec{p}$ and $\vec{n}$.

where R_s and R_p are the Fresnel reflection coefficients (see chapter 2) depending on the local angle of incidence $\delta_i(\vec{r}')$. The electromagnetic theory can also be applied to find the first derivative of the field $\vec{E}$ along the normal vector $\vec{n}$:

$$\frac{\partial \vec{E}}{\partial n}(\vec{r}') = j\,\vec{k_1}.\vec{n}\;\; e^{\,j(\vec{k_1}.\vec{r}' - \omega t)}\;\; [\,\vec{P} - \vec{P_s}(\vec{r}')\,] \qquad (4.9)$$

The Green function (4.4) and its derivatives along the normal vector are :

$$G(\vec{r}') = \frac{e^{jkR_o}}{R_o}\; e^{-j\vec{k_2}.\vec{r}'}$$

$$\frac{\partial G}{\partial n}(\vec{r}') = -j\,\vec{k_2}.\vec{n}\;\frac{e^{jkR_o}}{R_o}\; e^{-j\vec{k_2}.\vec{r}'} \qquad (4.10)$$

if the distance R_o between the receiving point and the surface is much greater than the wavelength. The expressions (4.8) to (4.10) can be applied to (4.6), leading to an original vectorial expression for the Helmholtz-Kirchhoff integral theorem :

$$\vec{E_s}(M) = j\,\frac{e^{j(kR_o-\omega t)}}{4\pi R_o}\int\!\!\int_S e^{\,j\vec{v}.\vec{r}'}\left((\vec{v}.\vec{n})\,\vec{P_s}(\vec{r}') - (\vec{w}.\vec{n})\,\vec{P}\right) dS$$

$$\vec{v} = \vec{k_1} - \vec{k_2} \qquad \text{and} \qquad \vec{w} = \vec{k_1} + \vec{k_2} \qquad (4.11)$$

Development for a plane finite surface

The corrugations of the surface are such that : $\xi(x,y) = 0$.

In this case, the polarization vector corresponding to the specularly reflected electric field ($\vec{P_s}$) does not depend on $\vec{r}'$:

$$\vec{P_s}(\vec{r}') = [\,-R_p A^+ \cos\theta_1,\; R_s A^-,\; R_p A^+ \sin\theta_1\,] \qquad (4.12)$$

Since the cartesian coordinates of the vector $\vec{r}'$ are [x,y,0] , the solution of the integral (4.11) gives :

$$\vec{E_s}(M) = jkS\,\frac{e^{j(kR_o-\omega t)}}{4\pi R_o}\;[\,\cos\theta_1\,(\vec{P} - \vec{P_s}) - \cos\theta_2\,(\vec{P} + \vec{P_s})\,]\;\mathrm{sinc}(v_x X)\;\mathrm{sinc}(v_y Y)$$

$$\mathrm{sinc}(x) = \frac{\sin x}{x} \qquad , v_x = \vec{v}.\vec{1}_x\,, \qquad v_y = \vec{v}.\vec{1}_y \qquad (4.13)$$

If the dimensions (X,Y) of the surface are much greater than the wavelength, then the scattered field is only significant for $v_x X = v_y Y = 0$. This condition is only fulfilled in the specular direction $\theta_1 = \theta_2$ and $\phi = 0$: it can be concluded that a plane finite surface reflects light as a mirror, if its dimensions are sufficiently great !

If the dimensions (X,Y) of the surface are of the same magnitude as the wavelength, then the electric field cannot be neglected outside the specular direction anymore. It is reflected along some lobes, determined by the maximum values of the product $\mathrm{sinc}(v_x X)\;\mathrm{sinc}(v_y Y)$.

Development for a rough surface

The coefficient of the vector $\vec{P}$ in (4.11) has been first developed in appendix 4.1, which gives :

$$\int\!\!\int_S e^{\,j\vec{v}.\vec{r}'}\,(\vec{w}.\vec{n})\,dS = -\frac{w_x}{jv_z}\int_{-Y}^{Y}\left[e^{\,j\vec{v}.\vec{r}'}\right]_{-X}^{X} dy \;-\; \frac{w_y}{jv_z}\int_{-X}^{X}\left[e^{\,j\vec{v}.\vec{r}'}\right]_{-Y}^{Y} dx \qquad (4.14)$$

It is more difficult to solve the term containing $\vec{P_s}$ in the expression (4.11), since this vector now depends on $\vec{r}'$. In order to overcome this difficulty, we can imagine the rough surface as being composed of many smaller plane facets. If the dimensions of each facet are much greater than the wavelength, then only the specularly oriented facets have a significant contribution to the scattered field in the direction (θ_2,ϕ). This assumption is only valid if the corrugations of the rough surface are not too steep, a condition which is similar to the Kirchhoff approximation (see also Bahar and Fitzwater [37]: "...in the high-frequency limit, in which the contribution to the scattered fields come primarily from the neighborhood of the specular points of the rough surface ...").

If this assumption is valid, the vector $\vec{P_s}(\vec{r}')$ can be replaced by $\vec{P_s}(\theta_1,\theta_2,\phi)$, i.e. the polarization vector corresponding to the field locally reflected by the specularly oriented facets. Doing this, an error is introduced in the less significant contributions, corresponding to the facets which are not

in the vicinity of the specular points. Finally, the following expression is obtained (see appendix 4.1 for the detailed mathematical developments) :

$$\vec{E_s}(M) = j \frac{e^{j(kR_o-\omega t)}}{4\pi R_o} \left[\vec{P_s}(\theta_1,\theta_2,\phi) \frac{\vec{v}.\vec{v}}{v_z} \int_{-X}^{X} dx \int_{-Y}^{Y} e^{j \vec{v}.\vec{r}'} dy + \vec{\varepsilon_E}(M) \right]$$

$$\vec{\varepsilon_E}(M) = \frac{w_x \vec{P} - v_x \vec{P_s}}{jv_z} \int_{-Y}^{Y} \left[e^{j \vec{v}.\vec{r}'} \right]_{-X}^{X} dy + \frac{w_y \vec{P} - v_y \vec{P_s}}{jv_z} \int_{-X}^{X} \left[e^{j \vec{v}.\vec{r}'} \right]_{-Y}^{Y} dx \qquad (4.15)$$

$\vec{\varepsilon_E}(M)$ is similar to the "edge effect", introduced by Beckmann [38] . It will be shown that this term leads to unsignificant contributions to the scattered intensity.

4.2.3. Expression of the electromagnetic intensity scattered by a rough surface

A similar development would lead to the magnetic field at point **M** :

$$\vec{H_s}(M) = j \sqrt{\frac{\varepsilon_0}{\mu_0}} \frac{e^{j(kR_o-\omega t)}}{4\pi R_o} \left[\vec{Q_s}(\theta_1,\theta_2,\phi) \frac{\vec{v}.\vec{v}}{v_z} \int_{-X}^{X} dx \int_{-Y}^{Y} e^{j \vec{v}.\vec{r}'} dy + \vec{\varepsilon_H}(M) \right]$$

$$\vec{Q} = [\, A^- \cos\theta_1,\ -A^+ ,\ A^- \sin\theta_1 \,]$$

$$\vec{Q_s}(\theta_1,\theta_2,\phi) = R_p \left(\vec{Q}.\vec{p} \right) \vec{p} + R_s \left(\left(\vec{Q}.\vec{n} \right) \vec{n} - \left(\vec{Q}.\vec{q} \right) \vec{q} \right) \qquad (4.16)$$

$\vec{Q}$ and $\vec{Q_s}$ are the polarization vectors corresponding respectively to the incident magnetic field, and to the field reflected in the direction (θ_2,ϕ) by the specularly oriented facets. The scattered intensity is defined by the Poynting vector :

$$I_s(M) = \left(\vec{E_s} \times \vec{H_s}^* \right) . \frac{\vec{k_2}}{k} \qquad (4.17)$$

Neglecting the "edge effect", it is shown in appendix 4.2 that the intensity is proportional to:

$$\vec{P_s} \times \vec{Q_s}^* = A^2 \, R^2(\theta_1,\theta_2,\phi) \, \frac{\vec{k_2}}{k}$$

$$A^2 = |A^-|^2 + |A^+|^2 \qquad (4.18)$$

N.B. : $\vec{Q_s}^*$ is the complex conjugate of $\vec{Q_s}$.

R^2 is a reflection factor depending on the direction of incidence (θ_1), on the scattering (or viewing) direction (θ_2,ϕ), on the Fresnel reflection coefficients at the specular points (R_s and R_p) and on the polarization of the incident wave (A^-, A^+). The expression of this factor has also been developed in appendix 4.2, for a scattering direction contained in the plane of incidence ($\phi=0$ or $\phi=\pi$) :

$$R^2(\theta_1,\theta_2) = \frac{|A^- R_s(\theta_1,\theta_2)|^2 + |A^+ R_p(\theta_1,\theta_2)|^2}{A^2} \qquad (4.19)$$

Neglecting again the "edge effect", we obtain from (4.15) to (4.18) :

$$I_s(M) \approx \sqrt{\frac{\varepsilon_0}{\mu_0}} \frac{1}{(4\pi R_o)^2} \left(\frac{\vec{v}.\vec{v}}{v_z} \right)^2 A^2 R^2(\theta_1,\theta_2,\phi) \int_{-X}^{X} dx \int_{-Y}^{Y} dy \int_{-X}^{X} dx' \int_{-Y}^{Y} e^{j(\vec{v}.\vec{r} - \vec{v}.\vec{r}')} dy'$$

$$\vec{r} = [x, y, \xi(x,y)] \quad \text{and} \quad \vec{r}' = [x', y', \xi(x',y')] \qquad (4.20)$$

Development for a random rough surface with normal distribution of the corrugations

The elevation of the surface $\xi(x,y)$ is a gaussian random variable, with mean 0 and variance σ^2. As $\vec{r}'$ depends on ξ, then the electric vector $\vec{E_s}(M)$ in the expression (4.15) and the scattered intensity $I_s(M)$ in (4.20) are also random variables. The coherent electric field is defined as the mean value of the electric vector at point **M**. Neglecting the "edge effect", the coherent electric field is :

$$\langle \vec{E_s}(M) \rangle = j \frac{e^{j(kR_o-\omega t)}}{4\pi R_o} \vec{P_s}(\theta_1,\theta_2,\phi) \frac{\vec{v}.\vec{v}}{v_z} \left(\int_{-X}^{X} dx \int_{-Y}^{Y} dy \; e^{j(v_x x + v_y y)} \langle e^{j v_z \xi} \rangle \right) \qquad (4.21)$$

The symbol <var> is used to represent the mean value of the random variable "var" and $<e^{jv_z\xi}>$ is defined as the characteristic function $\chi(v_z)$. It is shown that, for a gaussian (normal) distribution of the corrugations ξ :

$$\chi(v_z) = e^{-\frac{\sigma^2 v_z^2}{2}} \qquad (4.22)$$

which is introduced in (4.21), and leads to :

$$<\vec{E_s}(M)> \; + \; e^{-\frac{\sigma^2 v_z^2}{2}} \; \text{sinc}(v_x X) \quad \text{sinc}(v_y Y) \qquad (4.23)$$

The electric field is only coherent in the specular direction, for the surfaces with dimensions much greater than the wavelength. This coherence of the reflected waves in the specular direction is attenuated if the amplitude of the corrugations (σ) increases. So, for a very rough surface, the scattered electric field is totally incoherent, even in the specular direction. In other words, the phase of the electric vector has been totally randomized.

Neglecting again the "edge effects", the mean scattered intensity is proportional to :

$$<I_s(M)> \; + \; \int_{-X}^{X}\int_{-Y}^{Y}\int_{-X}^{X}\int_{-Y}^{Y} dx\,dy\,dx'\,dy' \; e^{j(v_x(x-x')+v_y(y-y'))} \; \chi_2(v_z,-v_z)$$

$$\chi_2(v_z,-v_z) \; = \; <e^{jv_z(\xi-\xi')}> \; = \; e^{-\sigma^2 v_z^2 (1-C)} \qquad (4.24)$$

To solve this quadruple integral, a more detailed description of the random rough surface is needed. In particular, the correlation coefficient "C" must be defined in equation (4.24). This coefficient expresses the dependence between the elevations ξ and ξ' , at two neighbouring points of the surface with position vectors $\vec{r}$ and $\vec{r'}$. The "horizontal" distance between them is noted "τ".

For τ=0, ξ and ξ' are of course fully correlated, and this implies C=1. However, ξ and ξ' become independent (C=0), if the distance τ is great enough . Beckmann [38] assumed that :

$$C(\tau) \; = \; e^{-\frac{\tau^2}{T^2}}$$

$$\tau = \sqrt{(x-x')^2 + (y-y')^2} \qquad (4.25)$$

where T is the "correlation length" of the rough surface. High values of T correspond to smooth corrugations.

With this additional assumption, it is now possible to solve the integral (4.24). Another assumption is necessary : the dimensions of the surface X and Y must be much greater than the correlation length T, which implies that the finite surface contains at least several corrugations (see appendix 4.3). The expression (4.24) becomes :

$$\pi S T^2 e^{-g} \sum_{m=1}^{\infty}\left(\frac{g^m}{m\,m!} \; e^{-\frac{v_{xy}^2 T^2}{4m}} \right) + S^2 e^{-g} \; \text{sinc}^2(v_x X) \; \text{sinc}^2(v_y Y)$$

$$g = v_z^2 \sigma^2 = \left(\frac{2\pi\sigma}{\lambda} \; (\cos\theta_1 + \cos\theta_2) \right)^2$$

$$v_{xy} = \sqrt{v_x^2 + v_y^2} \qquad (4.26)$$

The second term prevails for slightly rough surface (g and $\frac{\sigma}{\lambda}$ << 1). It represents a mirror-like behaviour, since it vanishes outside the specular direction. An image of the source clearly appears on the surface. This specular behaviour increases at grazing incidence, for a fixed value of $\frac{\sigma}{\lambda}$. So, the mathematical model is well in accordance with the visual inspection of illuminated surfaces (see chapter 2), even if the Kirchhoff approximation, which neglects the shadowing effects, is theoretically not valid at grazing incidence.

The first term of (4.26) prevails for significantly rough surfaces (g and $\frac{\sigma}{\lambda}$ >> 1), since [38] :

$$e^{-g} \sum_{m=1}^{\infty}\left(\frac{g^m}{m\,m!} \; e^{-\frac{v_{xy}^2 T^2}{4m}} \right) \approx \frac{1}{g} \; e^{-\frac{v_{xy}^2 T^2}{4g}} \qquad (4.27)$$

Applying the equations (4.20), (4.26) and (4.27) leads to :

$$I_s(M) \approx \sqrt{\frac{\varepsilon_0}{\mu_0}} \; \frac{\pi S T^2}{(4\pi R_0)^2} \left(\frac{\vec{v}.\vec{v}}{v_z} \right)^2 A^2 R^2_{(\theta_1,\theta_2,\phi)} \; \frac{1}{g} \; e^{-\frac{v_{xy}^2 T^2}{4g}} \qquad (4.28)$$

The vector $\vec{v}$ can be further developed, which gives :

$$I_s(M) \approx \sqrt{\frac{\varepsilon_0}{\mu_0}}\ \frac{\pi S}{(4\pi R_o)^2}\left(\frac{T}{\sigma}\right)^2 \frac{A^2\, R^2(\theta_1,\theta_2,\phi)}{\cos^4\alpha}\ e^{-\frac{T^2}{4\sigma^2}\tan^2\alpha}$$

$$\cos^2\alpha = \frac{v_z^2}{\vec{v}\,.\,\vec{v}} = \frac{(\cos\theta_1 + \cos\theta_2)^2}{2\,(1 + \cos\theta_1\cos\theta_2 - \sin\theta_1\sin\theta_2\cos\phi)} \qquad (4.29)$$

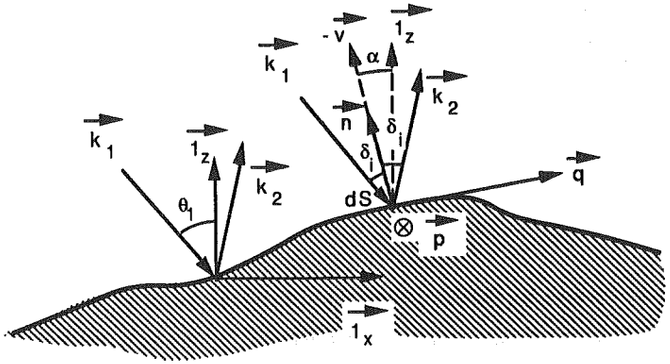

Figure 4.4 : Definition of the angle α between the axis $\vec{1}_z$ and the vector perpendicular to the specularly oriented facets, with respect to the viewing direction $\vec{k}_2$.

The angle α is defined in figure 4.4, as the angle between the axis $\vec{1}_z$, perpendicular to the mean plane of the corrugations, and the vector perpendicular to the specularly oriented facets, with respect to the direction $\vec{k}_2$. The expression (4.29) is analysed hereafter, as a function of the angle α. In a first step, the variation of R^2 is not considered (see figure 4.5) :

- if $T \geq 2.83\,\sigma$ (strong correlation), the scattered intensity is maximum at $\alpha=0$, i.e. in the specular direction $(\theta_1=\theta_2,\phi=0)$;
- if $T < 2.83\,\sigma$ (weak correlation), the scattered intensity is maximum at $\alpha=\alpha^*$, defined by $\cos^2\alpha^* = \frac{T^2}{8\sigma^2}$, and a local minimum appears at $\alpha=0$. However, this conclusion should be carefully considered, since the validity of the Kirchhoff approximation is here questionable.

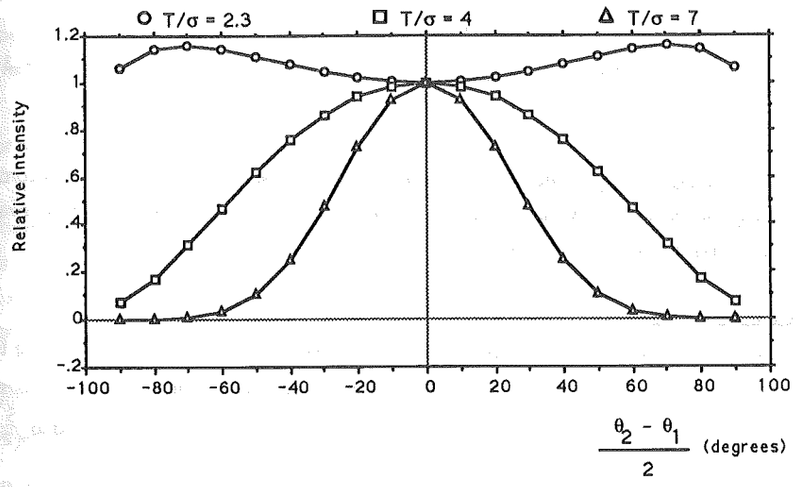

Figure 4.5 : Relative scattered intensity in the plane of incidence, expressed by the equation (4.31) with $R^2=1$, as a function of $\left(\frac{\theta_2-\theta_1}{2}\right)$ in degrees. $\frac{T}{\sigma}$ is the roughness parameter of the surface.

The expression (4.29) can be developed in the plane of incidence. In this case, the following notation has been adopted : θ_2 is positive if $\phi=0$ (forward scattering) and negative if $\phi=\pi$ (backward scattering)[6] :

$$\cos^2\alpha = \cos^2\left(\frac{\theta_1-\theta_2}{2}\right)$$

$$R^2(\theta_1,\theta_2) = \frac{|\,A^-\,R_s(\delta_i)\,|^2 + |\,A^+\,R_p(\delta_i)\,|^2}{A^2}$$

$$\delta_i = \left|\frac{\theta_1+\theta_2}{2}\right| \qquad (4.30)$$

δ_i is the local angle of incidence on the facets specularly reflecting in the viewing direction θ_2 (see appendix 4.2). The following expression can be written in the plane of incidence :

[6] "forward" means " in the half-plane of incidence containing the specular direction", and "backward" designates the other half-plane.

$$I_s(M) \propto \frac{R^2\left(\left|\frac{\theta_1+\theta_2}{2}\right|\right)}{\cos^4\left(\frac{\theta_1-\theta_2}{2}\right)} e^{-\frac{T^2}{4\sigma^2}tg^2\left(\frac{\theta_1-\theta_2}{2}\right)} \qquad (4.31)$$

This is our final expression for the scattered intensity at point M. This equation is in accordance with the principle of reciprocity, since the directions of incidence and scattering can be swapped without changing the scattered intensity.

About the edge effects

The determination of the scattered intensity could have been performed without neglecting the terms $\vec{\varepsilon}$ in the equations (4.15) and (4.16). Indeed, it can be shown, after long and tedious mathematical developments, that the terms in $\vec{\varepsilon}$ are proportional to $\frac{Y}{\lambda}$ or $\frac{X}{\lambda}$, instead to $\frac{S}{\lambda^2}$ for the main contribution (4.20). Therefore, if X and Y are much greater than λ, then the terms in $\vec{\varepsilon}$ can be neglected.

4.2.4. Validity of the model and transformation into photometric concepts

The equations (4.29) and (4.31) have been derived under the following assumptions :

- the incident electromagnetic wave is a monochromatic plane wave;
- the distance between the receiving point M and the rough surface is much greater than the dimensions X and Y of this surface. Furthermore, X and Y are much greater than the wavelength;
- the medium under the surface is homogeneous, linear and isotropic;
- the amplitude of the corrugations of the surface is a random, normally-distributed variable, with mean 0 and variance σ^2;
- the local radius of curvature of the surface and the correlation length T are much greater than the wavelength λ;
- $\lambda << T << X,Y$ and $\sigma >> \lambda$. An extra coherent and nearly-specular contribution must be added in (4.26), if σ is of the same magnitude as the wavelength;
- the shadows created on the surface by any element of this surface, and the multiple reflections between the surface elements have been ignored.

In their paper [58], Soto-Crespo and Nieto-Vesperinas compare the results of a numerical simulation and the results of the Kirchhoff approximation, for several perfectly conducting, one-dimensional rough surfaces. It is shown that the Kirchhoff approximation is valid for $T > 0.5\ \lambda$.

This conclusion is corroborated by the works of Eftimiu [41,42] on perfectly conducting and lossy dielectric surfaces.

Another conclusion cited by Soto-Crespo et al [59] is that the ratio $\left(\frac{T\cos\theta_1}{\sigma}\right)$ must be greater than 5, and that the angle of incidence θ_1 must be lower than 40°. Obviously, the shadowing effects which have been neglected must be more significant at grazing incidence ($\theta_1 > 40°$). Moreover, multiple reflections are created for $\sigma > T$, and the local radius of curvature tend to decrease. This is also a situation where enhanced back-scattering can appear, for σ and $T \approx \lambda$ [57,58]. The Kirchhoff approximation cannot predict these back-scattering effects (see figure 4.5).

The lambertian reflection can be observed for metallic surfaces such that $\sigma \approx T$ [58], but only at small angles of incidence ($\theta_1 \leq 20°$).

The equation (4.29) expresses the scattered intensity, i.e. the radiant energy passing through a surface of $1m^2$ perpendicular to the direction of scattering, in one second. Therefore, the scattered intensity I_e by unit solid angle is :

$$I_e(\theta_1,\theta_2,\phi) = \sqrt{\frac{\varepsilon_0}{\mu_0}}\frac{S}{16\pi}\left(\frac{T}{\sigma}\right)^2 \frac{A^2 R^2(\theta_1,\theta_2,\phi)}{\cos^4\alpha} e^{-\frac{T^2}{4\sigma^2}tg^2\alpha} \qquad (4.32)$$

The radiant flux incident on the rough surface is the product of the incident plane wave intensity ($\sqrt{\frac{\varepsilon_0}{\mu_0}}\vec{P} \times \vec{Q}$) and the section of the light beam intercepted by the surface :

$$\Phi_{ei} = \sqrt{\frac{\varepsilon_0}{\mu_0}}\left(|A^-|^2 + |A^+|^2\right) S\cos\theta_1 \qquad (4.33)$$

Equation (4.32) becomes :

$$I_e(\theta_1,\theta_2,\phi) = R^2(\theta_1,\theta_2,\phi)\frac{\Phi_{ei}}{16\pi\cos\theta_1}\left(\frac{T}{\sigma}\right)^2\frac{1}{\cos^4\alpha} e^{-\frac{T^2}{4\sigma^2}tg^2\alpha} \qquad (4.34)$$

The reflection factor R^2 is equal to 1 for a perfectly conducting surface, and the equation (4.34) can be integrated over all the scattering directions, to obtain the total scattered flux Φ_{es}. The table (4.1) gives the ratio between the total scattered flux (Φ_{es}) and the incident flux (Φ_{ei}). This ratio should be equal to 1 for a perfectly conducting surface.

This value is obtained (± 10%) by numerical integration, if the roughness parameter $\left(\frac{T}{\sigma}\right)$ is greater than 3 (for $\theta_1 \leq 70°$), or $\left(\frac{T}{\sigma}\right) > 5$ (for $\theta_1 = 80°$). The validity of the Kirchhoff approximation is again illustrated here. However, it must be emphasized that the validity will be extended later by experimentally taking into account the shadowing effects.

Table 4.1 : Ratio between the flux reflected by a perfectly conducting surface (eq. 4.34) and the incident flux

$\frac{T}{\sigma}$	angle of incidence : θ_1 (degrees)								
	0°	10°	20°	30°	40°	50°	60°	70°	80°
0.5	0.06	0.06	0.08	0.10	0.16	0.30	0.68	1.95	6.19
1.0	0.22	0.23	0.27	0.34	0.47	0.72	1.15	1.86	3.61
2.0	0.63	0.64	0.68	0.73	0.80	0.89	1.03	1.30	2.11
3.0	0.89	0.89	0.89	0.88	0.89	0.91	0.96	1.10	1.61
5.0	1.00	1.00	0.99	0.98	0.96	0.95	0.94	0.98	1.23
10.0	1.00	1.00	1.00	1.00	1.00	1.00	0.99	0.96	0.99
15.0	1.00	1.00	1.00	1.00	1.00	1.00	1.00	0.99	0.96
20.0	1.00	1.00	1.00	1.00	1.00	1.00	1.00	1.00	0.97
50.0	1.00	1.00	1.00	1.00	1.00	1.00	1.00	1.00	1.00

The radiance is the quotient of the radiant intensity I_e and the apparent surface $S\cos\theta_2$:

$$L_e(\theta_1,\theta_2,\phi) = \sqrt{\frac{\varepsilon_0}{\mu_0}}\ \frac{1}{16\pi\cos\theta_2}\left(\frac{T}{\sigma}\right)^2\ \frac{A^2\,R^{\,2}(\theta_1,\theta_2,\phi)}{\cos^4\alpha}\ e^{-\frac{T^2}{4\sigma^2}\tg^2\alpha} \qquad (4.35)$$

The radiance is equal to $\frac{\Phi_{ei}}{\pi S}$ for a perfect diffuser. Therefore, the radiance factor of the rough surface in the direction (θ_2,ϕ) is :

$$\beta_e(\theta_1,\theta_2,\phi) = R^{\,2}(\theta_1,\theta_2,\phi)\ \frac{1}{16\cos\theta_1\cos\theta_2}\left(\frac{T}{\sigma}\right)^2\ \frac{1}{\cos^4\alpha}\ e^{-\frac{T^2}{4\sigma^2}\tg^2\alpha} \qquad (4.36)$$

The expressions (4.34) and (4.36) can finally be particularized to the case of a naturally polarized incident light, which is a non-restrictive assumption for lighting engineers (see appendix 4.2, equation 4.A14) :

$$R^{\,2}(\theta_1,\theta_2,\phi) = \frac{|R_s|^2+|R_p|^2}{2} \qquad (4.37)$$

where R_s and R_p are the Fresnel reflection coefficients which depend on the local angle of incidence δ_i(4.A12).

4.2.5. First comparison with measured intensities

It is now intended to test the validity of the electromagnetic model described above. The material chosen for this study is a sample of frosted glass, because it fulfils the conditions of an homogeneous, linear and isotropic medium. In other words, the light reflected by the glass sample is due to surface scattering only, and not to volume scattering, since the material is transparent. Moreover, the optical properties of glass, such as its refractive index, are well known.

The scattered intensity has been measured in the plane of incidence with the apparatus described in chapter 3. The wavelength is 550 nm. The measurement process gives the spectral radiance factor $\beta_e(\theta_1,\theta_2,\lambda)$, for an angle of incidence θ_1 comprised between 0° and 80°, and a scattering angle $\theta_2 \neq \theta_1$ comprised between -70° and +70°. The negative scattering angles θ_2 correspond to backward scattering and the positive angle to forward scattering. The scattered intensity $I_e(\theta_1,\theta_2,\lambda)$ can then be obtained by the product of this radiance factor and the geometrical factor $(\cos\theta_1\ \cos\theta_2)$: see equations (4.32) and (4.36).

Three glass samples have been tested. Their surfaces have been frosted at the "Institut National du Verre" (I.N.V.) with fine-, middle- and coarse-grain abrasives. These samples will be referred to in the text by the letters A, B and C, respectively. The dimensions of the analysed surface are 10 cm x 10 cm, and the depth of the glass sample is 1cm.

To avoid light reflection on the reverse plane surface of the sample, it has been covered with two layers of black oil-paint. Indeed, it has been observed that this operation reduces the reverse plane reflection by at least 90%.

The intensities measured in the plane of incidence are first compared with equation (4.31). In this expression, $R^{\,2}$ is the reflection factor of a glass plane surface (n=1.52), for naturally polarized incident light (eq. 4.37 and figure 2.4, curve b). Following the model (4.31), the ratio

between the scattered intensity and the reflection factor R^2 would only depend on the difference between the angle of incidence θ_1 and the viewing angle θ_2.

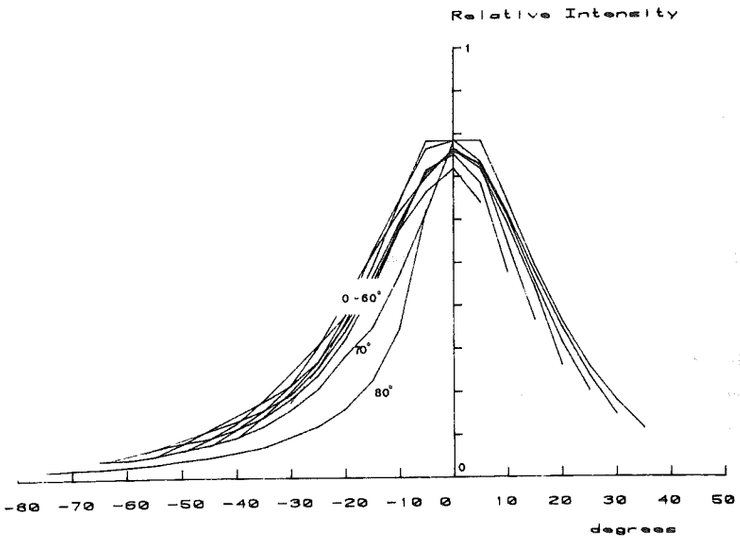

Figure 4.6 : Measured ratio $\frac{I_\theta}{R^2}$ (relative units) as a function of the difference $\frac{(\theta_2 - \theta_1)}{2}$, in degrees ($\lambda$ = 550 nm). These nine curves have been measured for the slightly rough sample A : they correspond to the angles of incidence from 0° to 80°, by 10° step.

This ratio $\frac{I_\theta}{R^2}$ has been derived[7] from the intensity measurements : the results are shown for the slightly rough sample in figure 4.6, as a function of the angles of incidence and viewing. The prediction of the dependence in $(\theta_1 - \theta_2)$ alone is fairly good, until θ_1 =70°. However, the curves at θ_1 =70° and 80° slightly differ from the others.

This difference is again observed and well accentuated in figure 4.7 (sample B), and especially for the very rough sample C in figure 4.8. In this case, the curves diverge from the "ideal" law for the incidence and scattering angles greater than 40°.

[7] The expressions (2.4) and (2.6) give the Fresnel reflection coefficients.

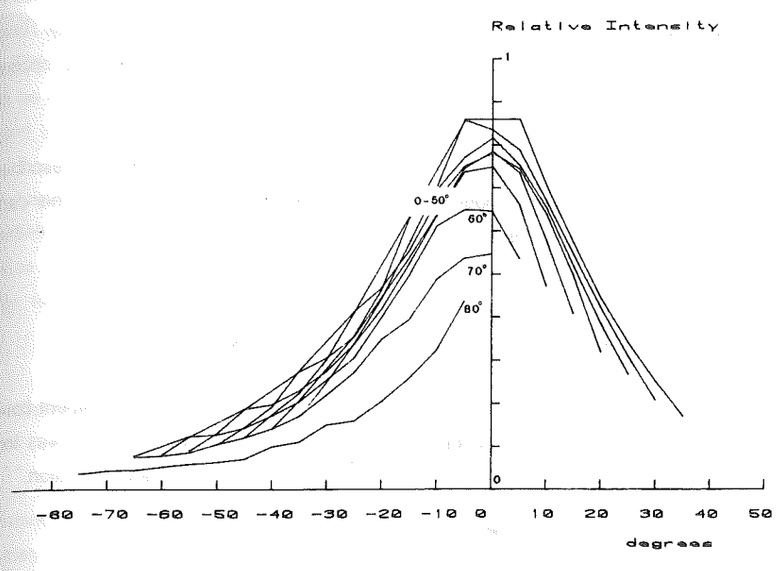

Figure 4.7 : Same as figure 4.6 for the moderately rough sample B.

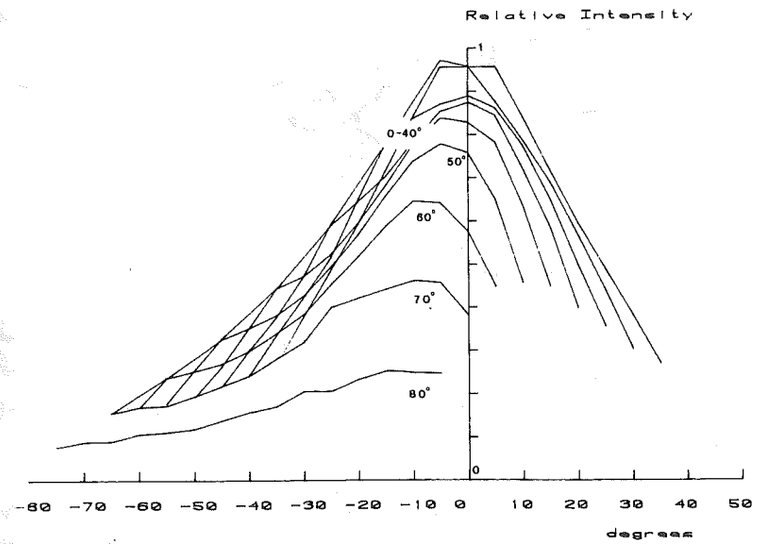

Figure 4.8 : Same as figure 4.6 for the very rough sample C.

It is again possible to relate these conclusions to the validity of the Kirchhoff approximation, which holds for the angles of incidence smaller than a given upper bound, which tends to increase with the roughness $\left(\frac{T}{\sigma}\right)$: see §4.2.4. Our measurements corroborate this statement, since the

sample A can be viewed as a slightly rough surface, with small amplitude (σ) and highly correlated (T>>) corrugations, whereas the very rough sample C would exhibit just the opposite behaviour.

Thus, a first conclusion from these measurements is that the crude theoretical model described by (4.31) should be corrected at grazing incidence. It will be shown in the following that this can be performed by taking the shadowing effects into account.

4.2.6. Shadowing effects and second comparisons with measured intensities

To derive equation (4.31), it has been assumed that the electric field at a surface element could be computed as the total field (direct + reflections) that would exist if the rough surface was locally replaced by the infinite tangent plane at this element : this is the Kirchhoff approximation.

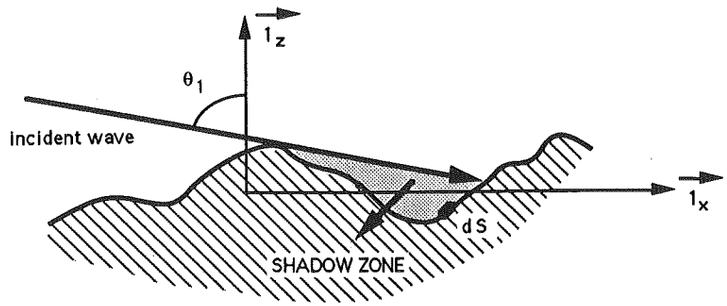

Figure 4.9 : The element of surface dS is situated in a shadow zone.

This assumption holds as long as the incident wave can reach the element of surface dS without obstruction. This is not the case in figure 4.9 where dS is situated in a shadow zone. A better approximation would be that the total electric field vanishes at dS, if the multiple reflections could be disregarded.

A correction factor $C(\theta_1)$ has been introduced in equation (4.31) to take these shadowing effects into account. Of course, this factor depends on the angle of incidence : if $\theta_1 = 0°$, the rough surface unequivocally defined by $\xi(x,y)$ is totally illuminated by the incident wave and C = 1. However, if $\theta_1 = 90°$, the shadow zone is covering the whole surface and C = 0. Between 0° and 90°, the function $C(\theta_1)$ is expected to decay monotonically.

The next argument is based on geometrical optics and the assumption that light propagates along rays. Therefore, the function $C(\theta_1)$ can be interpreted as the probability for a "useful" light ray not to be intercepted. A "useful" ray is here defined as a light ray falling upon a facet specularly oriented towards the scattering direction.

It can be imagined that this probability must also be applied to the scattered ray, i.e. that a second correction factor $C(|\theta_2|)$ must be introduced in the model. This second factor depends on the absolute value of the scattering angle : so is the Helmholtz principle of reciprocity satisfied. Finally, the corrected equation is :

$$I_e(\theta_1,\theta_2) + C(\theta_1)\ C(|\theta_2|)\ \frac{R^2\left(\left|\frac{\theta_1+\theta_2}{2}\right|\right)}{\cos^4\left(\frac{\theta_1-\theta_2}{2}\right)}\ e^{-\frac{T^2}{4\sigma^2}\,tg^2\left(\frac{\theta_1-\theta_2}{2}\right)} \qquad (4.38)$$

It remains to test that this correction can lead to a better model for the scattered intensity. The first step is to determine the function $C(\theta)$: all that is known about it, is that it must monotonically decrease from θ=0° (C=1) to 90° (C=0). The following mean square expression has been minimized to find the intermediate values :

$$\Delta = \frac{1}{N} \sum_i \sum_j \left[\log \hat{I}_e\,(\theta_{1i},\theta_{2j}) - \log I_e(\theta_{1i},\theta_{2j}) \right]^2$$

$$\theta_{1i} = 0°,\ 10°,\ .....,80°$$

$$\theta_{2j} = -70°,\ -60°,\ .....,\ 60°,\ 70°,\quad \theta_{2j} \neq \pm\,\theta_{1i} \qquad (4.39)$$

In this definition, I_e is the measured scattered intensity and $\hat{I}_e\,(\theta_{1i},\theta_{2j})$ is the corresponding calculated intensity, given by :

$$\hat{I}_e\,(\theta_{1i},\theta_{2j}) = C(\theta_{1i})\ C(|\theta_{2j}|)\ R^2\left(\left|\frac{\theta_{1i}+\theta_{2j}}{2}\right|\right)\ I_d\left(\frac{|\theta_{1i}-\theta_{2j}|}{2}\right) \qquad (4.40)$$

The unknows of the minimization problem are :

- the value of $C(\theta)$ for θ = 10°, 20°, ..., 80° ; C(0°) = 1;
- the value of $I_d(\omega)$ for ω = 5°, 10°, ..., 75°; I_d(0°) is left undetermined since the comparisons at $\theta_{2j} = \theta_{1i}$ have been excluded (see below).

The problem involves N=120 intensity comparisons and 23 unknows. Taking the logarithm in equation (4.39) ensures that the minimization process always converges to a unique solution, since the function Δ is convex [52, p.98]. The direction of retroreflection has been excluded since there was no measurement at $\theta_{2j} = -\theta_{1i}$. The specular direction has been excluded to prevent the coherent surface contribution from altering our conclusions (see eq. 4.26).

Several comparisons between measured and calculated (by 4.38) intensities have been undertaken. For example, it has been observed that it was not convenient to directly define the intensity I_d by :

$$I_d = \frac{c_1}{\cos^4\left(\frac{\theta_1-\theta_2}{2}\right)} e^{-c_2 \, tg^2\left(\frac{\theta_1-\theta_2}{2}\right)} \qquad (4.41)$$

Of course, this expression could be interesting since, on the one hand, it only involves two parameters c_1 and c_2 and, on the other hand, it allows a direct evaluation of the model of Beckmann. However, the least square minimization could lead to unrealistic values of c_1 and c_2 (for example, a negative value of c_2).

It must be recalled here that the surface corrugations are perhaps not normally distributed, or that the reverse side of the glass sample (though painted in black) perhaps reflects a significant luminous flux for some incidences.

It is therefore careful to keep the term I_d as general as possible.

The figure 4.10 shows the results of the optimization process (4.39) for the three frosted glass samples (A, B and C). The correction factor $C(\theta)$ not only depends on θ, but also on the roughness of the surface, as could be expected. It is worth noting that the function $C(\theta)$ converged to a function monotonically decreasing between the values 1 and 0, though no constraint has been put on its optimization.

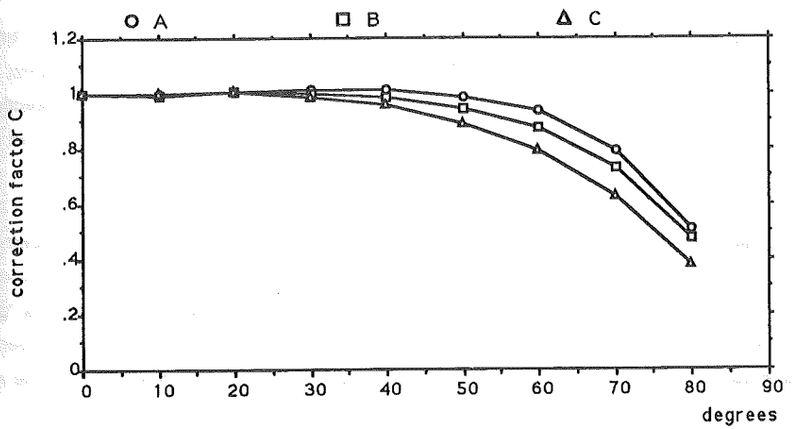

Figure 4.10 : Correction factor $C(\theta)$ calculated for the three frosted glass samples (A, B and C).

The figure 4.11 shows the function $I_d(\omega)$ calculated for the sample A : the curve is designated by "general model". This curve bears some resemblance to figure 4.5, which was based on equation (4.41).

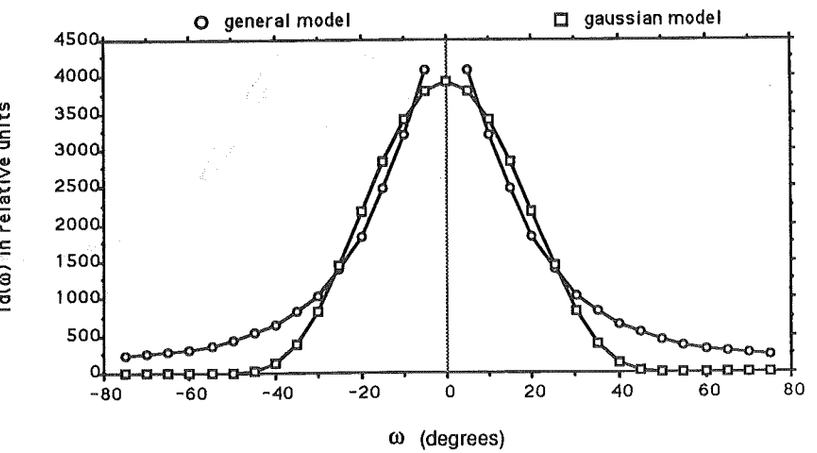

Figure 4.11 : Function $I_d(\omega)$ calculated for the slightly rough sample A. The curve (O) is the result of the minimization process (4.39). Best fit curve with equation (4.41) is also represented (gaussian model).

However, if the analysis is further proceeded, it is observed that the decreasing of the function predicted by the gaussian model is much more accentuated for $|\omega| > 30°$, i.e. for $|\theta_1 - \theta_2| > 60°$. In particular, this model predicts that the intensity should vanish, when the viewing direction significantly deviates from the specular direction : this behaviour has not been observed during the measurements.

A better illustration of this departure from the gaussian model is obtained by the following optimization : we have determined the values of the parameters (c_1 and c_2), by least square minimization between the model (4.41) and the curves "general model". So, the curves "gaussian model" have been derived in figures 4.11 to 4.13. The most significant difference between both model is the sharper decreasing of the gaussian model, and this is observed for the three rough samples. This difference is more accentuated for very rough surfaces.

Besides the possible non-gaussian distribution of the corrugations and the unwanted reflection on the reverse side of the glass sample, this behaviour could also be attributed to multiple reflections inside the corrugations of the surface, which should increase with the roughness of the sample.

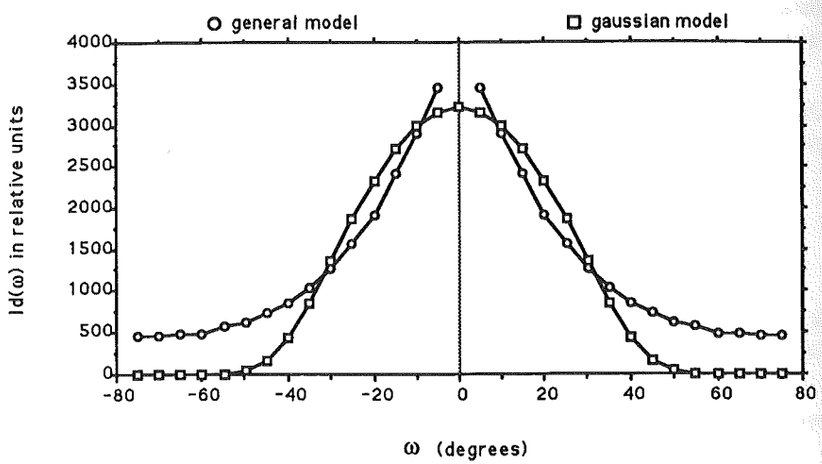

Figure 4.12 : Same as figure 4.11 for the moderately rough sample B.

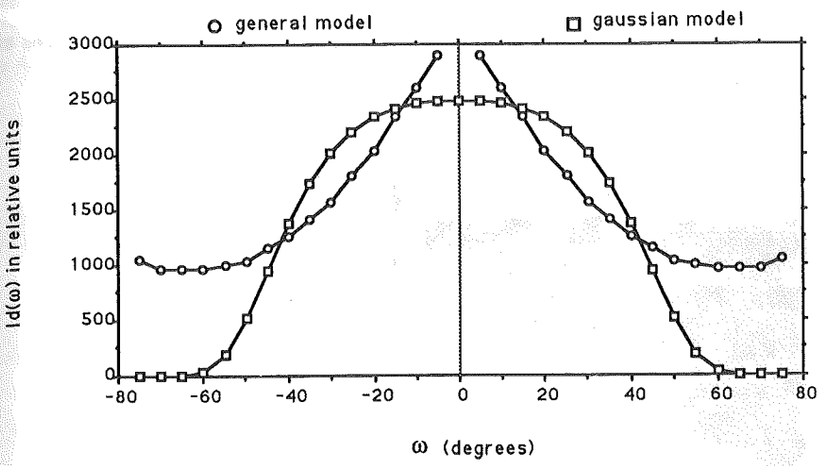

Figure 4.13 : Same as figure 4.11 for the very rough sample C.

The roughness parameters $\left(\frac{T}{\sigma}\right)$ derived by the optimization process are :

5.05 for the sample A (figure 4.11),
4.16 for the sample B (figure 4.12),
3.06 for the sample C (figure 4.13).

The general model (4.40) gives fairly good results, since the relative deviations between measured and calculated intensities for the glass sample A are 47% at ($\theta_1 = 80°$, $\theta_2 = 70°$) and less than 15% for all other pairs (θ_1, θ_2). For the sample B, the corresponding deviations are 33% and 14%. For the sample C, the relative deviations are always less than 10%.

However, the model (4.40) is not "user-friendly", since too many parameters are required to describe a rough surface. It is interesting, therefore, to analyse the deviations obtained with the gaussian model (4.38). Besides the parameters of the function $C(\theta)$, this model has only two parameters : an amplitude parameter (c_1) and a roughness parameter (c_2 or $\frac{T}{\sigma}$).

The relative deviation between measured intensities for the glass sample A and the gaussian equation (4.38) is less than 33% if $|\theta_1 - \theta_2| \leq 60°$, except at ($\theta_1 = 80°$, $\theta_2 = 70°$) for which the deviation is 50% (see figure 4.14). However, the deviations can reach 100 % in the other scattering directions, since I_d vanishes in the gaussian model, while the measured intensity is weak, but not zero. Therefore, the absolute deviations remain acceptable.

The agreement is even better for the very rough sample C, since the relative deviations are less than 30%, if $|\theta_1 - \theta_2| \leq 90°$.

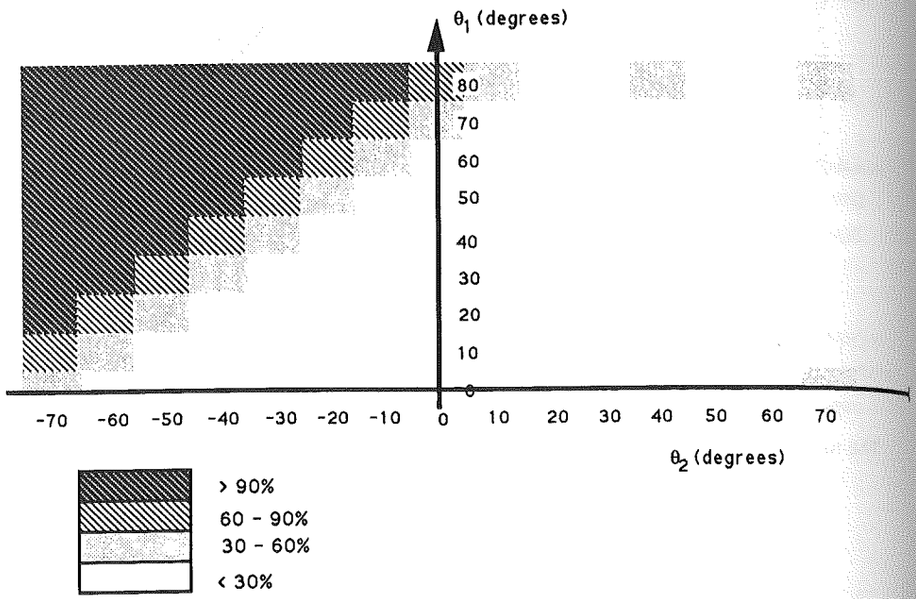

Figure 4.14 : Relative deviations between the measured scattered intensities and the two-parameters equation (4.38) . The deviations are expressed in percents, for several discrete values of the angles θ_1 and θ_2. Slightly rough sample A.

4.2.7. An analytical model to take the shadowing effects into account

The function $C(\theta)$ has been defined as the probability for a "useful" light ray not to be intercepted by the corrugations of the rough surface. It monotonically decreases from $\theta=0°$ (C=1) to $\theta=90°$ (C=0), and the slope of the decay depends on the roughness of the surface (fig. 4.10).

It would be interesting if the same roughness parameter $\left(\frac{T}{\sigma}\right)$ could be used for $I_d(\omega)$ and $C(\theta)$ in (4.40) : so, the shadowing function would not introduce extra parameters in our model. An analytical formulation of $C(\theta)$ is proposed here; it is based on very simple arguments.

Figure 4.15 shows a cross-section of the rough surface, containing the scattering direction θ_2,.

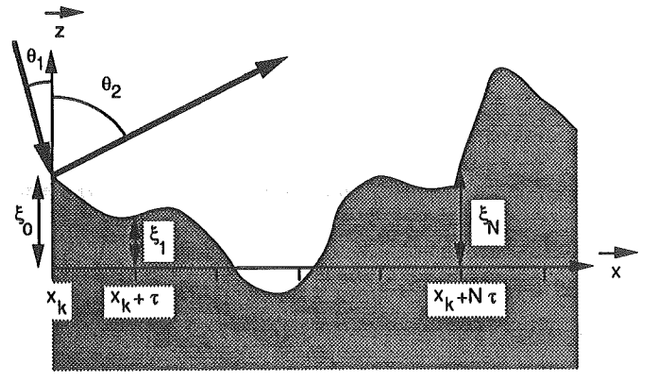

Figure 4.15 : Cross-section of the rough surface parallel to the $\vec{x}$ axis. Symbols are defined in the text.

Consider a "useful" ray which is reflected by the surface in $x=x_k$. The elevation of the surface in x_k is $\xi_0=\xi(x_k)$, and the slope in x_k is such that the surface element is specularly oriented. Imagine that the rough surface is described by its elevation at several equidistant points or elements of surface, i.e. at x_k, $x_k + \tau$, ... $x_k + N\tau$. The elevation in $(x_k + i\tau)$ is ξ_i : see figure 4.15. The elevations ξ_i are normally distributed, with mean $\xi=0$ and standard deviation σ.

The "useful" ray (θ_2) is not intercepted if :

$$
\begin{aligned}
& -\infty < \xi_0 < +\infty \\
\text{and} \quad & -\infty < \xi_1 < \xi_0 + \tau \operatorname{cotg} \theta_2 \\
& \ldots \\
\text{and} \quad & -\infty < \xi_N < \xi_0 + N\tau \operatorname{cotg} \theta_2
\end{aligned}
\qquad (4.42)
$$

If the distance τ is greater than the correlation length T, the elevations ξ_i can be considered as independent values. Therefore, the probability associated with the inequalities (4.42) is :

$$P(\tau, \theta_2, N) = \int_{-\infty}^{+\infty} p(\xi_0)\, d\xi_0 \int_{-\infty}^{\xi_0+\tau\cot g\theta_2} p(\xi_1)\, d\xi_1 \ \ldots \int_{-\infty}^{\xi_0+N\tau\cot g\theta_2} p(\xi_N)\, d\xi_N$$

$$p(\xi_I) = \frac{1}{\sigma\sqrt{2\pi}}\, e^{-\frac{\xi_I^2}{2\sigma^2}} \qquad (4.43)$$

Introducing $z_0 = \frac{\xi_0}{\sigma}$ and the normal cumulative distribution function f(v) leads to :

$$P(\tau, \theta_2, N) = \int_{-\infty}^{+\infty} \frac{1}{\sqrt{2\pi}}\, e^{-\frac{z_0^2}{2}} \left(\prod_{i=1}^{N} f(z_0 + i\,\frac{\tau}{\sigma}\cot g\,\theta_2) \right) dz_0 \qquad (4.44)$$

This probability only depends on the factor $(\frac{\tau}{\sigma}\cot g\,\theta_2)$.

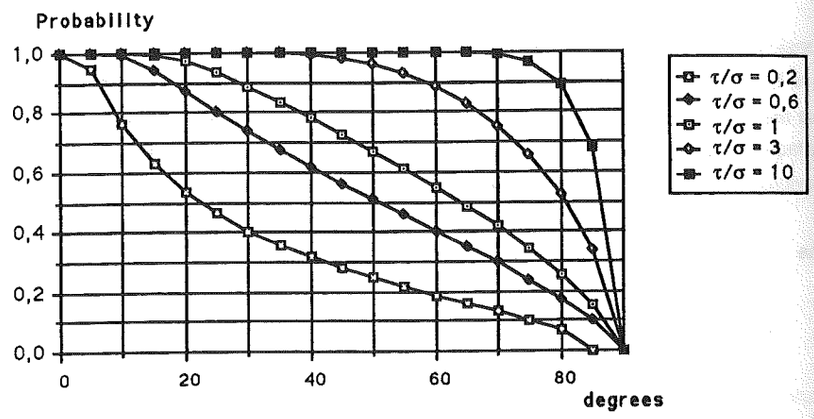

Figure 4.16 : Probability for a "useful" ray not to be intercepted, as a function of the viewing angle θ_2 (degrees) and the roughness parameter $\frac{\tau}{\sigma}$: see expression (4.44).

The limit of (4.44), for infinite values of N, has been computed by numerical integration. The results are shown in figure 4.16. A more detailed analysis would reveal that the curve

corresponding to $(\frac{\tau}{\sigma}=1)$ is very close to the function $\cos\theta_2$. Therefore, the following analytical expression is proposed for $C(\theta)$:

$$C(\theta) = \frac{\frac{\tau}{\sigma}\cot g\,\theta_2}{\sqrt{1 + \left(\frac{\tau}{\sigma}\cot g\,\theta_2\right)^2}} \qquad (4.45)$$

The distance τ must be greater than the correlation length T (see above). However, if it is too great, the rough surface would be incompletely described. A satisfying compromise consists in attributing the value τ=T in (4.45).

It must be recalled that the purpose of this study is not to perform a detailed and rigourous analysis on the shadowing effects, but rather to obtain a simple analytical expression depending only on the roughness parameter $\left(\frac{T}{\sigma}\right)$. It will be seen in the following that the introduction of this expression (4.45) in our general model for light reflection will lead us to very satisfying results.

4.2.8. Conclusion about the model for surface reflection

This model is based on the reflection of electromagnetic waves by rough surfaces, on the Kirchhoff approximation and the formulation of Beckmann [38]. The following amendments have been added :

- vectorial approach, to take into account non-conducting materials;
- introduction of the optical properties of the homogeneous material under the surface, through the reflection factor R^2.
- analysis of the intensity scattered in the plane of incidence and introduction of a correction factor to take the shadowing effects into account.

The final expression can be directly applied in lighting simulations. The following parameters are necessary :

- the angles of incidence (θ_1) and viewing (or scattering) (θ_2,ϕ);
- the roughness parameter $\left(\frac{T}{\sigma}\right)$;
- the Fresnel reflection coefficients of the surface R_s and R_p.

The radiance factor is :

$$\beta_e(\theta_1,\theta_2,\phi) = \frac{|R_s|^2+|R_p|^2}{3\,2}\,\frac{C(\theta_1)\,C(\theta_2)}{\cos\theta_1\cos\theta_2}\left(\frac{T}{\sigma}\right)^2\frac{1}{\cos^4\alpha}\;e^{-\frac{T^2}{4\sigma^2}\tan^2\alpha}$$

$$\cos^2\alpha = \frac{(\cos\theta_1+\cos\theta_2)^2}{2\,(1+\cos\theta_1\cos\theta_2-\sin\theta_1\sin\theta_2\cos\phi)}$$

$$\cos 2\delta_i = \cos\theta_1\cos\theta_2-\sin\theta_1\sin\theta_2\cos\phi \qquad (4.46)$$

The coefficients R_s and R_p depend on the local angle of reflection δ_i and on the refractive index (n) of the air/material interface : see equations (2.4) and (2.6). The correction factor taking into account shadowing effects is :

$$C(\theta) = \frac{\frac{T}{\sigma}\cot g\,\theta}{\sqrt{1+\left(\frac{T}{\sigma}\cot g\,\theta\right)^2}} \qquad (4.47)$$

Note : For slightly rough surfaces ($\sigma < \lambda$), an extra term corresponding to the coherent intensity must be added to (4.46) : see eq. 4.26.

The major interest of the model (4.46), associated with the expression (4.47), is that it is described by a small number of parameters, in particular concerning the surface roughness.

A second model is proposed hereafter, which is probably much closer to the real behaviour of non-gaussian surfaces, but which implies the determination of a great number of parameters :

$$\beta_e(\theta_1,\theta_2,\phi) = \frac{|R_s|^2+|R_p|^2}{3\,2}\,\frac{C(\theta_1)\,C(\theta_2)}{\cos\theta_1\cos\theta_2}\;I_d(\alpha) \qquad (4.48)$$

Besides R_s and R_p, these parameters are the value of $C(\theta)$, for θ = 10, 20, ..., 80° and the value of $I_d(\alpha)$, for α = 0, 5, 10, ..., 85°. They must be derived from a complete measurement of the luminance factor in the plane of incidence.

Lighting simulations by computer is an application where the model (4.46) could be very interesting. The model of Beckmann has already been applied in the field of image synthesis [60]. In this particular work, another approach is developed to describe the shadowing effects.

The Japanese Uetani and Matsuura [64] have proposed a geometrical optics approach, without taking into account these shadowing effects. Their expression for the surface reflection term is quite similar to our model (4.46) :

$$\beta_e = K\,\frac{|R_s|^2+|R_p|^2}{2}\,\frac{1}{\cos\theta_1\cos\theta_2}\,\frac{p_f(\theta_f,\phi_f)}{\cos\theta_f} \qquad (4.49)$$

$p_f(\theta_f,\phi_f)$ is the probability density function of the quotient of the total projected area of the specularly oriented facets and the reflecting surface S. The angles θ_f and ϕ_f define the direction perpendicular to these specularly oriented facets : θ_f is similar to the angle α appearing in equation (4.46).

The conclusion of the authors about their model is that it is not satisfying for incidences greater than 60° : this again illustrates the necessity to introduce a shadowing factor.

4.3. Volume scattering

It is the re-emission of light which has penetrated into the bulk of the material and has interacted with its heterogeneous structure. It has already been illustrated in chapter 2 that the volume reflection is distributed in all scattering directions, contrary to the surface reflection which is rather concentrated around the specular direction.

Uetani and Matsuura [64] even state that volume scattering is nearly isotropic and lambertian. Their assumption is based on their luminance factors measurements, during which the surface and volume contributions have been separated by polarization. Indeed, these authors assume that, if the incident wave is polarized in the plane of incidence or in the perpendicular direction, then the (rough) surface reflection is polarized in the same way. This is quite correct and can be justified by our equation (4.15), giving the scattered electric field. They also assume that the volume reflection is not (or naturally) polarized, and this allows them to separate both contributions by inserting two polarizers in the light ray [64].

Another technique is proposed here. The reflection on an air/glass interface is again used, since its optical characteristics are well known. More precisely, we use a plane opaline glass surface, which is of course an heterogeneous medium. The surface and volume contributions are geometrically separated, since the first one is only significant in the specular direction : in all other scattering directions, the measuring apparatus detects the volume reflection.

The size of the opaline glass sample is 20 cm x 13 cm. The reverse side of the sample has been covered with two layers of black oil-paint. Indeed, it has been observed that this reduces the reverse plane reflection by at least 90%.

The luminance factor is measured by the apparatus described in chapter 3, and the detector is the luminancemeter with its photopic filter V(λ). The results are shown in figure 4.17 and in table 4.2. The luminance factor has not been measured in the specular direction, because the mirror-like surface reflection was too intense.

Table 4.2 : Luminance factor of an opaline glass sample, measured for the angles of incidence ("inc") from 0° to 80° and for the viewing angles ("obs") from -70° to +70°. The luminance factor is here expressed in relative units : the value 100 has been attributed to $\beta_{40/0}$.

obs/inc	0	10	20	30	40	50	60	70	80
-70.0	85.6	90.8	89.0	83.8	89.0	89.4	86.4*******		58.2
-60.0	99.2	96.8	95.3	96.6	98.7	97.8*******		86.4	64.0
-50.0	100.6	98.4	99.7	100.9	101.5*******		97.8	89.4	68.8
-40.0	100.0	100.1	101.0	101.8*******		101.5	98.7	89.0	62.3
-30.0	100.4	101.0	102.1*******		101.8	100.9	96.6	83.8	67.8
-20.0	101.8	101.5*******		102.1	101.0	99.7	95.3	89.0	69.2
-10.0	102.7*******		101.5	101.0	100.1	98.4	96.8	90.8	61.0
.0*******		102.7	101.8	100.4	100.0	100.6	99.2	85.6	66.8
10.0	103.0*******		101.7	101.6	102.3	102.7	95.5	89.4	59.9
20.0	102.2	101.9*******		104.0	104.5	102.0	99.4	86.3	64.4
30.0	101.3	102.5	104.4*******		104.9	105.3	98.1	90.8	66.4
40.0	102.5	103.2	105.0	105.2*******		103.9	102.8	92.3	68.8
50.0	101.8	102.7	103.0	105.6	105.2*******		105.4	94.4	70.2
60.0	99.8	99.2	100.8	101.3	104.3	106.4*******		97.6	74.0
70.0	91.0	91.4	92.0	94.2	96.5	98.0	99.0*******		59.9

A first analysis of these results shows that the assumption of a possible lambertian behaviour is only valid :

- at a given angle of incidence;
- for the viewing angles comprised between -50° and +50°.

This behaviour had already been found for the keramics sample, in § 3.5.2. It can be attributed to the surface reflection, which is here perfectly specular, and which contains a significant part of the incident energy : $\rho_s(\hat{i})$. So, only the complementary part $(1-\rho_s(\hat{i}))$ is available for the volume reflection, and a more appropriate model than the lambert law would be :

$$\beta_V(\hat{o},\hat{i}) = (1-\rho_s(\hat{i}))\ \rho_d \qquad (4.50)$$

ρ_d is the diffuse reflection factor, defined as the quotient of the flux re-emitted by volume scattering and the flux entering the material. This quotient is assumed to be independent on the angle of incidence.

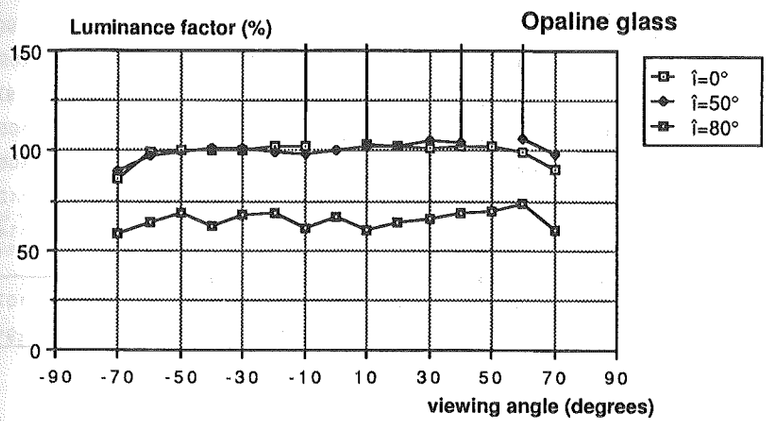

Figure 4.17 : Luminance factor of an opaline glass sample measured in the plane of incidence; î is the angle of incidence. This factor is expressed in relative units, with 100% being attributed to $\beta_V(\hat{i}=40°,\hat{o}=0°)$.

The ratio between the measured luminance factor (table 4.2) and the factor $(1-\rho_s(\hat{i}))$ has been computed, in order to test the model (4.50). The reflection factor $\rho_s(\hat{i})$ is given by the curve b) in figure 2.4, for the air/glass interface (n=1.52).

It can be observed in table 4.3 that the mean value of this ratio is constant, within an accuracy of ±1% . However, the deviations around the average value increase with the angle of incidence. If it is considered that these deviations include the measurements' errors, then it can be concluded that the model (4.50) is well satisfying, from ô=-50° to +50°.

Table 4.3 : Analysis of the ratio $\frac{\beta_V(\hat{o},\hat{i})}{1-\rho_s(\hat{i})}$ for the opaline glass

	Angle of incidence î (degrees)					
ô(degrees)	0	10	20	40	70	80
-50	104.8	102.5	103.8	106.4	107.8	112.4
-40	104.2	104.3	105.2	-----	107.3	101.8
-30	104.6	105.2	106.3	106.7	101.1	110.8
-20	106.0	105.7	-----	105.9	107.4	113.1
-10	107.0	-----	105.7	104.9	109.5	99.7
0	-----	107.0	106.0	104.8	103.3	109.2
+10	107.3	-----	105.9	107.2	107.8	97.9
+20	106.5	106.2	-----	109.5	104.1	105.2
+30	105.5	106.8	108.8	110.0	109.5	108.5
+40	106.8	107.5	109.4	------	111.3	112.4
+50	106.4	107.0	107.3	110.2	113.9	114.7
Average	105.9	105.8	106.5	107.3	107.6	107.8
Deviation	±2%	±3%	±3%	±3%	±6%	±9%

For greater viewing angles (in magnitude), the model (4.50) is not accurate, probably because it does not satisfy the Helmholtz principle of reciprocity. The following expression should be preferred :

$$\beta_V(\hat{o},\hat{i}) = (1-\rho_s(\hat{i}))\ (1-\rho_s(|\hat{o}|))\ \rho_d \qquad (4.51)$$

ρ_d is not considered as a reflection factor anymore, but rather as a constant value which does not depend on the angles î and ô. It is one of the parameters of the model which depends on the kind of material, as does the refractive index (n) which is used to determine $\rho_s(\hat{i})$ and $\rho_s(|\hat{o}|)$. It can now be explained why the model (4.50) was valid between ô = -50° and +50° : this is because the factor $\rho_s(|\hat{o}|)$ is approximately constant within this interval.

The application of the model (4.51) to the opaline glass sample leads to maximum deviations of 5% (î=10°), 12% (î=80°, ô<60°) and 18% (î=80°, ô≥60°), between the calculated and measured luminance factors.

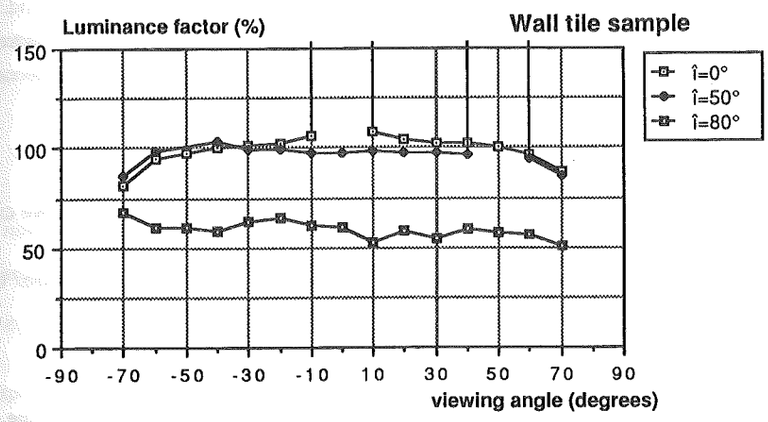

Figure 4.18: Luminance factor of a wall tile sample measured in the plane of incidence; î is the angle of incidence. This factor is expressed in relative units, with 100% being attributed to $\beta_V(\hat{i}=40°,\hat{o}=0°)$.

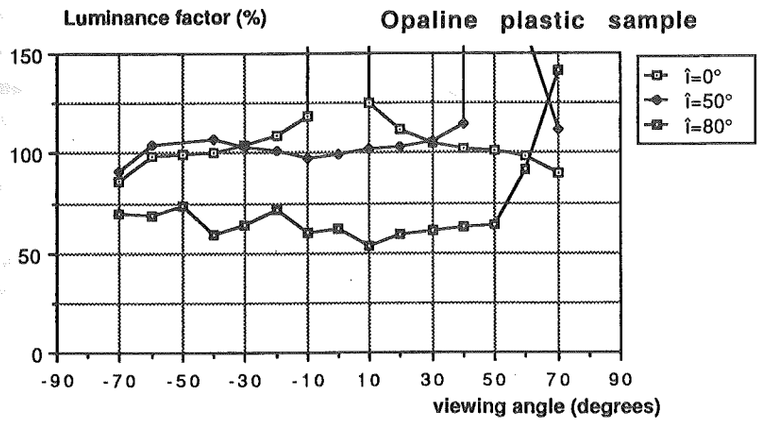

Figure 4.19 : Luminance factor of an opaline plastic sample measured in the plane of incidence; î is the angle of incidence. This factor is expressed in relative units, with 100% being attributed to $\beta_V(\hat{i}=40°,\hat{o}=0°)$.

Similar conclusions can be drawn for a wall tile sample and an opaline plastic sample (2mm thick). Of course, the refractive index cannot be accurately predicted for both samples, but it is

again observed that the luminance factor is approximately constant between δ=-50° and +50°, for a fixed angle of incidence. The deviations around the average value are of the same magnitude as the deviations observed for the opaline glass, and they also increase with the angle of incidence (fig. 4.18 and 4.19).

Therefore, given that :

- the model (4.51) is fairly accurate for the opaline glass and two other samples (we can also add here the keramics sample analysed in §3.5.2),
- the physical phenomena involved in the process of volume scattering are so complex that a detailed analytical approach would be extremely difficult,
- and given the measurements results obtained by Uetani and Matsuura [64],

it has been decided to adopt the expression (4.51) as our mathematical model for volume reflection.

Note
In this expression, ρ_s is practically independent on the wavelength, for most non-conducting materials. On the contrary, ρ_d is strongly affected by the wavelength and is mainly responsible for the colour associated with the volume reflection.

4.4. General model for light reflection and determination of the parameters for any material

4.4.1. General model including surface and volume scattering

The combination of the results obtained in §4.2 and 4.3 gives the following expression, which is valid for the luminance factor β_v, as well as for the radiance factor β_e :

$$\beta_e(\theta_1,\theta_2,\phi) = \rho_s(\theta_1)\frac{2\pi\,\delta(\theta_2-\theta_1)\,\delta(\phi)}{\sin 2\theta_1}$$

$$+ \alpha_{sc}\frac{|R_s|^2+|R_p|^2}{2}\frac{C(\theta_1)\,C(\theta_2)}{\cos\theta_1\cos\theta_2}\frac{1}{\cos^4\alpha}\,e^{-\frac{T^2}{4\sigma^2}tg^2\alpha}$$

$$+ (1-\rho_{surf}(\theta_1))\,(1-\rho_{surf}(\theta_2))\,\rho_d \qquad (4.52)$$

Note : the angles are defined in §4.2.

The coherent intensity which creates the image of the source is expressed by the first term; this term vanishes outside the specular direction ($\theta_2 = \theta_1$, ϕ= 0). The specular reflection factor ρ_s depends on the angle of incidence θ_1, the refractive index (n) and the roughness of the surface :

$$\rho_s(\theta_1) = \alpha_s\frac{|R_s(\theta_1)|^2+|R_p(\theta_1)|^2}{2} \qquad (4.53)$$

It must now be decided which value must be attributed to "α_s". The equation (4.26) expresses the dependence of this factor on the ratio $\left(\frac{\sigma\cos\theta_1}{\lambda}\right)$, i.e. on the roughness of the surface, but also (explicitely) on the wavelength of the incident light.

Now, experiments and observations (see chapter 2) have shown that the colour of the image reflected by a non-conducting material was approximately the same as the colour of the source, except in the case described in §2.2.3. This contradicts equation (4.53).

The apparent discrepancy is eliminated, if it is considered that the ratio $\left(\frac{\sigma\cos\theta_1}{\lambda}\right)$ is much greater than one, for usual roughness conditions and not too grazing incidence. As the ratio appears as an exponential factor in α_s (more precisely in the term e^{-g} in equation 4.26), then this contribution to the luminance factor is often unsignificant ($\alpha_s \to 0$). It is only significant at grazing incidence or for slightly rough surfaces : in these cases, α_s is close to unity. Intermediate values can hardly be found in practice : for e^{-g} to be comprised between 0.01 and 0.99, σ must be of the order of some tenths of wavelength (neither greater, nor smaller). This is the only situation where α_s is significantly different from 0 and 1, in an angular interval extending at least on several degrees. This is the only situation where a complex dependence of the coherent term on the surface roughness(σ), the angle of incidence(θ_1) and the wavelength(λ) can be found.

In practice, two characteristic values are proposed for α_s :
•) α_s = 0, for significantly rough surfaces;
•) α_s = 1, for plane surfaces, or at grazing incidences.

The second term of (4.52) represents the incoherent intensity reflected by the surface (cfr. §4.2). The angle α and the shadowing function $C(\theta)$ are defined in equations (4.46) and (4.47). R_s and R_p are the Fresnel reflection coefficients, which depend on the local angle of incidence δ_i on the specularly oriented facets, and on the refractive index "n". The parameter α_{sc} is the relative magnitude of this contribution.

The third term is the contribution of the volume reflection (§4.3). The equation (4.51) has been adapted for a rough interface, since the factor $\rho_{surf}(\theta)$ is the part of incident light energy reflected by the (rough) surface, for an angle of incidence θ : this factor involves the coherent and incoherent intensities :

$$\rho_{surf}(\theta_1) = \rho_s(\theta_1) + \alpha_{sc} \frac{C(\theta_1)}{\cos\theta_1} \int_0^{2\pi} d\phi \int_0^{\pi/2} \frac{|R_s|^2+|R_p|^2}{2\pi} \frac{C(\theta_2)}{\cos^4\alpha} e^{-\frac{T^2}{4\sigma^2} tg^2\alpha} \sin\theta_2 \, d\theta_2 \qquad (4.54)$$

The five parameters of the model (4.52) are :

- the refractive index "n" of the air/material interface, used to calculate the Fresnel reflection coefficients and $\rho_s(\theta)$;
- α_s, the magnitude of the coherent surface reflection contribution (eq. 4.53);
- α_{sc}, the magnitude of the incoherent term;
- ρ_d, the magnitude of the volume contribution;
- $\frac{T}{\sigma}$, the roughness parameter of the surface.

The following phenomena can be simulated by the general model (4.52) :

- specular reflection;
- scattering effects due to surface roughness;
- two kinds of surface reflections, and angular transition zone between them, if the general expression is kept for α_s ;
- shadowing effects;
- influence of the angle of incidence on the scattering indicatrix : the magnitude of the surface component tends to increase at grazing incidence (as the Fresnel coefficients increase) and, therefore, the volume component decreases (since ρ_{surf} increases);
- influence of the wavelength on non-metallic and metallic materials. For non-metallic materials, only ρ_d depends on λ (in usual conditions : α_s=0 or 1);
- for metals, ρ_d=0 (no volume reflection), and the Fresnel reflection factor possibly depends on the wavelength;
- reflection on transparent materials : ρ_d=0 ;
- reflexion on materials "without surface" (or very rough : see chapter2) : ($\alpha_s = \alpha_{sc}$= 0) and (ρ_{surf} = 0) leads to $\beta_e = \rho_d$ (Lambert).

The following phenomena cannot be simulated by the general model (4.52) :

- multiple scattering between surface elements, though this effect could be included in ρ_d;
- retroreflection, since the random elevation of the rough surface is supposed to be normally distributed. A more general surface term like (4.48) or (4.49) could possibly be used to include this phenomenon;
- the reflection on multi-layer materials, on diffraction gratings and, more generally, on all non-random rough surfaces (for the same reason as above).

4.4.2. Principle of the determination of the parameters

It is not sufficient to determine the parameters from only a few measurements. Several unsuccessful attempts have been tried, for example through the measurement of the luminance factor at $\hat{i}$=50° and $\hat{o}$=-40° to +40°. It would be theoretically possible to derive the five parameters of the model from these nine measurements. However, some parts of the diffusion indicatrix (for $\hat{i}$=70° or 80°) would not be accurately approximated, since the model would be fitted to another part where the angular gradient is weaker.

Therefore, the best solution to determine these parameters seems to be a least square approximation between the mathematical model and all the measurement results obtained in the plane of incidence.

A simplification would be to fix the refractive index to a value of 1.5 or 1.55 (glass), as it is suggested by some authors [8,64] . But this is not justified in a general sense, and the refractive index will be considered as a variable parameter in this work, even though this choice implies a much complex determination.

The "least square" function to minimize is a non-linear expression of the parameters (see eq. 4.52). This kind of optimization process raises two major problems :

- on the one hand, it requires the determination of initial values for the parameters [52]. The minimization process is then carried out until a local minimum of the function has been found: one can never be sure that the true (smallest) minimum has been reached;
- on the other hand, we should impose some constraints on the parameters (for example : n>1), which would imply a more complicated minimization procedure.

Though it is always possible to apply this classical optimization technique, another method is proposed here to evaluate the parameters. This more simple method will avoid the two problems raised above, by first assuming that, in the model (4.52) :

- the term $(1- \rho_{surf}(\theta_2))$ does not depend on the angle θ_2, for fixed values of "n" and $\left(\frac{T}{\sigma}\right)$, and for $0° \leq \theta_2 \leq 80°$;
- the factor α_s, appearing in the coherent term, is constant and comprised between 0 and 1.

Obviously, the first assumption is only a crude approximation, and it will be left in the following. It is justified by the relative uniformity of the factor $(1- \rho_{surf}(\theta))$, which has been computed in table 4.4. It is shown that this assumption should be verified, after the determination of the parameters : this is particularly the case if the optimum parameter $\left(\frac{T}{\sigma}\right)$ is less than 1, or for high values of the parameters (α_s or α_{sc}).

Table 4.4 : Value of $(1- \rho_{surf}(\theta))$ calculated by (4.54) with $\alpha_s=0$ and $\alpha_{sc}=1$

	angle θ (degrees)					0≤ θ≤80°
	0	20	40	60	80	Deviation
$\left(\frac{T}{\sigma}\right)=0.5$:						
n=1.1	0.998	0.998	0.997	0.995	0.980	±1.0%
n=1.5	0.960	0.961	0.955	0.920	0.760	±12.%
n=2.0	0.892	0.895	0.880	0.791	0.398	±38.%
$\left(\frac{T}{\sigma}\right)=2$:						
n=1.1	0.996	0.996	0.994	0.989	0.972	±1.2%
n=1.5	0.933	0.928	0.910	0.879	0.830	±5.8%
n=2.0	0.818	0.805	0.766	0.711	0.667	±10.%
$\left(\frac{T}{\sigma}\right)=5$:						
n=1.1	0.998	0.998	0.998	0.995	0.979	±1.0%
n=1.5	0.975	0.975	0.972	0.962	0.929	±2.4%
n=2.0	0.931	0.931	0.931	0.925	0.899	±1.7%

The second assumption is justified by the discussion on the equation (4.53). A simplified transition between the characteristic values of α_s (0 and 1) is accepted. This simplification implies a constant value of α_s which will allow, for some materials, to reduce the deviations between the measurements and the model (4.52).

Once these assumptions have been adopted, the following expression can be written. It is valid in the plane of incidence and for $\theta_1 \neq \theta_2$ (see 4.38 and 4.52) :

$$\Delta\beta_e(\theta_1,\theta_2) = \beta_e(\theta_1,\theta_2) - \beta_e(\theta_1,0)$$

$$= \alpha_{sc}\left(R^2\left(n, \left|\frac{\theta_1+\theta_2}{2}\right|\right) F\left(\theta_1,\theta_2, \frac{T}{\sigma}\right) - R^2\left(n, \frac{\theta_1}{2}\right) F\left(\theta_1,0, \frac{T}{\sigma}\right)\right)$$

$$= \alpha_{sc}\, D\left(\theta_1,\theta_2,n, \frac{T}{\sigma}\right)$$

with : $R^2(n, \theta) = \frac{|R_s(n, \theta)|^2+|R_p(n, \theta)|^2}{2}$

$$F\left(\theta_1,\theta_2, \frac{T}{\sigma}\right) = \frac{C(\theta_1)\, C(\theta_2)}{\cos\theta_1 \cos\theta_2} \frac{1}{\cos^4\alpha} e^{-\frac{T^2}{4\sigma^2} tg^2\alpha}, \quad \alpha = \left(\frac{\theta_1-\theta_2}{2}\right)$$

(4.55)

In this expresion, the angle θ_2 is positive in the half-plane containing the specular direction and negative in the other half-plane.

In the specular direction ($\theta_1 = \theta_2$), the expression (4.55) is not complete, since the coherent term has been omitted. In fact, this direction will not be taken into account during the comparison between calculated and measured luminance factors, because :

- on the one hand, the calculated luminance factor can reach infinite values, and this of course raises an important mathematical problem;
- on the other hand, the measurement procedure described in chapter 3 is not accurate in the specular direction.

The direction of incidence ($\theta_2 = -\theta_1$) will also be omitted, since the measurement of the luminance factor is here impossible (see chapter 3).

Let $\beta_{eM}(\theta_1,\theta_2)$ be the measured value of the luminance factor. The optimum value of the parameter α_{sc} will minimize the following expression :

$$\Delta_1 = \sum_{i,\ j} \left(\frac{\beta_{eM}(\theta_{1i},0) + \alpha_{sc}\ D\ \left(\theta_{1i},\theta_{2j},n,\ \frac{T}{\sigma}\right) - \beta_{eM}(\theta_{1i},\theta_{2j})}{\beta_{eM}(\theta_{1i},\theta_{2j})} \right)^2$$

θ_{1i} = 10°, 20°, ..., 80° ($\theta_{1i} \neq 0°$)

θ_{2j} = -70°, -60°, ..., -10°, +10°, ..., +70° (see footnote[8])

$\theta_{2j} \neq \pm\theta_{1i}$ (4.56)

The interest of this first step, i.e. the minimization of (4.56), is to reduce the number of parameters from five to three (α_{sc}, n, and $\frac{T}{\sigma}$). Let $D_{i,j} = D\left(\theta_{1i},\theta_{2j},n,\ \frac{T}{\sigma}\right)$. The optimum value of the parameter $\overset{*}{\alpha}_{sc}$ is (for fixed "n" and $\frac{T}{\sigma}$) :

$$\overset{*}{\alpha}_{sc} = \frac{\displaystyle\sum_{i,\ j} \frac{\left(\beta_{eM}(\theta_{1i},\theta_{2j}) - \beta_{eM}(\theta_{1i},0)\right) D_{i,j}}{\beta^2_{eM}(\theta_{1i},\theta_{2j})}}{\displaystyle\sum_{i,\ j} \frac{D^2_{i,j}}{\beta^2_{eM}(\theta_{1i},\theta_{2j})}} \qquad (4.57)$$

The minimum value of the deviation Δ_1(eq. 4.56), corresponding to $\overset{*}{\alpha}_{sc}$, must then be analysed as a function of the two other parameters (n , $\frac{T}{\sigma}$). This will be done at some sampled value of n and $\left(\frac{T}{\sigma}\right)$, in the following intervals : $1.1 \leq n \leq 2$ and $2 \leq \frac{T}{\sigma} \leq 25$. The optimum values $\overset{*}{n}$ and $\left(\frac{T}{\sigma}\right)^*$ are those which minimize Δ_1 : this will be illustrated by an example later.

It remains to determine the parameters α_s and ρ_d in the model (4.52). At this moment, the first assumption concerning (1- $\rho_{surf}(\theta_2)$) is left, and this term is again dependent on θ_2 and α_s. The minimization process is the following :

---

[8] Most samples of materials have been measured up to a viewing angle of 70°. If the term (1- $\rho_{surf}(\theta_2)$) exhibits significant variations, this would not be in accordance with the first assumption. Then, the viewing angle θ_{2j} could be limited to another value, less than 70° : $|\theta_{2j}| \leq \theta_{max} < 70°$.

•) the value of α_s is fixed between 0 and 1, and this is repeated every 0.1 step;

•) the surface reflection factor $\rho_{surf}(\theta)$ is calculated every 10° by numerical integration, as it is described in (4.54);

•) the following deviation must be minimized, with respect to ρ_d :

$$\Delta_2 = \sum_{i,j} \left(\frac{V_{ij} + \rho_d\ W_{ij} - \beta_{eM}(\theta_{1i},\theta_{2j})}{\beta_{eM}(\theta_{1i},\theta_{2j})} \right)^2$$

θ_{1i} = 0°, 10°, ..., 80°

θ_{2j} = -70°, -60°, ..., +70°

$\theta_{2j} \neq \pm\ \theta_{1i}$

with :

$$V_{ij} = \overset{*}{\alpha}_{sc}\ R^2\left(\overset{*}{n}, \left|\frac{\theta_{1i}+\theta_{2j}}{2}\right|\right) F\left(\theta_{1i},\theta_{2j}, \left(\frac{T}{\sigma}\right)^*\right)$$

$$W_{ij} = (1-\rho_{surf}(\theta_{1i}))(1-\rho_{surf}(\theta_{2j})) \qquad (4.58)$$

and this leads to the optimum value of ρ_d :

$$\overset{*}{\rho}_d = \frac{\displaystyle\sum_{i,j} \frac{\left(\beta_{eM}(\theta_{1i},\theta_{2j}) - V_{ij}\right) W_{ij}}{\beta^2_{eM}(\theta_{1i},\theta_{2j})}}{\displaystyle\sum_{i,\ j} \frac{W^2_{ij}}{\beta^2_{eM}(\theta_{1i},\theta_{2j})}} \qquad (4.59)$$

The optimum value of α_s is the one which minimizes the deviation Δ_2 for $\rho_d = \overset{*}{\rho}_d$.

4.4.3. Example of the determination of the parameters

This example will illustrate the principles which have been defined in the previous section (§4.4.2).

Sample of plywood

The measured luminance factors are shown in table 4.5. They are expressed in relative units, the 100% value being attributed to the measurement at $\hat{i}=40°$ and $\hat{o}=0°$. The absolute value of the luminance factor has been determined for this particular geometry ($\hat{i}=40°$, $\hat{o}=0°$) by a simultaneous measurement of luminance and illuminance (see §3.5.1) : the value of 0.391 has been found.

It can be observed in table 4.5 that the measurement is possible in the specular direction for this sample, since the value of the luminance factor is not infinite. Therefore, the coherent surface reflection term is expected to vanish ($\alpha_s = 0$). This is corroborated by the fact that no clear image of the source is visible on the material sample, even at grazing incidence (80°).

Table 4.5 : Luminance factor of a sample of plywood, measured for several angles of incidence ("inc" in degrees) and several viewing angles ("obs" in degrees). The value 100% corresponds to β_V=0.391.

obs/inc	0	10	20	30	40	50	60	70	80
-70.0	98.1	93.1	90.1	90.3	92.7	97.2	106.0*******		138.1
-60.0	99.6	92.6	88.7	90.0	91.1	94.7*******		106.0	117.7
-50.0	98.9	92.3	89.7	89.2	90.9*******		94.7	97.2	107.1
-40.0	100.0	95.1	90.4	90.4*******		90.9	91.1	92.7	100.7
-30.0	105.4	97.0	93.9*******		90.4	89.2	90.0	90.3	96.9
-20.0	112.4	105.3*******		93.9	90.4	89.7	88.7	90.1	96.3
-10.0	128.3*******		105.3	97.0	95.1	92.3	92.6	93.1	96.3
.0	*******	128.3	112.4	105.4	100.0	98.9	99.6	98.1	100.7
10.0	122.3	136.1	127.0	116.1	111.3	109.9	108.2	106.9	114.3
20.0	107.4	122.3	137.6	133.9	127.8	124.4	123.1	125.0	131.3
30.0	100.7	109.8	128.8	151.4	150.2	146.1	149.3	149.0	150.0
40.0	94.4	104.7	120.8	144.6	173.5	179.8	180.7	181.0	186.4
50.0	92.7	102.4	118.0	139.8	171.9	218.7	224.8	233.1	245.9
60.0	91.8	101.5	117.0	137.0	171.2	220.9	305.0	332.9	375.5
70.0	91.0	100.7	113.7	136.4	169.6	219.6	321.3	569.9	744.9

The first step of the optimization process consists in the derivation of the parameters α_{sc}^*, n^* and $\left(\frac{T}{\sigma}\right)^*$. This is performed by a calculation program called "fctref", which has been conceived for this application.

The minimum value of Δ_1(eq. 4.56), corresponding to α_{sc}^*, has been calculated for several pairs $(n, \frac{T}{\sigma})$. The results of this first study are shown in table 4.6 : they are expressed by the mean deviation $100\sqrt{\frac{\Delta_1}{n_{ij}}}$ (%), where n_{ij} is the total number of comparisons involved in (4.56). A minimum (7.32%) clearly appears at n=2.9 and $\frac{T}{\sigma}$ = 6.5. A more detailed analysis would lead to the following optimum values :

$$n^* = 2.9$$
$$\left(\frac{T}{\sigma}\right)^* = 6.60$$
$$\alpha_{sc}^* = 0.645$$

Note : The optimum parameter n^* which has been determined by this process is the one which minimizes the deviations between a mathematical model and measured luminance factors. It is not pretended here that this is the refractive index of the plywood sample, though the theoretical developments leading to the model (4.52) were based on this physical concept. The possible correspondence between this value of the optimum parameter and the value of the refractive index (which could be measured by other optical methods) will not be considered in this work. The same remark can be done for the parameter $\frac{T}{\sigma}$ which also derives from a physical concept.

Table 4.6 : Mean deviations Δ_1 (defined in the text), calculated for several values of the parameters "n" and $\frac{T}{\sigma}$ ("tsig"), and for the sample of plywood.

n/tsig	.50	1.50	2.50	3.50	4.50	5.50	6.50	7.50	8.50	9.50
1.500	28.68	28.70	24.51	18.07	14.80	14.12	14.61	15.49	16.44	17.34
1.700	28.69	28.70	26.08	18.66	13.64	11.90	12.05	12.96	14.06	15.13
1.900	28.69	28.70	27.06	19.43	13.17	10.42	10.14	11.04	12.26	13.48
2.100	28.69	28.70	27.66	20.16	13.12	9.53	8.83	9.69	11.01	12.35
2.300	28.70	28.70	28.02	20.79	13.27	9.09	8.01	8.82	10.21	11.64
2.500	28.70	28.70	28.25	21.30	13.51	8.92	7.56	8.32	9.75	11.22
2.700	28.70	28.70	28.39	21.71	13.77	8.93	7.36	8.06	9.51	11.01
2.900	28.70	28.70	28.48	22.04	14.01	9.01	7.32	7.97	9.42	10.93
3.100	28.70	28.70	28.54	22.31	14.24	9.14	7.36	7.97	9.41	10.92
3.300	28.70	28.70	28.58	22.52	14.44	9.28	7.44	8.02	9.45	10.95

The second step of the optimization process consists in the derivation of the remaining parameters (ρ_d^* and α_s^*), through equation (4.59). The value of ρ_d^* = 0.400 is obtained for α_s= 0. The table 4.7 shows the optimum values of Δ_2(4.58), for α_s comprised between 0 and 1. It is indeed observed that the value α_s= 0 corresponds to the minimum deviation between the model and the

measurements. So, the optimization process and the visual observation come to the same conclusion, that the coherent surface reflection term must vanish for this sample.

Table 4.7 : Mean deviations Δ_2 (defined in the text), calculated for several values of the parameter α_s, and for the sample of plywood.

α_s	0	0.1	0.2	0.3	0.4	0.5	0.6	0.7	0.8	0.9	1
ρ_d^*	0.40	0.42	0.45	0.47	0.50	0.54	0.57	0.61	0.65	0.70	0.75
Mean Δ_2 (%)	7.91	8.30	8.74	9.21	9.73	10.3	10.9	11.6	12.4	13.2	14.0

It can be verified that the factor $(1-\rho_{surf}(\theta))$ is approximately constant (±0.2%) for $|\theta| \leq 70°$. The direct comparison between the model and the measurements is illustrated in table 4.8, and in figure 4.20. The results obtained by the model (4.52) are fairly good. Indeed, the relative deviation is less than 20%, except in three geometrical configurations (î=80°, ô= -70°, -60° and +20°). The mean deviation is about 5%.

Table 4.8 : Deviations (%) between the measured luminance factors and the model (4.52) described by the optimum values of the parameters. Sample of plywood. The angles of incidence ("inc") and viewing ("obs") are expressed in degrees.

obs/inc	0	10	20	30	40	50	60	70	80
-70.0	5.5	1.5	1.7	1.5	1.2	5.6	13.3	.0	33.7
-60.0	4.4	.2	3.4	1.9	.7	3.0	.0	13.3	22.2
-50.0	1.0	2.3	2.8	2.8	.8	.0	3.0	5.6	14.6
-40.0	6.8	3.6	4.0	1.9	.0	.8	.7	1.2	9.2
-30.0	9.1	8.5	4.4	.0	1.9	2.8	1.9	1.5	5.8
-20.0	9.3	7.8	.0	4.4	4.0	2.8	3.4	1.7	5.2
-10.0	.1	.0	7.8	8.5	3.6	2.3	.2	1.5	5.2
.0	.0	.1	9.3	9.1	6.8	1.0	4.4	5.5	9.2
10.0	5.0	3.3	3.0	8.5	6.5	.1	5.4	9.6	18.5
20.0	14.4	6.9	1.5	1.7	3.6	.7	5.5	14.0	23.7
30.0	14.2	14.8	5.7	5.3	2.5	1.1	7.2	12.8	19.7
40.0	13.1	13.2	9.6	1.2	8.9	7.7	6.5	7.0	11.2
50.0	7.7	7.5	6.2	3.4	3.5	14.4	7.9	2.5	2.6
60.0	3.7	.8	.6	1.1	1.3	6.2	16.8	5.3	9.7
70.0	1.9	4.0	5.4	4.7	.8	3.5	1.9	19.9	2.7

Ecart moyen : 6.00 %
Ecart moyen (sans speculaire) : 5.77 %
Ecart maximum : 33.72 %

The influence of the surface reflection contribution is clearly observed, even at an angle of incidence of 20°, with a maximum luminance factor of 0.53. Obviously, this influence is more significant at 80°. This is due to the factor $\frac{1}{\cos\theta_2}$ and to the Fresnel reflection factor which, for $n^* = 2.9$, rises from R^2=0.238 at an incidence of 20° to R^2=0.433 at 80°.

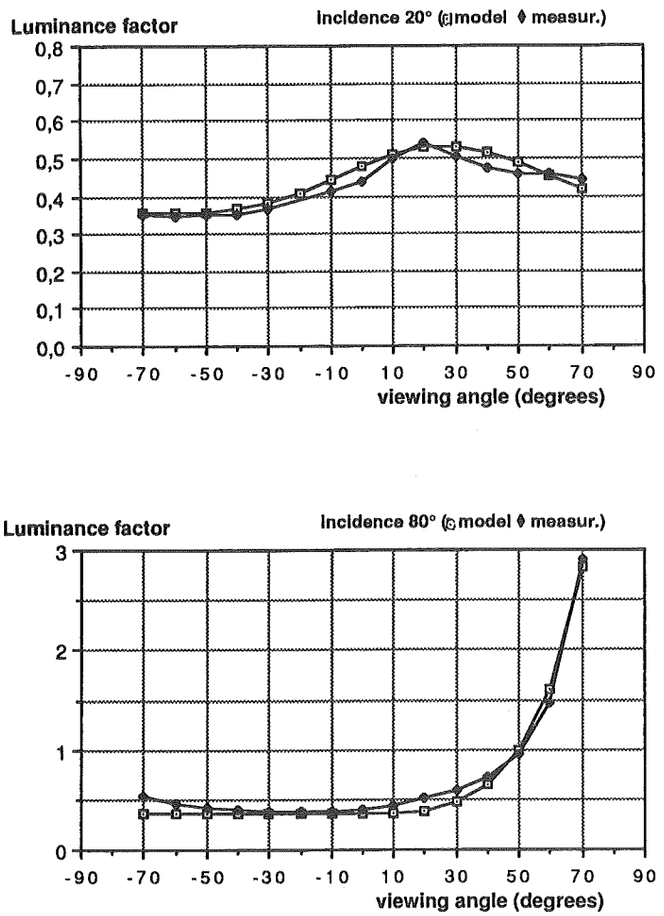

Figure 4.20 : Sample of plywood : comparison between the measured luminance factors and the model (4.52).

White sheet of paper

This sheet of paper has been fixed on a sample of agglomerated wood. All the measurement results are given in appendix 3.2. It must be observed that the coherent surface reflection term is again unsignificant for this sample (no image of the source).

The program "fctref" gives the following optimum parameters :

$$n^* = 1.87$$
$$\left(\frac{T}{\sigma}\right)^* = 6.22$$
$$\alpha_{sc}^* = 1.468$$
$$\rho_d^* = 0.950$$
$$\alpha_s^* = 0$$

It can be verified that the factor $(1-\rho_{surf}(\theta))$ is approximately constant (±2.0%) for $|\theta| \leq 70°$. The direct comparison between the model and the measurements is illustrated in table 4.9, and in figure 4.21. The correspondence is even better than for the plywood sample : the mean deviation is less than 3% and the maximum deviation is only 21% ($\hat{i}$=70° and $\hat{o}$=70°). This is considered as a very good result, more especially as the measured specular values are taken into account, though they are not involved in the optimization process. If they are excluded from the comparison, the maximum deviation is only 14% !

Table 4.9 : Deviations (%) between the measured luminance factors and the model (4.52) described by the optimum values of the parameters. White sheet of paper. The angles of incidence ("inc") and viewing ("obs") are expressed in degrees.

obs/inc	0	10	20	30	40	50	60	70	80
-70.0	.3	.9	.2	1.5	.4	1.1	1.9	.0	13.6
-60.0	1.1	1.2	.6	.4	.7	.7	.0	1.9	9.5
-50.0	.4	.2	1.9	.7	.4	.0	.7	1.1	6.3
-40.0	2.3	.4	.2	1.0	.0	.4	.7	.4	3.8
-30.0	1.1	.2	.9	.0	1.0	.7	.4	1.5	4.7
-20.0	1.8	1.2	.0	.9	.2	1.9	.6	.2	.4
-10.0	1.1	.0	1.2	.2	.4	.2	1.2	.9	1.4
.0	.0	1.1	1.8	1.1	2.3	.4	1.1	.3	2.7
10.0	.9	.6	.7	4.0	2.2	.2	.8	.1	11.7
20.0	2.7	.2	.7	1.1	2.1	2.8	2.7	6.9	10.6
30.0	2.6	5.8	1.1	1.1	1.9	3.0	1.6	4.1	8.9
40.0	4.9	3.7	3.0	2.3	2.5	4.4	1.0	.5	1.3
50.0	2.7	2.2	4.6	3.5	3.5	9.6	5.3	2.1	8.3
60.0	2.1	3.3	3.1	.5	.4	5.1	13.5	5.1	12.4
70.0	4.7	2.2	.1	1.3	2.9	4.5	3.8	20.8	11.3

Ecart moyen : 2.64 %
Ecart moyen (sans speculaire) : 2.39 %
Ecart maximum : 20.81 %

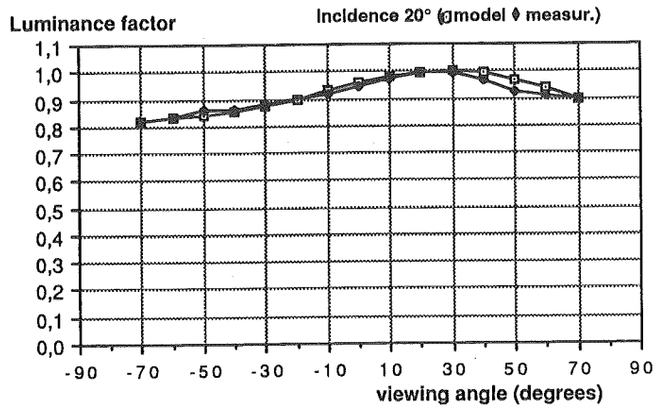

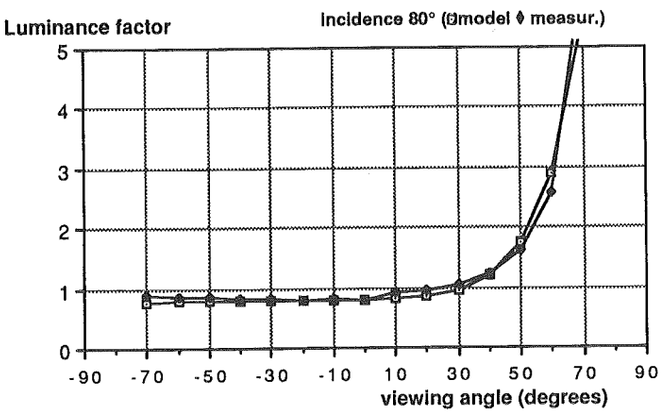

Figure 4.21 : White sheet of paper on agglomerated wood : comparison between measured luminance factors and the model (4.52).

Opaline glass sample

This sample has already been analysed (see table 4.2), since it has been used to derive the model for volume reflection.

The image of the source clearly appears in the specular direction. In this direction, the measurement cannot be performed, since the luminance of the sample is too high. The measurement is also very sensitive to any variation of the angles $\hat{i}$ and $\hat{o}$. These observations confirm the existence of the coherent surface reflection term : $\alpha_s \neq 0$.

However, the incoherent term is unsignificant, since the surface is plane. Indeed, the results given in table 4.2 don't show any significant increase of the luminance factor around the specular direction.

Therefore, the introduction of the parameter α_s in the model (4.52) is very important. Not to attribute an accurate value of the luminance factor in the specular direction : in fact, this value is of little interest, since neither the measurement, nor the model, are significant in this direction. However, the influence of α_s on the factor $(1-\rho_{surf}(\theta))$ is important, since it represents the decreasing of the luminance factor when $\hat{i}$ and/or $|\hat{o}|$ approach 80°. If there were no coherent term (with α_s), the model would reduce to the Lambert law for $\hat{o} \neq \hat{i}$ and, obviously, it would not be sufficiently accurate : see fig. 4.17.

Finding the optimum value of the parameters with the program "fctref" is here particularly difficult. Indeed, there is no optimum value for n^* and $\left(\frac{T}{\sigma}\right)^*$, since all pairs $(n, \frac{T}{\sigma})$ lead to the same minimum deviation Δ_1(eq. 4.56), for $\alpha_{sc}^* = 0$. Therefore, a realistic value has to be chosen, such as, for example, the refractive index of glass n^*=1.52. This value cannot be undefined, since it will influence the factor $(1-\rho_{surf}(\theta))$. The optimum parameters are :

$n^* = 1.52$
$(\frac{T}{\sigma})^* =$ undefined
$\alpha_{sc}^* = 0$
$\rho_d^* = 0.472$
$\alpha_s^* = 1$

It can be verified that the factor $(1-\rho_{surf}(\theta))$ is approximately constant (±11%) for $|\theta| \leq 70°$. The mean deviation between the model and the measurements is 2.8% (excluding the specular direction) and the maximum deviation is 15% (at $\hat{i}$=80° and $\hat{o}$=60°).

White opaline plastic sample

From the visual observation of the illuminated sample, a significant coherent surface reflection term can also be expected. Furthermore, the measurements have detected a weak, but significant, incoherent term (see appendix 3.2 and figure 4.22 at 80°).

As it was the case for the opaline glass sample, there is no minimum value of Δ_1, which would be necessary to derive optimum values for n^* and $\left(\frac{T}{\sigma}\right)^*$. The refractive index of most plastic materials can be estimated at 1.5, and this value is attributed to n^*. So, the optimum values of the parameters are :

$n^* = 1.50$
$\left(\frac{T}{\sigma}\right)^* = 9$
$\alpha_{sc}^* = 0.181$
$\rho_d^* = 0.598$
$\alpha_s^* = 1$

These values are in agreement with the visual and experimental observations, since the surface reflection has a weak incoherent contribution ($\alpha_{sc}^* \neq 0$) and a significant coherent term ($\alpha_s^* = 1$).

It can be verified that the factor $(1-\rho_{surf}(\theta))$ is approximately constant (±12%) for $|\theta| \leq 70°$. The mean deviation between the model and the measurements is 6.2% (excluding the specular direction) : see table 4.10 and figure 4.22.

Table 4.10 : Deviations (%) between the measured luminance factors and the model (4.52) described by the optimum values of the parameters. White opaline plastic sample. The angles of incidence ("inc") and viewing ("obs") are expressed in degrees.

obs/inc	0	10	20	30	40	50	60	70	80
-70.0	6.1	.2	5.6	10.0	1.2	1.8	10.3	.0	17.2
-60.0	2.1	5.5	7.5	2.1	.7	5.4	.0	10.3	7.7
-50.0	4.7	6.4	2.6	.2	3.9	.0	5.4	1.8	10.5
-40.0	5.3	2.8	1.2	1.6	.0	3.9	.7	1.2	11.9
-30.0	1.9	1.4	.8	.0	1.6	.2	2.1	10.0	4.3
-20.0	2.4	1.9	.0	.8	1.2	2.6	7.5	5.6	6.4
-10.0	9.4	.0	1.9	1.4	2.8	6.4	5.5	.2	11.5
.0	.0	9.4	2.4	1.9	5.3	4.7	2.1	6.1	7.7
10.0	14.6	.0	6.3	2.6	3.4	1.6	5.1	5.4	24.5
20.0	4.5	15.2	.0	5.8	1.7	1.1	2.4	10.0	12.0
30.0	.5	2.8	15.8	.0	6.9	.7	4.1	4.9	9.3
40.0	3.5	.8	4.1	17.4	.0	7.0	2.0	4.3	8.8
50.0	3.0	1.6	1.3	7.0	29.2	.0	12.7	2.3	15.8
60.0	1.8	1.3	.3	3.0	11.2	35.6	.0	28.8	4.4
70.0	1.7	1.3	.8	1.7	5.0	13.2	48.0	.0	14.7

Ecart moyen : 6.18 %
Ecart moyen (sans speculaire) : 6.18 %
Ecart maximum : 48.01 %

It is quite difficult here (for the optimization process) to accurately modelize the incoherent surface reflection contribution : indeed, the maximum deviation (48% at $\hat{i}$=60° and $\hat{o}$=70°) and, more generally, the greatest deviations between the measurements and the model, can be found around the specular direction. The deviations observed at ($\hat{i}$=80°) are probably due to measurements errors, since the oscillations of the measured luminance factor (fig. 4.22) do not seem to have any other physical meaning.

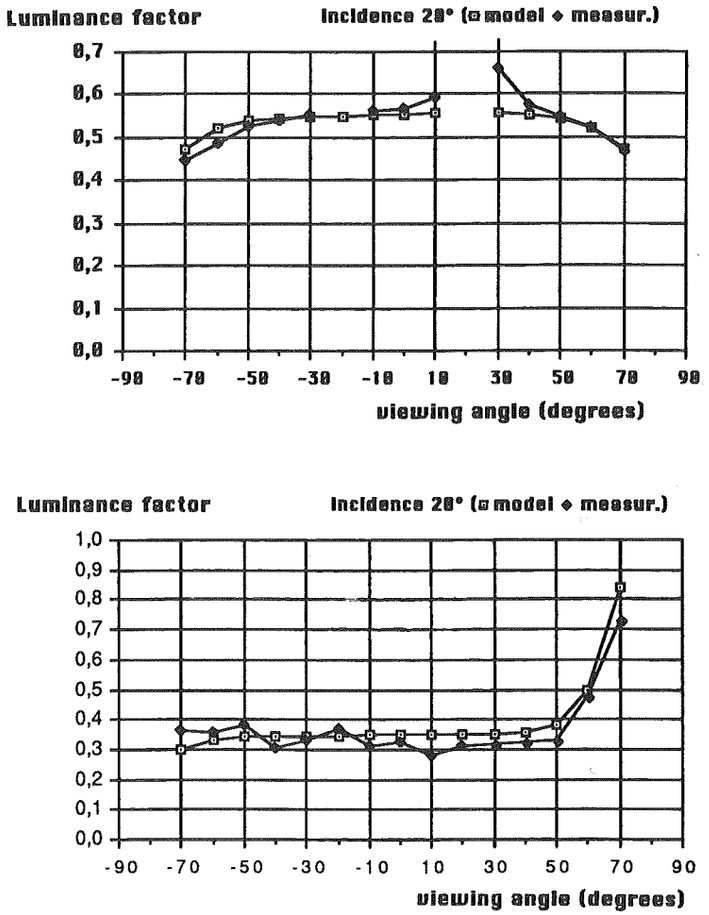

Figure 4.22 : White opaline plastic sample : comparison between the measured luminance factors and the model (4.52).

The main conclusion that can be drawn from this example is that it is difficult to attribute a value to the parameter n^*, for the samples with a plane surface. The same behaviour has been observed for a wall tile sample. A local minimum of Δ_1(4.56) was found in the vicinity of ($\frac{T}{\sigma}$ = 0.04), which is not a realistic value since the surface is plane. Furthermore, this minimum was not very sharp. By fixing n^*=1.5, a satisfying solution was derived, with α^*_{sc}=0 and $\left(\frac{T}{\sigma}\right)^*$ undefined (mean deviation of 3.2% and maximum deviation of 23%).

Keramics sample (used as wall pavement in a tunnel)

The measured luminance factors have been illustrated in §3.5.2 (fig. 3.22). They are also given in the appendix 3.2.

This is a first example for which the optimum value of the parameter α^*_s is comprised between 0 and 1. The visual inspection of the illuminated sample is already not convincing, concerning the existence of an image of the source : in fact, the image which is detected is rather fuzzy. Moreover, the measured luminance factor in the specular direction has a high, but finite value : the measurement is still possible.

It is surprising that this uncertainty is also found in the evaluation of the optimum value of the parameter α^*_s. In the case of the keramics sample, this value is α^*_s = 0.4.

The results of the model are again very good : the mean deviation between the model and the measurements is only 2.5% (excluding the specular values) and the maximum deviation is 16% ($\hat{i}$=80°, $\hat{o}$=0°) : see figure 4.23.

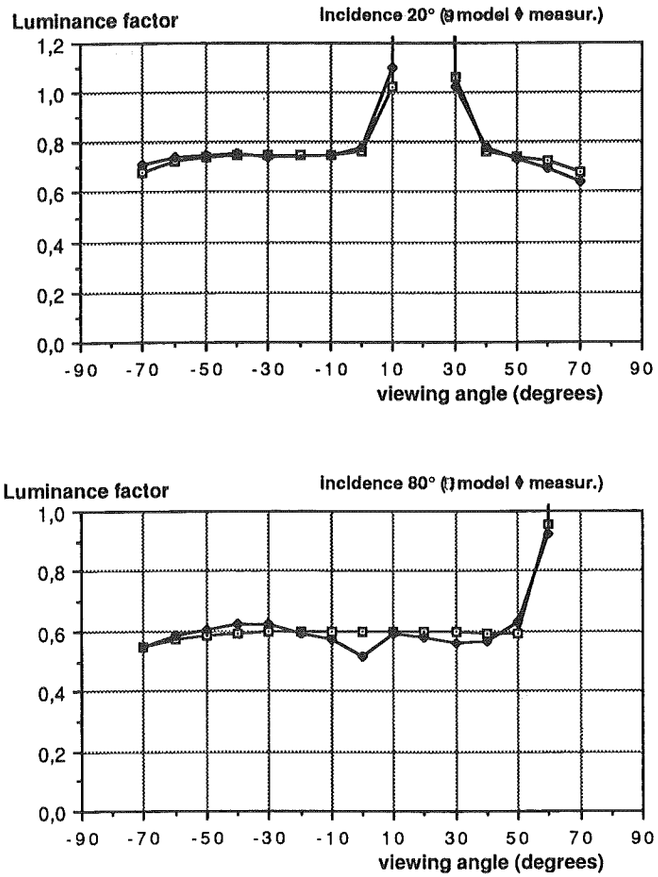

Figure 4.23 : Keramics sample : comparison between the measured luminance factors and the model (4.52).

The same behaviour has been observed for a laminated wood panel : $\alpha^{*}_{s}=0.2$.

Concrete block

This sample has an original behaviour : it is illustrated in figure 4.24. The luminance factor of the concrete block is approximately constant for all viewing angles, except at the negative grazing angles where it significantly increases. This behaviour is more accentuated, as the angle of

incidence increases. Of course, at grazing incidence, the luminance factor also increases at the positive viewing angles.

A significant retroreflection effect can then be observed at grazing incidence. This phenomenon, which has been detected by the measurement of the luminance factor, can also be detected by visual inspection of the illuminated sample. If it is assumed that luminance is correlated with perceptual brightness, then a significant decrease of the luminance can be observed from $\hat{o}$=-80° to $\hat{o}$=0°, and also from $\hat{o}$=80° to $\hat{o}$=0°.

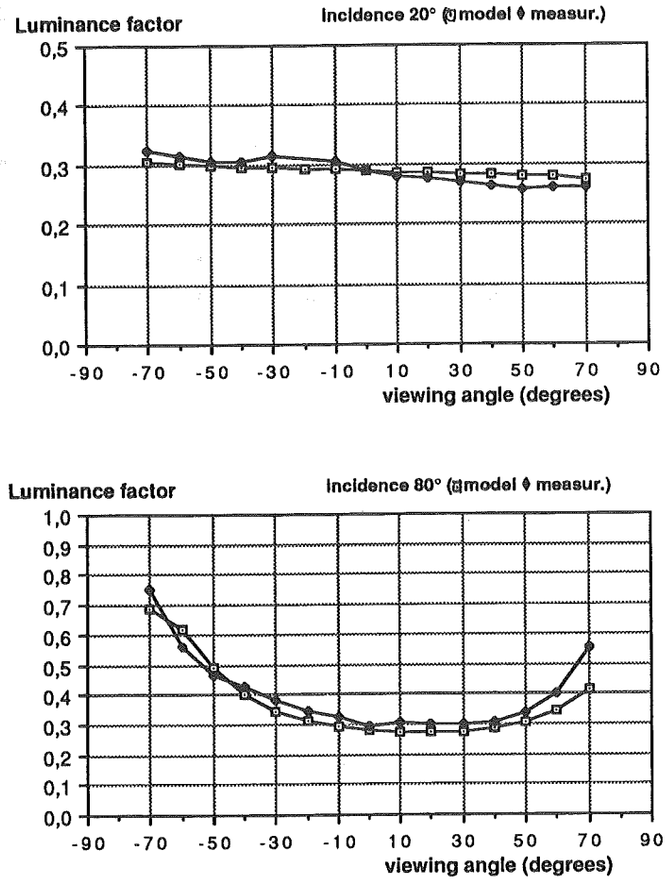

Figure 4.24 : Concrete block : comparison between the measured luminance factors and the model (4.52).

It is interesting to examine if the model (4.52) can take this particular behaviour into account.

The optimum value of the parameter $\frac{T}{\sigma}$ is less than 2.83, which means that the surface reflection contribution has two maxima outside the specular zone (see fig. 4.5) : this is well in accordance with the measured values (figure 4.24). The optimum values of the parameters are:

$$n^* = 1.26$$
$$\left(\frac{T}{\sigma}\right)^* = 0.75$$
$$\alpha_{sc}^* = 2.079$$
$$\rho_d^* = 0.283$$
$$\alpha_s^* = 0$$

The table 4.11 and the figure 4.24 again illustrate the satisfying performance of the model.

Table 4.11 : Deviations (%) between the measured luminance factors and the model (4.52) described by the optimum values of the parameters. Concrete block. The angles of incidence ("inc") and viewing ("obs") are expressed in degrees.

obs/inc	0	10	20	30	40	50	60	70	80
-70.0	.4	4.2	6.3	7.1	5.3	3.2	2.8	.0	7.8
-60.0	.5	2.0	4.3	5.0	8.8	11.6	.0	2.8	10.5
-50.0	.9	.5	1.9	5.5	11.4	.0	11.6	3.2	4.6
-40.0	1.5	.4	2.7	8.9	.0	11.4	8.8	5.3	6.8
-30.0	1.6	.9	6.1	.0	8.9	5.5	5.0	7.1	10.0
-20.0	.1	4.4	.0	6.1	2.7	1.9	4.3	6.3	9.7
-10.0	3.6	.0	4.4	.9	.4	.5	2.0	4.2	9.9
.0	.0	3.6	.1	1.6	1.5	.9	.5	.4	4.0
10.0	2.8	.9	2.8	3.3	3.2	4.1	2.4	3.3	10.6
20.0	1.0	3.0	4.0	4.3	5.8	4.9	6.5	.7	9.9
30.0	3.2	4.6	5.3	7.1	6.2	8.8	7.0	2.1	7.5
40.0	3.3	5.1	6.9	7.3	8.9	8.3	6.7	1.9	7.0
50.0	3.0	6.6	8.6	8.9	9.7	7.0	5.6	.9	9.0
60.0	4.0	6.0	6.3	8.6	7.4	7.8	3.4	2.8	13.6
70.0	1.6	2.7	5.6	5.5	5.3	3.2	0.0	8.8	25.3

Ecart moyen : 5.08 %
Ecart moyen (sans speculaire) : 5.04 %
Ecart maximum : 25.27 %

Conclusion of the examples

The general model for light reflection expressed by the equation (4.52) can approach the real behaviour of materials with a fairly good accuracy. The mean deviation between the measured luminance factors and the model is often less than 5%. The deviations are also usually less than

10%. The greatest deviations are observed around the specular direction and/or at grazing incidence.

The following problems have been detected :

- it is difficult to evaluate n^* for the samples with a plane surface;
- a clear understanding of the physical phenomena should allow the elimination of unrealistic solutions, such as $\frac{T}{\sigma} = 0.04$ for a smooth wall pavement.

4.4.4. Comparison with other mathematical models

It is proposed here to compare the mathematical model (4.52) with the results of other models which are more simple in their mathematical expression, to examinate if the relative complexity of the equation (4.52) and the five parameters are necessary.

Four other models will be used in this test[9] :

- the Lambert law : $\beta_v(\theta_1,\theta_2) = \rho_d$, which has been chosen because it is very simple, and still widely used in lighting applications.

- the Beckmann+Lambert model :

$$\beta_v(\theta_1,\theta_2) = \alpha_{sc} \frac{R^2\left(n, \left|\frac{\theta_1+\theta_2}{2}\right|\right)}{\cos\theta_1 \cos\theta_2} \frac{1}{\cos^4\alpha} e^{-\frac{T^2}{4\sigma^2} tg^2\alpha} + \rho_d \qquad (4.60)$$

This is a more simple expression than (4.52) with only three parameters : α_{sc}, $\frac{T}{\sigma}$ and ρ_d. The refractive index has been fixed at a value close to the index of an air/glass interface (n=1.55). Shadowing effects are not taken into account, and the volume reflection contribution is constant.

---

[9] The expressions proposed here are valid in the plane of incidence, and the viewing angle θ_2 can have negative or positive values.

- the Uetani+Matsuura model :

$$\beta_v(\theta_1,\theta_2) = \alpha_{sc} \frac{R^2\left(n, \left|\frac{\theta_1+\theta_2}{2}\right|\right)}{\cos\theta_1 \cos\theta_2} \frac{e^{-\frac{\alpha^2}{2\sigma_f^2}}}{\cos\alpha} + \rho_d \qquad (4.61)$$

The symbols are the same as in (4.60). This model is proposed in reference [64], with a gaussian distribution of the specularly oriented facets (see also equation 4.49). Three parameters are here necessary : α_{sc}, σ_f and ρ_d. The refractive index has the value n =1.55.

- the Hori+Lambert model :

$$\beta_v(\theta_1,\theta_2) = \alpha_{sc} \frac{R^2(n, \theta_1)}{\cos\theta_1 \cos\theta_2} (1 - \sin X)^{\alpha} + \rho_d$$

$$X = |\theta_2-\theta_1| \frac{90°}{90°\pm\theta_1} \text{ if } \theta_2 \lesseqgtr \theta_1 \qquad (4.62)$$

The surface reflection component is an experimental model described in reference [47]. This is also a model with three parameters α_{sc}, ρ_d and the "specularity factor" α. It must be noted that the original model contains a factor $I(\theta_1)$, appearing in equation (4.1). This factor has not been developed in the original paper. So, in order to compare this model with the others, the following assumption has been made : the surface reflection term shall have the same expression as the models (4.60) and (4.61) in the specular direction ($\theta_2=\theta_1$). This explains the introduction of the factor $R^2(n, \theta_1)$ in (4.62). The refractive index has also the value n =1.55.

These expressions have been tested on eight samples of materials, ranging from opaline glass to concrete. The parameters of each model have been determined by a least square fit with the measured luminance factors in the plane of incidence. The minimization procedure has always been illustrated in the previous section, for the model (4.52) . For the other models, the procedure is more simple since there are only three parameters (one for the Lambert law) and since the dependence is linear for two of them (α_{sc} and ρ_d).

For all models and all materials, the mean and maximum deviations (%) between the model and the measured luminance factors have been recorded, excluding the specular direction. The results of the test are summarized in figure 4.25. It can be observed that the best model is the five parameters expression (4.52). This comparison will help us to evaluate the benefit that can be obtained with this model.

Figure 4.25 : Comparison of the deviations (%) obtained with five models for light reflection, between computed and measured luminance factors in the plane of incidence. The test-samples are numbered as follows : (1) plywood , (2) white sheet of paper, (3) opaline glass, (4) opaline plastic sample, (5) wall tile, (6) laminated wood panel, (7) white wall keramics, (8) concrete block.

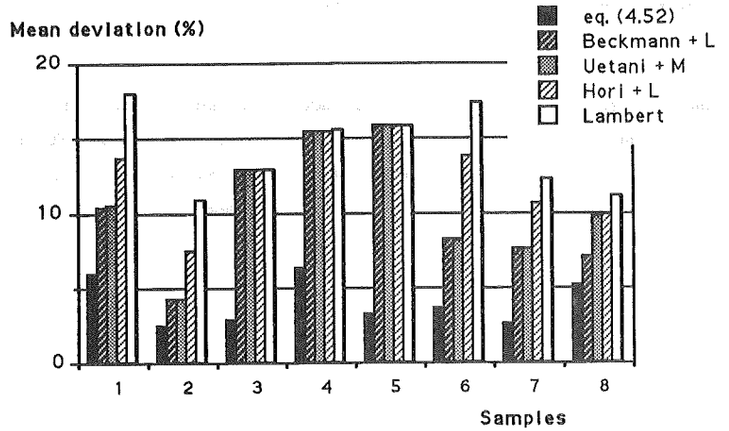

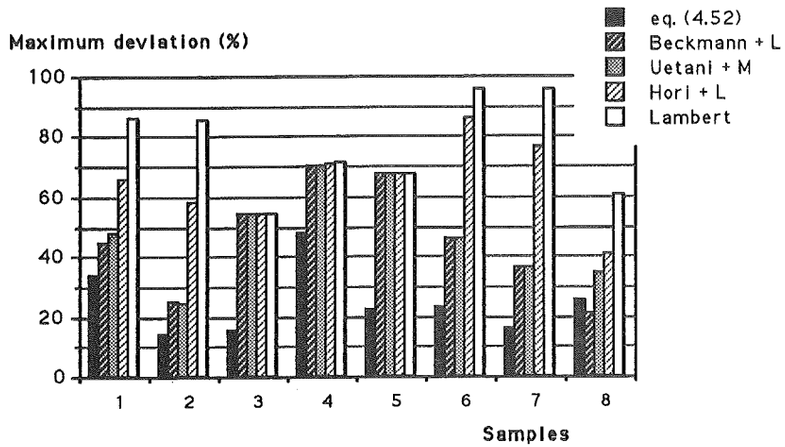

The model (4.52) is much more accurate than the Lambert law, for which the mean deviation is comprised between 10 and 20% , instead of less than 5% for the general model. This discrepancy is even more accentuated if the maximum deviations are considered. The experimental surface

model of Hori is not well suited for the materials tested, since the deviations are nearly as high as with the Lambert law.

A significant benefit can also be obtained if we compare (4.52) with the two remaining models (4.60 and 4.61). But this benefit strongly depends on the type of material. For slightly rough surfaces (samples number 3, 4 and 5 in figure 4.25), both models give the same results as the Lambert law, and the benefit is important. However, their performance increases with the magnitude of the incoherent surface reflection term.

As could be expected, it is for the very rough surfaces (like sample number 8) that the performances of all models are quite similar. It is also for this particular sample that both models (4.60) and(4.61) can be distinguished, probably because the Uetani and Matsuura model cannot represent the effect observed at grazing negative viewing angles.

Appendix 4.1. Solution of the integral (4.14)

The following integral must be solved[10] :

$$I_1 = \int_S \int e^{j \vec{v} \cdot \vec{r}'} (\vec{w} \cdot \vec{n}) \, dS \qquad (4.A1)$$

with :

$$\vec{r}' = [\, x, y, \xi(x,y) \,]$$

$$\vec{N} = \frac{\partial \vec{r}'}{\partial x} \times \frac{\partial \vec{r}'}{\partial y} \quad \text{and} \quad J = \sqrt{\vec{N} \cdot \vec{N}}$$

$$dS = J \, dx \, dy$$

$$\vec{n} = \frac{\vec{N}}{J} = \left[-\frac{\partial \xi}{J \partial x}, -\frac{\partial \xi}{J \partial y}, \frac{1}{J} \right] \qquad (4.A2)$$

Introducing (4.A2) in (4.A1) leads to :

$$I_1 = \int_{-X}^{+X} dx \int_{-Y}^{+Y} e^{j(v_x x + v_y y + v_z \xi(x,y))} \left[-w_x \frac{\partial \xi}{\partial x} - w_y \frac{\partial \xi}{\partial y} + w_z \right] dy \qquad (4.A3)$$

The first term of the integrand is developed as :

$$e^{j \vec{v} \cdot \vec{r}'} \frac{\partial \xi}{\partial x} = \frac{1}{v_z} \left(\frac{1}{j} \frac{\partial}{\partial x} \left(e^{j \vec{v} \cdot \vec{r}'} \right) - v_x \, e^{j \vec{v} \cdot \vec{r}'} \right) \qquad (4.A4)$$

A similar expression is obtained for the y-derivative of ξ . Introducing (4.A4) in (4.A3) leads to :

$$I_1 = \frac{\vec{w} \cdot \vec{v}}{v_z} \int_{-X}^{X} dx \int_{-Y}^{Y} e^{j \vec{v} \cdot \vec{r}'} dy - \frac{w_x}{j v_z} \int_{-Y}^{Y} \left[e^{j \vec{v} \cdot \vec{r}'} \right]_{-X}^{X} dy - \frac{w_y}{j v_z} \int_{-X}^{X} \left[e^{j \vec{v} \cdot \vec{r}'} \right]_{-Y}^{Y} dx \qquad (4.A5)$$

---

[10] These mathematical developments can be found in Beckmann [38].

The equation (4.14) is derived, if it is considered that the dot product $\vec{w}.\vec{v}=0$. The same calculation can be performed, replacing $\vec{w}$ by $\vec{v}$, which gives :

$$\int_S \int e^{j\vec{v}.\vec{r}'} (\vec{v}.\vec{n})\, dS =$$

$$\frac{\vec{v}.\vec{v}}{v_z} \int_{-X}^{X} dx \int_{-Y}^{Y} e^{j\vec{v}.\vec{r}'} dy \; - \frac{v_x}{jv_z} \int_{-Y}^{Y} \left[e^{j\vec{v}.\vec{r}'} \right]_{-X}^{X} dy \; - \frac{v_y}{jv_z} \int_{-X}^{X} \left[e^{j\vec{v}.\vec{r}'} \right]_{-Y}^{Y} dx \qquad (4.A6)$$

Appendix 4.2. Calculation of the cross product (4.18)

The following cross product has to be solved :

$$\vec{P_s} \times \vec{Q_s}^* = \left(R_s P_p \vec{p} + R_p (P_n \vec{n} - P_q \vec{q}) \right) \times \left(R_p Q_p \vec{p} + R_s (Q_n \vec{n} - Q_q \vec{q}) \right)^* \qquad (4.A7)$$

The definitions of $\vec{P_s}$ and $\vec{Q_s}$ are given in equations (4.8) and (4.16) respectively. Developing (4.A7) leads to :

$$\vec{P_s} \times \vec{Q_s}^* = \left(|R_s|^2 P_p Q_n^* - |R_p|^2 P_n Q_p^* \right) \vec{q} + \ldots$$

$$\ldots \left(|R_s|^2 P_p Q_q^* - |R_p|^2 P_q Q_p^* \right) \vec{n} + R_p R_s^* \left(P_q Q_n^* - P_n Q_q^* \right) \vec{p} \qquad (4.A8)$$

The unit vectors $\vec{q}$, $\vec{n}$ and $\vec{p}$ must be expressed for the specularly oriented facets. The vector $\vec{n}$ is parallel to $-\vec{v}=\vec{k_2}-\vec{k_1}$ (figure 4.4) :

$$\vec{n} = \frac{\vec{k_2}-\vec{k_1}}{2\,k\cos\delta_i} \qquad \vec{p} = \frac{\vec{k_2} \times \vec{k_1}}{k^2 \sin 2\delta_i}$$

$$\vec{q} = \vec{p} \times \vec{n} = \frac{\vec{k_2}+\vec{k_1}}{2\,k\sin\delta_i} = \frac{\vec{k_1}}{k\sin\delta_i} + \mathrm{cotg}\delta_i \vec{n} \qquad (4.A9)$$

By applying the definitions of $\vec{P}$ and $\vec{Q}$, given in equations (4.7) and (4.16), the following expressions are obtained :

$$P_q = \vec{P}.\vec{q} = \mathrm{cotg}\delta_i P_n$$

$$Q_q = \vec{Q}.\vec{q} = \mathrm{cotg}\delta_i Q_n$$

$$\vec{P_s} \times \vec{Q_s}^* = \left(|R_s|^2 P_p Q_n^* - |R_p|^2 P_n Q_p^* \right) \left(\vec{q} + \mathrm{cotg}\delta_i \vec{n} \right)$$

$$\vec{q} + \mathrm{cotg}\delta_i \vec{n} = \frac{\vec{k_2}}{k \sin\delta_i} \qquad (4.A10)$$

and, also :

$$P_n = \vec{P}.\vec{n} = \frac{\vec{P}.\vec{k_2}}{2k\cos\delta_i} =$$

$$\frac{A^+ \cos\theta_1 \sin\theta_2 \cos\phi + A^- \sin\theta_2 \sin\phi + A^+ \sin\theta_1 \cos\theta_2}{2\cos\delta_i}$$

$$Q_n = \vec{Q}.\vec{n} = \frac{\vec{Q}.\vec{k_2}}{2k\cos\delta_i} =$$

$$\frac{A^- \cos\theta_1 \sin\theta_2 \cos\phi - A^+ \sin\theta_2 \sin\phi + A^- \sin\theta_1 \cos\theta_2}{2\cos\delta_i}$$

$$P_p = \vec{P}.\vec{p} = \frac{(\vec{k_1} \times \vec{P}).\vec{k_2}}{k^2 \sin 2\delta_i} = \frac{\vec{Q}.\vec{k_2}}{k \sin 2\delta_i} = \frac{Q_n}{\sin\delta_i}$$

$$Q_p = \vec{Q}.\vec{p} = \frac{(\vec{k_1} \times \vec{Q}).\vec{k_2}}{k^2 \sin 2\delta_i} = \frac{-\vec{P}.\vec{k_2}}{k \sin 2\delta_i} = \frac{-P_n}{\sin\delta_i} \qquad (4.A11)$$

Finally :

$$\vec{P_s} \times \vec{Q_s^*} = A^2 R^2(\theta_1,\theta_2,\phi) \frac{\vec{k_2}}{k} \qquad \text{avec } A^2 = |A^+|^2 + |A^-|^2$$

$$A^2 R^2(\theta_1,\theta_2,\phi) =$$

$$\frac{|R_s|^2 |A^- \cos\theta_1 \sin\theta_2 \cos\phi - A^+ \sin\theta_2 \sin\phi + A^- \sin\theta_1 \cos\theta_2|^2}{\sin^2 2\delta_i} + \ldots$$

$$\ldots \frac{|R_p|^2 |A^+ \cos\theta_1 \sin\theta_2 \cos\phi + A^- \sin\theta_2 \sin\phi + A^+ \sin\theta_1 \cos\theta_2|^2}{\sin^2 2\delta_i}$$

$$\sin^2 2\delta_i = 1 - \cos^2 2\delta_i = 1 - \left(\frac{\vec{k_1}.\vec{k_2}}{k^2}\right)^2$$

$$= 1 - (\cos\theta_1 \cos\theta_2 - \sin\theta_1 \sin\theta_2 \cos\phi)^2 \qquad (4.A12)$$

The expression (4.A12) can be written as :

$$A^2 R^2(\theta_1,\theta_2,\phi) = \frac{|R_s|^2}{\sin^2 2\delta_i} |aA^- - bA^+|^2 + \frac{|R_p|^2}{\sin^2 2\delta_i} |aA^+ + bA^-|^2$$

$$a = \cos\theta_1 \sin\theta_2 \cos\phi + \sin\theta_1 \cos\theta_2$$
$$b = \sin\theta_2 \sin\phi \qquad (4.A13)$$

For natural polarization, the relative proportion between A^- and A^+ randomly fluctuates (see chapter 2.1.1). Therefore, the reflected intensity, which is proportional to R^2 (eq. 4.34), also fluctuates around an average value. It is this value which is representative of the reflected intensity, for a naturally polarized wave.

We introduce the angle of polarization ψ , between the fluctuating direction of vibration (or the direction of the electric vector) and the direction perpendicular to the plane of incidence, in order to calculate the mean intensity. It follows that : $A^- = A \cos\psi$ and $A^+ = A \sin\psi$. The complex amplitude "A" of the electric field is not time-dependent. However, the phase ψ randomly fluctuates between 0 and 2π, with a constant probability density function.

Replacing A^- and A^+ by their value in (4.A13) leads to[11] :

[11] Considering also that $\sin^2 2\delta_i = a^2 + b^2$: see (4.A12) and (4.A13).

$$R^2(\theta_1,\theta_2,\phi) = \frac{|R_s|^2+|R_p|^2}{2} + \frac{|R_p|^2-|R_s|^2}{2 \sin^2 2\delta_i} \left((b^2-a^2) \cos 2\psi + 2ab \sin 2\psi\right) \qquad (4.A14)$$

The first term is the mean value of this expression, whereas the second term fluctuates with ψ around a zero mean value.

The equation (4.A12) can be expressed in the plane of incidence :

$$A^2 R^2(\theta_1,\theta_2) = \frac{|R_s|^2 |A^-|^2 + |R_p|^2 |A^+|^2}{\sin^2 2\delta_i} \sin^2(\theta_1 + \theta_2)$$

$$\sin^2 2\delta_i = 1 - \cos^2(\theta_1 + \theta_2) = \sin^2(\theta_1 + \theta_2) \qquad (4.A15)$$

In this expression, θ_2 is positive for $\phi=0$ (forward scattering) and negative for $\phi=\pi$ (backward scattering). Finally, we have :

$$R^2(\theta_1,\theta_2) = \frac{|A^- R_s(\delta_i)|^2 + |A^+ R_p(\delta_i)|^2}{A^2}$$

$$\delta_i = \left|\frac{\theta_1+\theta_2}{2}\right| \qquad (4.A16)$$

Appendix 4.3. Solution of the integral (4.24)

The following integral must be solved[12] :

$$I_2 = \int_{-X}^{X} dx \int_{-Y}^{Y} dy \int_{-X}^{X} dx' \int_{-Y}^{Y} dy' \; e^{j(v_x(x-x')+v_y(y-y'))} \chi_2(v_z,-v_z)$$

$$\chi_2(v_z,-v_z) = \langle e^{jv_z(\xi-\xi')} \rangle \qquad (4.A17)$$

First, the cartesian coordinates are transformed into polar coordinates : $(x-x') = \tau \cos\omega$ and $(y-y') = \tau \sin\omega$. The equations (4.24) and (4.25) have indicated that the function χ_2 only depends on the coordinate τ. Therefore :

[12] These mathematical developments can be found in Beckmann [38].

$$I_2 = \int_{-X}^{X}\int_{-Y}^{Y}\int_{0}^{2\pi}\int_{0}^{\rho(x',y',\omega)} e^{j\tau(v_x\cos\omega+v_y\sin\omega)}\,\chi_2(v_z,-v_z,\tau)\,\tau\,d\tau\,dx'\,dy'\,d\omega \qquad (4.A18)$$

The elevations ξ and ξ' are independent random variables if the points (x,y) and (x',y') are sufficiently far from one another. Therefore, the fonction χ_2 becomes independent of τ :

$$\chi_2(v_z,-v_z) = \langle e^{jv_z\xi}\rangle \langle e^{-jv_z\xi'}\rangle = |\chi(v_z)|^2 \qquad (4.A19)$$

The integral I_2 can now be separated into two terms. The first one is :

$$I_3 = \int_{-X}^{X}\int_{-Y}^{Y}\int_{0}^{2\pi}\int_{0}^{\rho(x',y',\omega)} e^{j\tau(v_x\cos\omega+v_y\sin\omega)}\,\chi_d(\tau)\,\tau\,d\tau\,dx'\,dy'\,d\omega$$

$$\chi_d(\tau) = \chi_2(v_z,-v_z,\tau) - |\chi(v_z)|^2 \qquad (4.A20)$$

and the second one is :

$$I_4 = \int_{-X}^{X}\int_{-Y}^{Y}\int_{-X}^{X}\int_{-Y}^{Y} e^{j(v_x(x-x')+v_y(y-y'))}\,|\chi(v_z)|^2\,dx\,dy\,dx'\,dy'$$

$$= |\chi(v_z)|^2\,(4XY)^2\,\mathrm{sinc}^2(v_xX)\,\mathrm{sinc}^2(v_yY) \qquad (4.A21)$$

The integrand of (4.A20) is only significant in the vicinity of τ=0. Therefore, the upper bound of integration $\rho(x',y',\omega)$ can be extended to infinity, if the dimensions (X,Y) of the surface are much greater than the correlation length T :

$$I_3 = 4XY \int_0^{\infty} \chi_d(\tau)\,\tau\,d\tau \int_0^{2\pi} e^{j\tau(v_x\cos\omega+v_y\sin\omega)}\,d\omega \qquad (4.A22)$$

The solution of the integral in ω can be found in reference [12], and gives : $2\pi J_0(\tau\sqrt{v_x^2+v_y^2})$, with J_0 being the Bessel function of order zero. Using the notations S=4XY and $v_{xy}=\sqrt{v_x^2+v_y^2}$, the following expression is obtained :

$$I_3 = 2\pi S \int_0^{\infty} J_0(\tau\,v_{xy})\,\chi_d(\tau)\,\tau\,d\tau \qquad (4.A23)$$

The expressions (4.22) and (4.24) are now applied to the case of a normal (gaussian) rough surface :

$$\chi_d(\tau) = e^{-\sigma^2 v_z^2}\,(e^{\sigma^2 v_z^2 C} - 1)$$

$$C(\tau) = e^{-\frac{\tau^2}{T^2}} \qquad (4.A24)$$

The exponential factor can be written as :

$$e^{\sigma^2 v_z^2 C} = \sum_{m=0}^{\infty}\left(\frac{g^m}{m!}\,e^{-\frac{m\tau^2}{T^2}}\right)$$

$$g = v_z^2\,\sigma^2 \qquad (4.A25)$$

Introducing (4.A25) in (4.A24) and (4.A23) leads to :

$$I_3 = 2\pi S\,e^{-g}\sum_{m=1}^{\infty}\frac{g^m}{m!}\left(\int_0^{\infty} J_0(\tau\,v_{xy})\,\tau\,e^{-\frac{m\tau^2}{T^2}}\,d\tau\right) \qquad (4.A26)$$

The integral in (4.A26) can be found in reference [12], and gives : $\frac{T^2}{2m}\,e^{-\frac{v_{xy}^2 T^2}{4m}}$, which finally leads to :

$$I_3 = \pi S T^2\,e^{-g}\sum_{m=1}^{\infty}\left(\frac{g^m}{m\,m!}\,e^{-\frac{v_{xy}^2 T^2}{4m}}\right) \qquad (4.A27)$$

The equation (4.26) is derived, simply by adding I_3 (4.A27) to I_4 (4.A21).

Chapter 5 : Application of the general model for light reflection to the radiosity technique used in Lighting Science

5.1. Computerized lighting simulations : a short review

The use of the computer as a calculation tool in lighting applications started with a crude reproduction of the simple tabulated methods [97], such as the "Zonal-Cavity Method" [67,90,91], or the "BZ Method" used in Belgium [103]. Appropriate methods will appear only at the beginning of the 70's.

One of these methods is the finite-element method, or radiosity method. Each surface of the illuminated scene is divided into several smaller surfaces called the "finite elements", upon which some assumptions are made. For example, the illuminance or the luminance is supposed to be constant on each finite element.

The direct contributions of the light sources are first calculated on each element of surface. Then, the mutual exchange coefficients corresponding to each pair of surface elements are calculated, and this finally leads to the determination of their total illuminance (direct + reflections). The size of the finite elements must be carefully chosen : the assumptions are only valid if they are small enough, but the computing time is also higher !

In particular, the radiosity technique described by Di Laura and Mistrick [82,83,99,100] introduces an original method for calculating the direct contribution of the light sources, in developing their spatial intensity distributions as series of Fourier-Hermite polynomials.

The first applications were performed with empty rooms. However, their shape could already be rather complex. Afterwards, the illuminated spaces were modelized with their furniture, which were described as additional polygonal surfaces [76,84,116] or volumes [70,71,75]. Taking into account the furniture and complex geometries has led to hybrid methods where the radiosity and light rays techniques were combined. The light rays were used to evaluate the influence of the obstructions on the direct illuminance of any element of surface, or on the mutual light exchange between two finite elements [70,75].

Other methods are the light rays methods, also called Monte-Carlo methods. The first attempts to implement these techniques were made between 1985 and 1990 [80,88,94,110,114]. The principle is the following : each light source emits a great number of light rays (also called

"particles" by some authors), each of them carrying a part of the luminous flux of the source. The number of rays per solid angle can be constant [94] or not [110]. In the first case, the luminous flux carried by each ray is proportional to the intensity emitted by the source in this direction, whereas, in the second case, this flux is constant for each ray and the number of rays per solid angle is proportional to the intensity.

Each time the light ray reaches a surface in the room, it generates only one reflected or transmitted ray. The new direction attributed to this ray is determined from the scattering indicatrix of this surface, and the flux carried by the ray is attenuated by the absorption at the point of impact. Each time the light ray reaches a receiving surface or volume, is the contribution to the illuminance recorded.

The emission of a great number of randomly chosen light rays is statistically equivalent to a deterministic method [110]. Of course, increasing the number of rays improves the statistical accuracy of the results, but the computing time is also increased.

Image synthesis [72,73,74,76,81,95,98,109, 114] is an original method of displaying lighting calculation results : the 3D view of the simulated space is computed, with screen luminances at the monitor directly related to the calculated luminances in the real situation. The following problems have to be solved in this respect :

- the luminances must be determined in a great number of points in the space, in order to create an image with sufficient resolution;
- a satisfying correspondence between screen luminances and calculated luminances must be established [98,109].

The image synthesis is generally operated once the distribution of luminances in the lighted scene has been fully determined, either by the radiosity or the light rays techniques. The observer is fixed in the scene and the image is then constructed, pixel by pixel, each pixel representing an element of surface of the real space.

This procedure can of course be very time consuming (several hours are needed for only one image). Powerful computers are required for fast image generations or for more detailed descriptions of the real space [68,107,115].

Geometrical models are more and more sophisticated. More and more research works are dedicated to a better calculation of direct illuminances. The presentation of the calculated illuminances and luminances are also more and more attractive. So, in this context, it is surprising that the

modelization of light reflection is always lambertian and that no significant progress has been done in this field.

Therefore, it is hoped that the general model for light reflection (4.52) proposed in the preceding chapter will give new inspiration to lighting engineers, in order to develop new calculation techniques taking into account non-diffuse reflections.

In principle, ray-tracing methods can be easily adapted to account for general light reflection, once they can rely on a sufficiently accurate model. It must be noted that some programs have already been developed with imaginary scattering indicatrices.

It is proposed here to adapt the radiosity technique, in order to include the general model for light reflection (4.52). The practical influence of this adaptation on the calculated results and on the computing time will be analysed.

5.2. Adaptation of the radiosity method : the theoretical aspect

5.2.1. Assumptions

Given the location and light intensity distribution of all sources, the distribution of illuminances on all surfaces in the room must be calculated, with the following assumptions :

- the room may be of any shape, but it must be described by plane surfaces and plane obstructions. Each surface is divided into smaller surfaces called the facets;
- the light sources are punctual, and their light flux is supposed to be stable enough. Line and area sources must be divided into several equivalent point sources;
- the luminance factor is supposed to be constant on a facet, and it generally depends on the incidence and viewing directions;
- the illuminance due to interreflections is supposed to be constant on a facet : this approximation is verified if the size of the facets is small enough. Anyway, this approximation is better than the usual assumption of constant direct or total illuminance on a facet [82];

- the incidence of the interreflections on a facet is assumed to be uniformly diffuse : the opportunity of this assumption will be discussed later.

5.2.2. Determination of the radiosity equations

Consider the element of surface[1] dS_i, which belongs to the facet number "i". The illuminance due to interreflections is written as :

$$E_{ir}(dS_i) = \frac{1}{\pi} \sum_{i \neq k=1}^{N} \iint_{S_k} \left(\sum_{L} \beta(L,dS_k,dS_i)\, E_{dir}(dS_k,L) \right) CC(dS_i,dS_k)\, dS_k + \ldots$$

$$\frac{1}{\pi} \sum_{i \neq k=1}^{N} \iint_{S_k} \beta(diffus,dS_k,dS_i)\, E_{ir}(dS_k)\, CC(dS_i,dS_k)\, dS_k \qquad (5.1)$$

The first term of this expression is the contribution of the first-order reflections : $E_{dir}(dS_k,L)$ is the direct illuminance (Eclairement, in french) of the element dS_k, due to the lamp "L", and $\beta(L,dS_k,dS_i)$ is the luminance factor[2] of dS_k, for an incidence defined by the point source "L" and the viewing direction defined by the location of dS_i.

$\left(\sum_{L}\right)$ indicates that the contributions of all lamps "L" must be added. "N" is the total number of facets.

The geometrical factor $CC(dS_i,dS_k)$ is defined by (see fig. 5.1) :

$$CC(dS_i,dS_k) = \frac{\cos\theta_{ik} \cos\theta_{ki}}{r_{ik}^2} \qquad (5.2)$$

[1] The element of surface must be distinguished from the facet : the first one is infinitely small, whereas the second one has finite dimensions.

[2] In this chapter, the confusion of the luminance factor with an angle β is no more possible. So, the subscript "v" which was added to this symbol is no more reproduced here. The following developments which are established for the luminance factor, would be the same for the radiance factor, if the assumptions were identical.

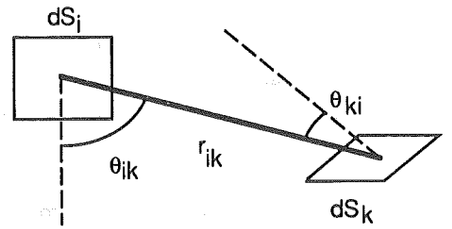

Figure 5.1 : Flux exchange between the elements of surface dS_i and dS_k . Definition of the angles θ_{ik} (between the normal to dS_i and the vector $\vec{r}_{ik}$) and θ_{ki} (between the normal to dS_k and the vector $-\vec{r}_{ik}$). The distance between the elements is noted r_{ik}.

The second term of the expression (5.1) is the contribution of higher order reflections (>1). It is also the contribution of the indirect illuminances $E_{ir}(dS_k)$. Now, the opportunity of the last assumption of (§ 5.2.1) clearly appears : without this assumption would the second term of (5.1) be replaced by an infinite sum of terms, each of them corresponding the contribution of reflections of a given order (from the second order to infinity).

This problem does not arise if all surfaces in the room are supposed to be diffuse. Indeed, the classical Lambert law imposes that the luminance factor of dS_k is equal to the reflection factor (ρ_k) of the facet number "k", whatever the incidence of light may be. The equation (5.1) is then greatly simplified. Therefore, the introduction of a general (non-lambertian) reflection implies :

- on the one hand, more complex equations, mainly for the contributions of the first-order reflections;
- on the other hand, an assumption on the incidence of the interreflections.

This assumption is discussed in an appendix to this thesis. It is shown that it can be verified in usual lighted scenes, where the proportion of "glossy surfaces"[3] is limited. Of course, the distribution of wall luminances which creates the indirect illuminance of dS_k is not uniform. However, it does not exhibit excessive variations.

For example, the assumption would not be verified in the extreme case of only one luminous wall element on a black surround. The case of several discrete luminous wall elements on a black surround is also not propitious to the assumption. This situation could happen in the metallic

[3] What is called a "glossy surface" is a surface which exhibits a significant coherent specular reflection.

reflector of a luminaire[4] : the luminous wall elements would correspond to the locations of the image sources. However, in this particular case, the great number of image sources and their geometrical extents could attenuate the discrepancy between the assumption and the real distribution of luminances.

In the equation (5.1), the indirect illuminance E_{ir} is supposed to be constant on any facet. We assume that this constant value can be expressed by the mean illuminance of the facet ($E_{ir,i}$) :

$$E_{ir,i} = \frac{1}{S_i} \iint_{S_i} E_{ir}(dS_i)\, dS_i = E_{1r,i} + \frac{1}{S_i} \sum_{i \neq k=1}^{N} E_{ir,k}\, H_{ik} \qquad \text{, for i=1 to N} \qquad (5.3)$$

with :

$$E_{1r,i} = \frac{1}{\pi\, S_i} \iint_{S_i} dS_i \sum_{i \neq k=1}^{N} \iint_{S_k} \left(\sum_{L} \beta(L,dS_k,dS_i)\, E_{dir}(dS_k,L) \right) CC(dS_i,dS_k)\, dS_k$$

$$H_{ik} = \frac{1}{\pi} \iint_{S_i} dS_i \iint_{S_k} \beta(diffus,dS_k,dS_i)\, CC(dS_i,dS_k)\, dS_k \qquad (5.4)$$

$E_{1r,i}$ is the mean illuminance of the facet number "i" due to first-order reflections. H_{ik} is the mutual exchange coefficient between the facets S_i and S_k , if the factor $\beta(diffus,dS_k,dS_i)$ is omitted (see the definition of the I.L.V. 845-09-71).

The equations (5.3) can be expressed as a matrix equation. If[5] $\mathbf{E_{ir}}$ is the column-matrix (dimensions : Nx1) of the indirect illluminances, $\mathbf{E_{1r}}$ the column-matrix of the mean illuminances due to first-order reflections and $\mathbf{G}$, a matrix NxN :

$$\mathbf{E_{ir}} = \mathbf{G}^{-1}\, \mathbf{E_{1r}} \qquad \text{with } G_{ii} = 1 \text{ and } G_{ik} = -\frac{H_{ik}}{S_i} \text{ , } i \neq k \qquad (5.5)$$

In the matrix equation (5.5), the unknown is the column-matrix $\mathbf{E_{ir}}$. The elements of the matrix $\mathbf{E_{1r}}$ must be determined by numerical integration, because the product $(\beta\, E_{dir})$ has no simple analytical expression. The same remark can be made for H_{ik} , because :

---

4 Private communication with Mark Jongewaard (Lighting Technologies)

5 Symbols in bold characters represent matrices.

- the geometrical function $CC(dS_i,dS_k)$ depends on the obstructions in the lighted scene;
- $\beta(diffus,dS_k,dS_i)$ is not constant for non-lambertian diffusers. If $\theta_2=\theta_{ki}$ is the angle between the vector $-\vec{r}_{ik}$ and the normal to the facet number "k", the model (4.52) gives :

$$\beta(diffus,\theta_2) = \rho(\theta_2) = \rho_{surf}(\theta_2) + \rho_d\, (\, 1-\rho_{surf}(d)\,)\ (\, 1-\rho_{surf}(\theta_2)\,)$$

$$\rho_{surf}(d) = 2 \int_0^{\frac{\pi}{2}} \rho_{surf}(\theta_2)\, \cos\theta_2\, \sin\theta_2\, d\theta_2 \qquad (5.6)$$

In this expression, $\rho(\theta_2)$ is the reflection factor under an angle of incidence θ_2, $\rho_{surf}(\theta_2)$ is the contribution of the surface reflection to the reflection factor (4.54), and $\rho_{surf}(d)$ is the surface reflection factor under diffuse incidence.

Figure 5.2 illustrates the dependence of the luminance factor $(\beta(diffus,\theta_2) = \rho(\theta_2))$ on the angle θ_2, for three materials analysed in the preceding chapter : the tunnel wall keramics, the concrete block and the opaline glass.

The reflection factor is approximately constant up to 60°, since it mainly depends on the volume reflection contribution. Above 60°, the surface reflection significantly increases : this is particularly the case when the coherent specular term is important, such as for the opaline glass.

In the following, the luminance factor will keep its general expression $\beta(diffus,dS_k,dS_i)$.

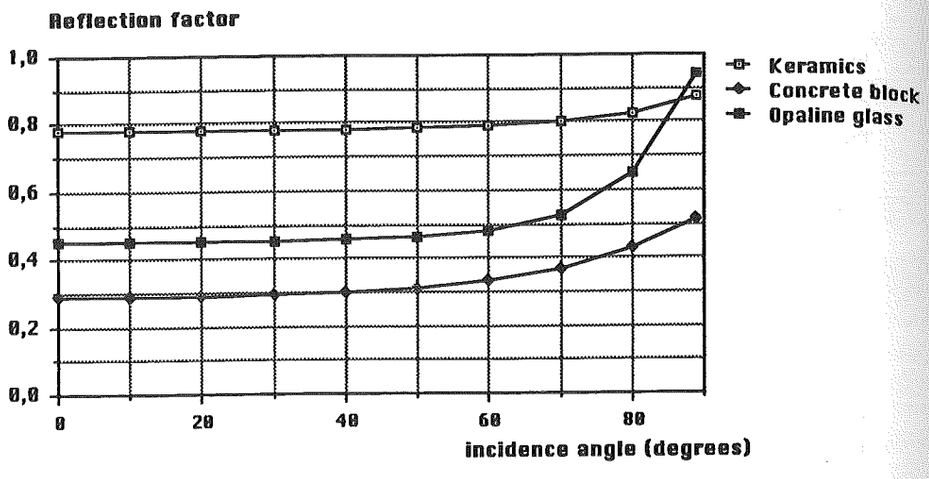

Figure 5.2 : Reflection factors of three materials, as functions of the angle of incidence θ_2 (degrees). This factor is identical to the luminance factor $\beta(diffus,\theta_2)$, by the Helmholtz principle of reciprocity.

5.2.3. Calculation of illuminances and luminances : principles

The main steps of the algorithm are the following :

1) Data : room and obstructions geometry, sources locations and photometry, luminance factors of all surfaces in the lighted scene;

2) Each surface is divided into several facets : "N" is the total number of facets;

3) Calculate , by numerical integration, the quantities $E_{1r,i}$ (i=1,N) and H_{ik} (i=1,N and k=1,N, $i \neq k$);

4) Compute the solution of the matrix equation (5.5) , which gives the indirect illuminance on each facet;

5) Calculate the illuminance E, on each element of surface dS which has been specified as a detector :

$$E(dS) = \sum_L E_{dir}(dS,L) + E_{ir}(dS) \qquad (5.7)$$

$E_{ir}(dS)$ is calculated through the equation (5.1) : in this expression, $E_{ir}(dS_k)$ must be replaced by $E_{ir,k}$, the mean indirect illuminance of the facet number "k", which has been calculated during the preceding step;

6) Once the location of the observer's eye has been fixed in the scene (at point V), the luminance distribution can be calculated as follows :

$$L(dS) = \sum_L \frac{\beta(L,dS,V)\ E_{dir}(dS,L)}{\pi} + \frac{\beta(diffus,dS,V)\ E_{ir}(dS)}{\pi} \qquad (5.8)$$

It is also assumed in this expression that the incidence of the indirect illuminance $E_{ir}(dS)$ is uniformly diffuse.

5.3. Transformation of the finite-element (radiosity) method : the LUXCALC program

5.3.1. Data

A program named LUXCALC has been conceived on the basis of the preceding algorithm. It is written in Fortran. The present version 2.0 has been developed on a personal computer.

Our intention is not to develop a commercial, user-friendly software, but rather a computer tool which will enable to implement and analyse a new original method to calculate interreflections. It must also be noted that no software presently available could be adapted to perform this task, and that the conception of a new software was necessary.

The main options of LUXCALC are described hereafter. First of all are listed the data describing the room geometry and the lighting installation.

The walls and the obstructions are rectangular surfaces. Each surface is described by (see figure 5.3) :

- its number;
- the local axis $\vec{h}$ and $\vec{v}$, defined by their vector-coordinates in the main cartesian system XYZ;
- the coordinates of its centre (P_c), in the same XYZ system;
- its dimensions along $\vec{h}$ and $\vec{v}$, in metres;
- its reflection factor, or its luminance factor described by the five parameters of the model (4.52);
- a digit to indicate if the surface is recto (only the positive side, facing the normal vector $\vec{h} \times \vec{v}$, is considered[6]), verso (negative side) or recto/verso.

All surfaces with the same local axis $\vec{h}$ and $\vec{v}$ are grouped in the same plane, in order to reduce the computing time during the obstructions analysis.

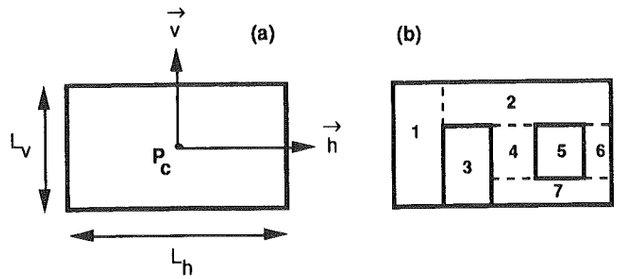

Figure 5.3 :
(a) Parameters describing any rectangular surface.
(b) All these seven surfaces belong to the same plane.

Each surface is then divided into facets. The size of the facets can be estimated if it is considered that the assumptions of §5.2.1 must be verified on each facet. In the present version of LUXCALC, it is the user himself who specifies the number of facets along $\vec{h}$ (n_h) and $\vec{v}$ (n_v) : see fig. 5.4.

The receiving surface is a particular surface which is transparent for the light flux exchanges between facets. A mesh of points is defined on this surface to indicate the detectors on which the direct and indirect illuminances will be calculated.

6 $\vec{h} \times \vec{v}$ is the cross product of two vectors.

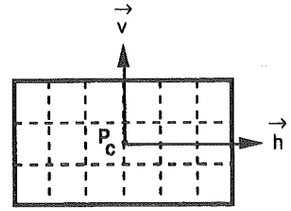

Figure 5.4 : This surface is divided into 18 facets : n_h=6 and n_v=3.

Each point source is described by the following data :

- its number;
- the coordinates XYZ of its location (P_s);
- its luminous flux, in lumens;
- its intensity distribution, in candelas/1000 lm;
- the vectors $\vec{axe}$ and $\vec{nadir}$, which define the local system attached to the intensity distribution curves : their coordinates are given in the main system XYZ.

LUXCALC presently supports two local systems :

- the classical system (C,γ) : see figure 5.5. "C" is the angle between the vertical plane containing the direction of light emission considered, and the vertical plane perpendicular to the vector $\vec{axe}$ (C=0);
- the system of C.I.E. publication 30.2 [14].

Finally, LUXCALC supports two models for light reflection :

- the classical Lambert law with only one parameter, which is the reflection factor of the surface;
- our general model described by the equations (4.52) and (4.53), with five parameters.

These data are written in an ASCII file.

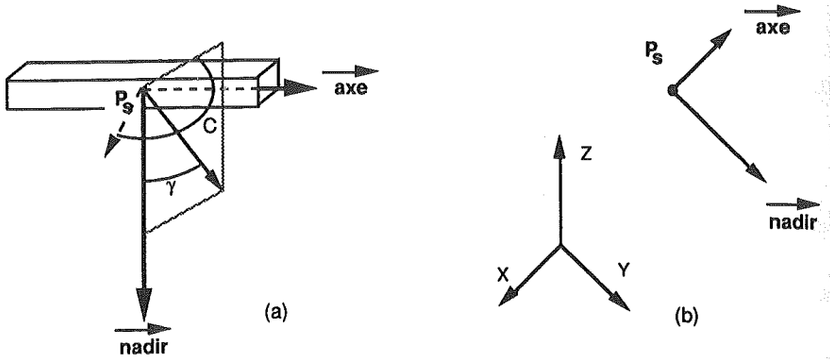

Figure 5.5 :

(a) The intensity distribution of the luminaire is described in the system (C,γ), for several angles γ = 0° to 180°, by 10° steps, and for the angles C=0°, 90°, 180°, 270°.
***P_s** is the luminous centre of the luminaire.*
(b) Geometrical parameters describing any point source.

5.3.2. Accuracy of the calculated results

Once the assumptions of §5.2.1 have been fixed, the distribution of illuminances and luminances can be calculated in the space. The solution of the equations described in §5.2.2 is unique.

The calculations performed by any lighting computer program (based on the radiosity or the ray-tracing method) must lead to the determination of this unique solution. However, the exact analytical solution cannot be calculated in most situations. The computer programs are then forced to introduce other assumptions, which allow them to find an approximation of this solution. Sometimes, very crude and inaccurate approximations are adopted in order to reduce the computing time.

The following errors in the lighting calculations can be distinguished :

the modelization errors
due to the assumptions adopted to simplify the real situation. Among them are the assumption of point sources, the assumptions about the light propagation and light reflection, and the assumptions in the geometrical description of the lighted scene. In the case of non-lambertian diffusers, the assumption about the diffuse incidence of the indirect illuminance must also be

mentioned. The modelization errors can only be estimated by a comparison of the calculated results with corresponding measurements in the real situation.

the discretization errors
inherent in the finite-element method, these errors decrease with the size of the facets. They are related to the assumptions of constant indirect illuminance and constant luminance factor on each facet, which of course are verified when the facet becomes very small.

approximation errors
Some errors are deliberately generated during the calculation process to improve convergence of the algorithm. Some of them will be introduced during steps 3) and 4) of the algorithm described in §5.2.3.

In most cases, the user of any lighting computer program is hardly aware of the magnitude of these errors. In this work, we have deliberatly designed the accuracy as a fundamental parameter, and the user will be allowed to specify a maximum bound to the approximation errors.

It is noted that this option will generally lead to time-consuming calculations. However, it must be recalled that the "user-friendliness" is not one of our major objectives.

5.3.3. Calculation of first-order reflections and mutual exchange coefficients

The calculation of $E_{1r,i}$ and H_{ik} (eq. 5.4) requires the solution of quadruple integrals. These integrals will be solved by the simple "rectangle rule" [78]. In this method, the truncature errors result from the approximation of the integral by a sum : their magnitude is proportional to h^2, if "h" is the integration step [78].

It is always possible to translate the integration intervals of $E_{1r,i}$ and H_{ik} to the interval [-1,1], since all surfaces are rectangular. So, the general expression is :

$$\int_{-1}^{1} dx_1 \int_{-1}^{1} dx_2 \int_{-1}^{1} dx_3 \int_{-1}^{1} f(x_1,x_2,x_3,x_4)\, dx_4 =$$

$$h^4 \sum_{x_1=x_i}^{x_f} \sum_{x_2=x_i}^{x_f} \sum_{x_3=x_i}^{x_f} \sum_{x_4=x_i}^{x_f} f(x_1,x_2,x_3,x_4) \qquad +o(h^2)$$

$$x_i = -1+h/2, \qquad x_f = 1-h/2 \qquad (5.9)$$

The truncature error is divided by four, if the integration step is divided by two, and if this step is small enough. This leads to the Richardson extrapolation [78] : in this iterative algorithm, the expression (5.9) is calculated with several steps "h" , which are halved at each iteration. The value of the integral calculated at iteration number "i" (F_i) is then corrected, taking into account the preceding values (F_1, ... , F_{i-1}), in such a way that the convergence to the exact value is accelerated. The iteration is stopped when the difference between two successive values (F_i - F_{i-1}) falls below a given threshold.

In our algorithm, this threshold precisely corresponds to the maximum error specified by the user.

Figure 5.6 illustrates the calculation of $E_{1r,i}$ and H_{ik} .

The main drawback of this procedure is that it requires a great number of evaluations of the function f(). For example, 256 evaluations are needed at the third iteration and 4096 at the fourth iteration. Therefore, the computing time can be excessive if the accuracy specified by the user is too important.

To overcome this, the integration can be performed as two double integrals, instead of one quadruple integral. This procedure is faster as early as the third or the fourth iteration. This is illustrated in figure 5.6 : in the original method, the next iteration creates four times more elements dS_k , for each dS_i. This multiplication is often not necessary for all dS_i, except for some of them (for example those which are closer to the surface S_k). The calculation of two double integrals can take this particular problem into account, by attributing at each surface element dS_i the required number of elements dS_k .

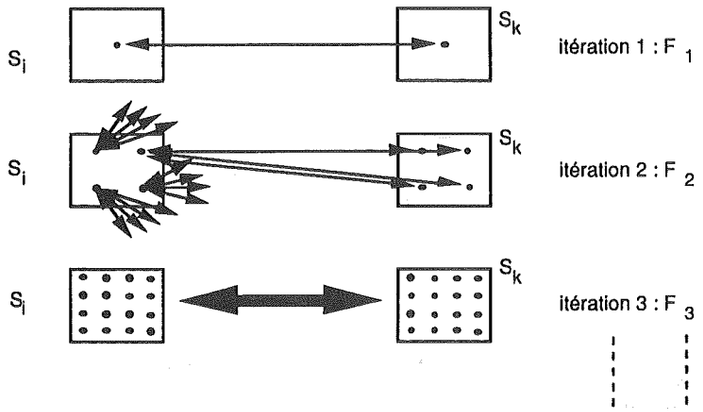

Figure 5.6 : Principles of the iterative calculation of the quadruple integrals in $E_{1r,i}$ and H_{ik} .

The algorithm described in figure 5.7 indicates that the solution of the integrals in $E_{1r,i}$ and H_{ik} is carried out in two steps :

- the first step is the calculation of the quadruple integral by Richardson extrapolation, which is efficient when the function f() is not varying too much in the expression (5.9). This is the case when the distance between the facets S_i and S_k is much greater than their dimensions;
- if the convergence of the first step is too low, a second step is carried out. It consists in the solution of two double integrals, with a Richardson extrapolation for both of them.

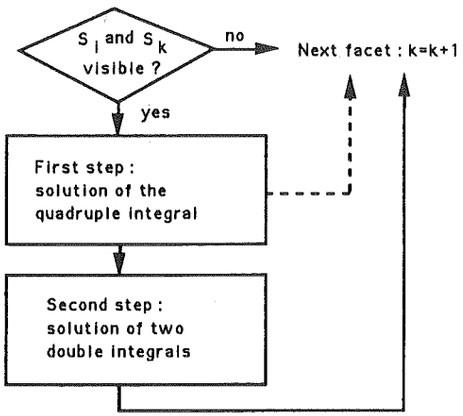

Figure 5.7 : Calculation algorithm of $E_{1r,k}$, the mean indirect illuminance of S_k due to first-order reflections on S_i , and H_{ki} , the mutual exchange coefficient including $\beta(diffus,dS_i,dS_k)$.

Figure 5.7 (bis) : Calculation algorithm of $E_{1r,k}$ and H_{ki} : first step.

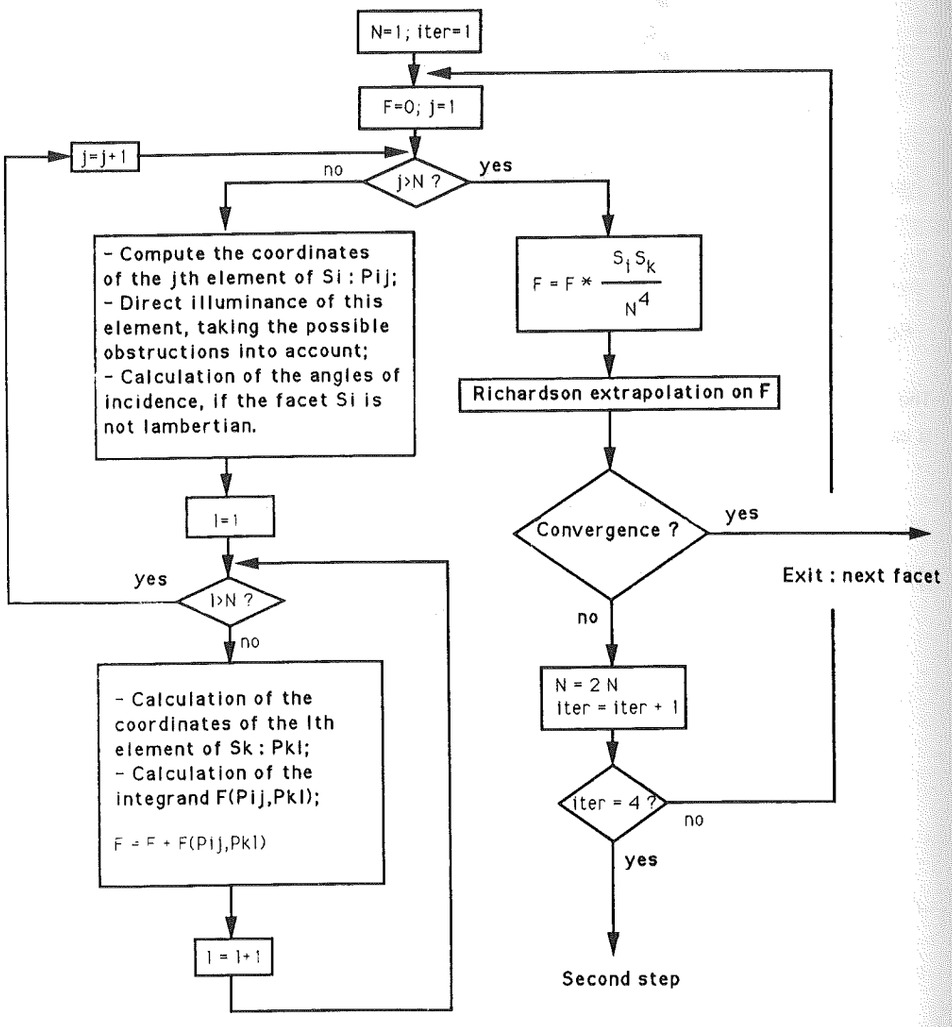

Figure 5.7 (ter) : Calculation algorithm of $E_{1r,k}$ and H_{ki} : second step.

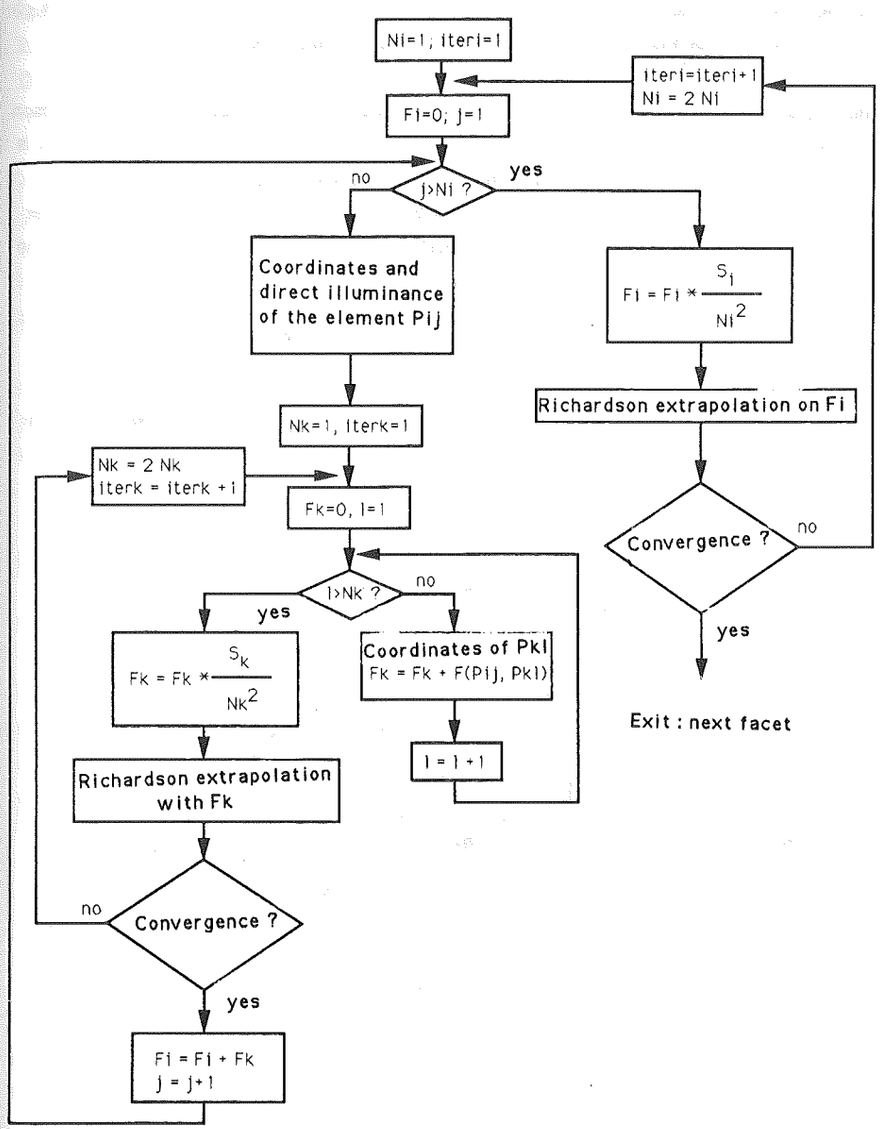

Notes :

- The number of iterations is limited to 10 within the Richardson extrapolations (4^9 points per facet !). This has been considered as sufficient in most situtations tested.

- The expression (5.9) is not valid if the integrand is discontinuous. Therefore, the Richardson extrapolation can theoretically not be applied, if the visibility between the facets S_i and S_k is partially obscured by the obstructions in the room. The following option has then been adopted: the Richardson extrapolation is carried out on the result without obstruction. After convergence, the result ($E_{1r,i}$ or H_{ik}) is proportionally corrected by the contribution of the obstructions detected between S_i and S_k .

The following example illustrates the interest of the procedure which has been developed to calculate the mutual exchange coefficients[7] H_{ik}. These coefficients are calculated in a simple rectangular enclosure, for which an analytical solution of the integrals (5.4) can be performed (figure 5.8).

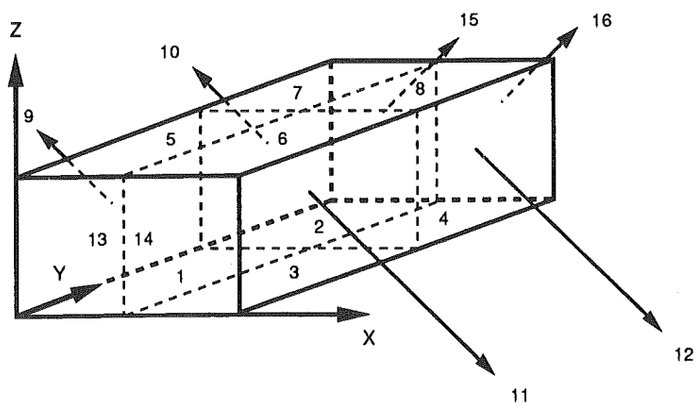

Figure 5.8 : Test room. The facets are numbered from 1 to 16 . The dimensions are : 10m along X, 20m along Y and 4m along Z.

[7] In this example, H_{ik} is really the mutual exchange coefficient, since the luminance factor is equal to 1.

Table 5.1.

Calculation of the mutual exchange coefficients H_{ik} between the 16 facets of the example described in figure 5.8. The three versions of the algorithm are described in the text. Only the values of H_{ik} differing from zero are indicated. Also, when several H_{ik} have the same value, only one of them is indicated. The luminance factor of all facets is equal to 1.

Exact analytical solution	Version 1	Version 2	Version 3
$H_{1,5}$ = 17.8	18.0	17.9	17.9
$H_{1,6}$ = 6.65	6.72	6.68	6.72
$H_{1,7}$ = 2.98	2.97	2.97	2.97
$H_{1,8}$ = 1.46	1.45	1.47	1.43
$H_{1,9}$ = 10.9	12.0	11.0	11.0
$H_{1,10}$ = 1.01	1.04	1.00	1.00
$H_{1,11}$ = 1.87	1.88	1.88	1.87
$H_{1,12}$ = .567	.570	.570	.570
$H_{1,13}$ = 5.22	5.54	5.16	5.35
$H_{1,14}$ = 1.18	1.23	1.22	1.21
$H_{1,15}$ = .208	.208	.208	.206
$H_{1,16}$ = .165	.165	.163	.163
$H_{9,11}$ = 3.82	3.85	3.85	3.82
$H_{9,12}$ = 1.59	1.58	1.58	1.59
$H_{9,13}$ = 4.23	4.33	4.17	4.39
$H_{9,14}$ = 1.09	1.09	1.08	1.08
$H_{9,15}$ = .201	.202	.202	.199
$H_{9,16}$ = .382	.382	.382	.382
$H_{13,15}$ = .308	.308	.308	.310
$H_{13,16}$ = .275	.275	.275	.275
Maximum deviation[8]	10 % ($H_{1,9}$)	4 % ($H_{1,14}$)	4 % ($H_{9,13}$)
C.P.U. time (sec)[9]	288	74	47

[8] Relative deviation from the analytical value. The element corresponding to this maximum deviation is indicated between brackets. The maximum error specified by the user is 10%.

[9] On a Macintosh SE30.

The exact analytical solution of the integrals can be found in table 5.1, together with the solutions of three algorithms :

- version 1 : four simple integrals;
- version 2 : quadruple integral;
- version 3 : combination of the solution of the quadruple integral (first step, during three iterations) and the solution of two double integrals (algorithm described in figure 5.7).

The execution of the third algorithm is significantly faster than the others. In this example, the maximum approximation error specified by the user is 10%. This upper bound is respected by the program, if the results are compared with the analytical solutions. The accuracy obtained with the algorithms is even much better than the minimum accuracy specified by the user. Indeed, only four among the 20 values calculated by the third algorithm lead to errors greater than 2% (see table 5.1).

If an interior obstruction is introduced in the room (see figure 5.9), the performance of the third algorithm is still more obvious : 3334 seconds C.P.U. for the version 1, 139 seconds for the version 2, and 57 seconds for the version 3.

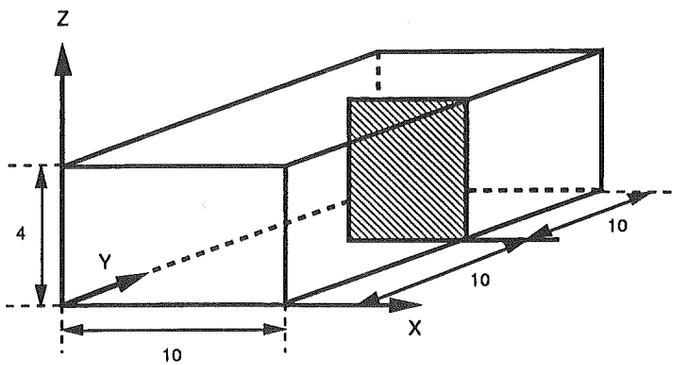

Figure 5.9 : Test room with one obstruction. The dimensions are indicated in metres.

The maximum approximation error specified by the user is also 10% : it has also been verified in the example of figure 5.9, at least for the coefficients H_{ik} for which an analytical solution could be computed.

5.3.4. Calculation of the illuminances (or luminances) of the receiving surface

The expressions (5.7) or (5.8) must now be calculated.

The direct illuminance of the element of surface dS, due to the point source L, is calculated following the usual laws of photometry. The luminous intensity (in candelas), emitted by the light source, is determined by linear interpolation between the data provided by the user at discrete angular values (see §5.3.1).

The indirect illuminances are calculated following expression (5.1), with $E_{ir}(dS_k) = E_{ir,k}$. This calculation requires the solution of double integrals, and the Richardson extrapolation is again applied here.

Note

The assumptions made about the facets are not used to calculate the illuminances due to first-order reflections : so, these illuminances are not affected by discretization errors.

5.3.5. Comparison of LUXCALC with an analytical solution

This test is described in an appendix to this work. The conclusions are summarized hereafter.

Two situations have been analysed. In the first situation, all surfaces of the illuminated space obeyed the Lambert law of reflection. In the second one, the ceiling was characterized by a luminance factor obeying equation (4.52). In both situations, the accuracy specified by the user has been respected by the program, except for three intermediate results.

In the first test, two intermediate results were calculted with an error of, respectively, 12% and 14% (instead of 10% maximum specified by the user). In the second test, only the indirect illuminance of the detector due to high-order reflections (>1), and coming from the ceiling, has been estimated with an error greater than 10% (12%).

It can then be concluded that the accuracy of the computation can be guaranteed. This conclusion has been confirmed by several other tests not reported here (see also §5.3.3).

5.3.6. Comparison of LUXCALC with in-situ measurements

It has already be mentioned that this kind of comparison is difficult to analyse, since it encompasses all sources of errors : approximation and discretization errors, of course, but also the modelization errors. The comparison between calculated and measured results is only significant, if a detailed error analysis is carried out at the same time. Otherwise, there are so much factors influencing the results that a good agreement could eventually be obtained by chance.

The interest of this particular test is of course to illustrate the good performance of LUXCALC, but also to discuss about the problems raised during the "validation"[10] of the program.

The proposed example is an office with only some pieces of furniture (figure 5.10). This simple configuration will allow us to approach the real situation with a reasonable accuracy and, therefore, to minimize the modelization errors. The measurements have been undertaken in collaboration with the members of the French "Institut National de Recherche et de Sécurité (I.N.R.S.)" from Nancy (Service de Physiologie Environnementale[11]) , during a common research on the simulation techniques used in Lighting Science [105].

The horizontal illuminances (workplane at 0.85m height) have been measured at several points located on a mesh defined in figure 5.11, with a LMT illuminance-meter. The luminances have been measured on the walls X=5m and Y=3.5m, on the centre of the ceiling, on the center of the table and on one point of the floor (point "I" in figure 5.11). The Hagner luminance-meter has an aperture of 1°.

The artificial lighting is provided by two luminaires equipped with fluorescent lamps. A black curtain (shown in fig. 5.10) has been hung in front of the windows to prevent daylight entering the room. The luminaires are of the type Mazda, Major 258GL. Both of them are equipped with two tubular fluorescent lamps of 58W (5400 lumens). The relative luminous intensities (in candelas per 1000 lumens) have been measured by the "Laboratoire Central des Industries Electriques (L.C.I.E.)" of Paris : they are shown in figure 5.12, in the vertical plane perpendicular to the luminaire axis, and in the vertical plane containing this axis.

[10] This term means the test of a computer simulation program which consists in comparing its results with measurements of illuminances or luminances in a real situation.

[11] The author wishes to thank S.Salsi and A.Barlier for their co-operation, and also for their authorization to publish these results.

Figure 5.10 : Geometry of the test room

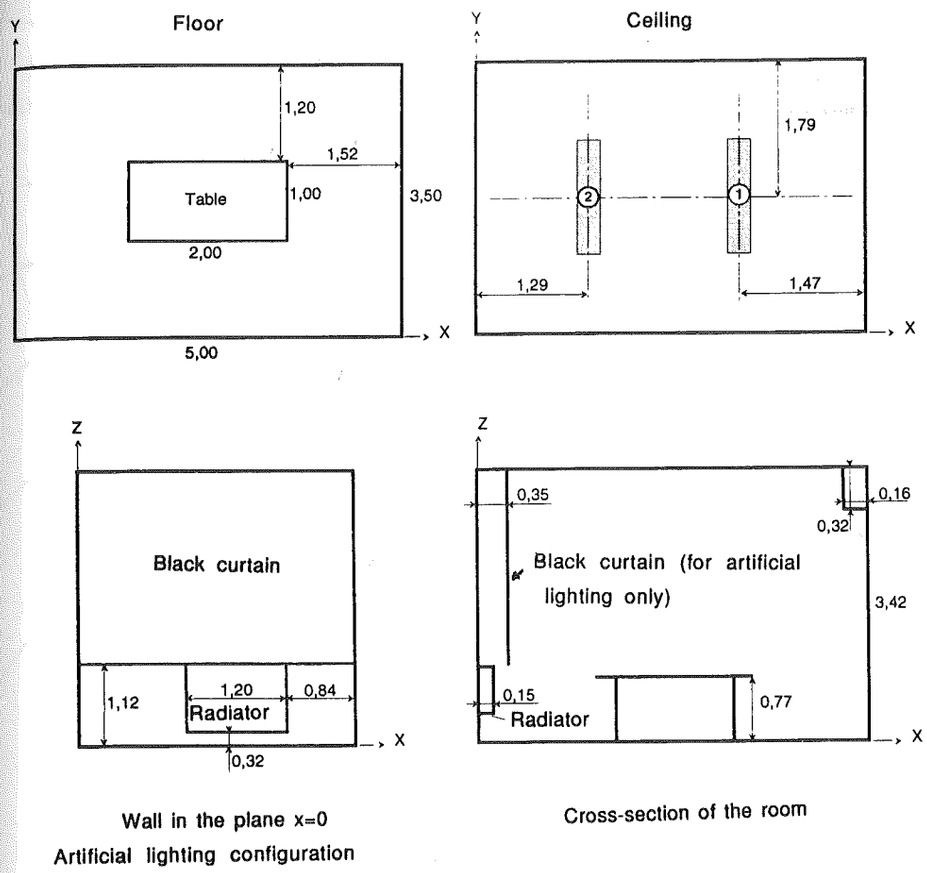

Wall in the plane x=0

Artificial lighting configuration

Cross-section of the room

Figure 5.11 : Location of the measurement points

Points of the workplane (height 0.85m) where the illuminances have been measured

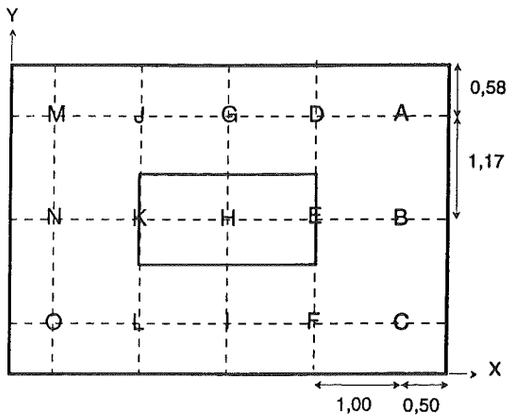

Points of the wall y=3.5m where the luminances have been measured

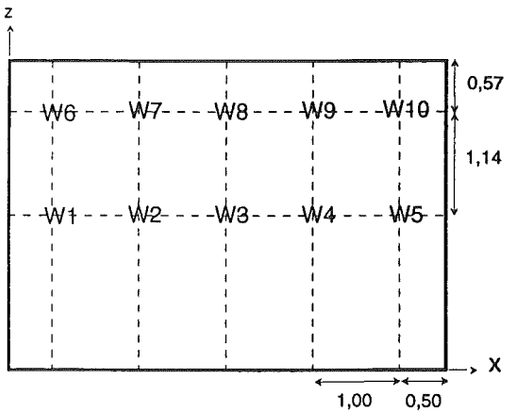

Points of the wall y=5m where the luminances have been measured

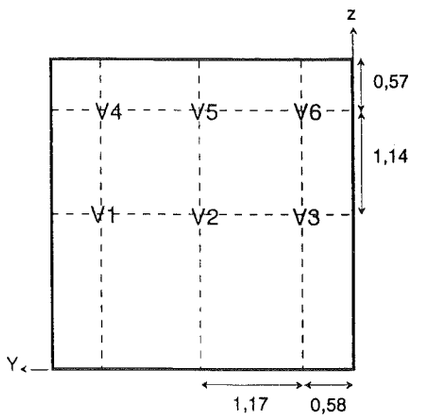

Figure 5.12 : Luminous intensity distribution curves of the luminaire Mazda Major 258GL, in candelas per 1000 lumens.

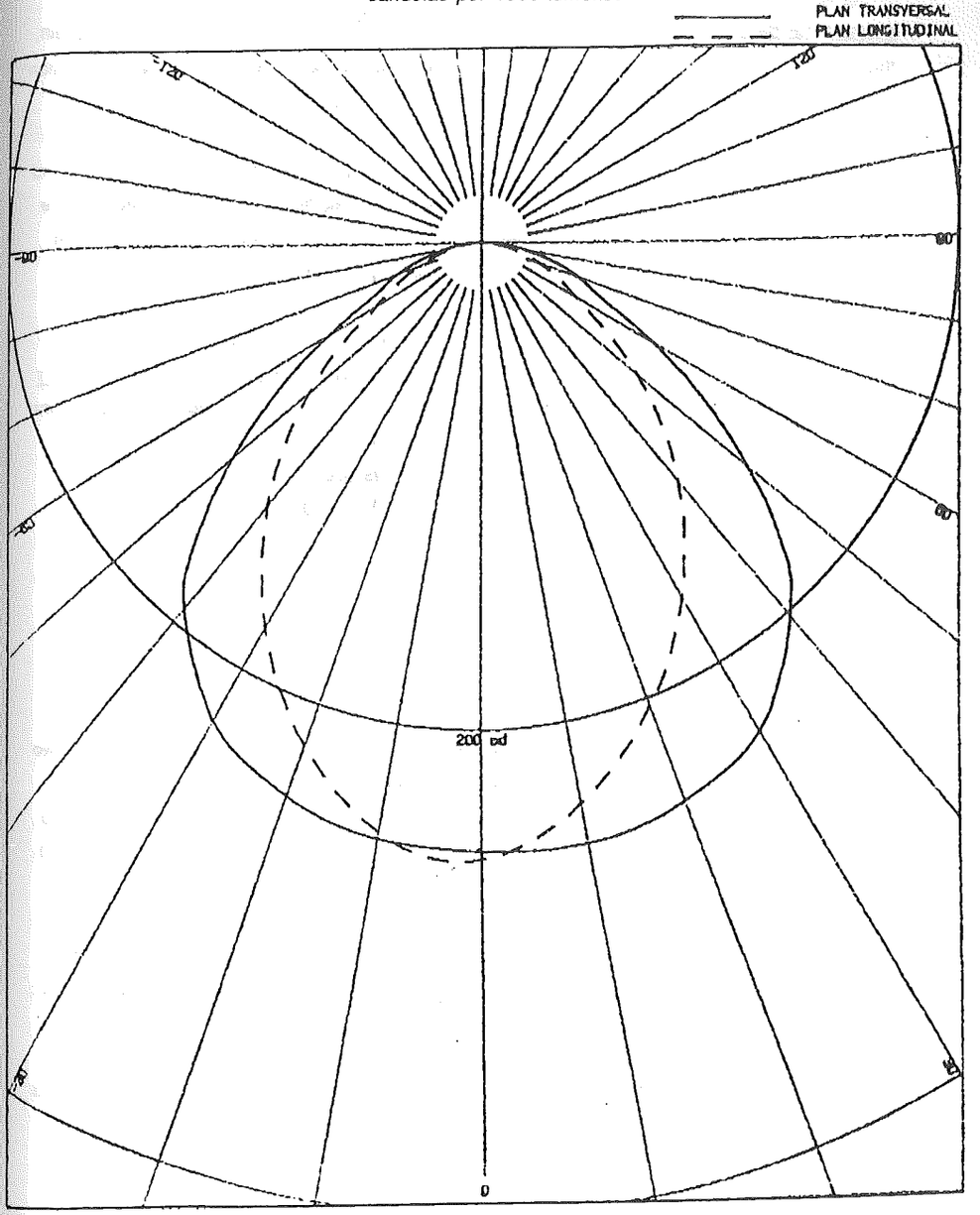

The following data must be given to LUXCALC :

- geometrical data : coordinates of the six faces of the rectangular enclosure, the black curtain, the radiator and the table (recto/verso surface). The door of the office has the same reflection factor as the adjacent wall and, therefore, it has not been modelized as a separate surface;

- each luminaire has been modelized by three point sources, located in Y=1.205m, 1.715m and 2.225m, and 0.04m below the ceiling (i.e., approximately the height of the luminous centre of the luminaire). Each point source emits a flux of 3600 lumens (10800 lumens for each luminaire), distributed following the curves described in figure 5.12;

- the reflection of the surfaces is represented by the Lambert law, as no other data were available. This assumption seems rather realistic here, except perhaps for the table. The reflection factors have been measured *in-situ*, through the ratio between the luminance of the wall viewed along its normal, and the luminance of a standard white diffuser. This ratio approximates the factor $\beta(\text{diffus},0°) = \rho(0°)$. The results are :

carpet covering the walls :	$\rho=0.63$
ceiling :	$\rho=0.80$
floor :	$\rho=0.79$
black curtain :	$\rho=0.04$
radiator :	$\rho=0.49$
table :	$\rho=0.09$

The measurement results are compared with the corresponding calculated values in table 5.2. Two configurations have been tested : first, with only the luminaire number 1 switched on and, secondly, with both luminaires "on". The calculated values have been obtained with LUXCALC : the maximum approximation error has been fixed at 10%. The computing times on a Macintosh SE30 are 11188 sec. for one luminaire "on" and 14759 sec. for both luminaires "on".

The first conclusion is that there exists a systematic deviation of about 10 to 20% between the calculated and measured values. This deviation can be explained by (one of) the following reasons :

- the luminous flux emitted by the lamps has been found in the technical description provided by the manufacturer. However, the lamps were probably aged, and this value of the flux could not be valid anymore;

- the linear interpolation in the luminous intensity data cannot be incriminated here, because the curves in the C0 and C90 planes are very similar for this luminaire. However, it could be

argued that these intensity curves have been measured at 25m distance, and that they are applied here to calculate illuminances at only 2m55 from the luminaire (distance to workplane). This could lead to a fundamental error, which could possibly be overcome with the help of near-field photometry [66,89,101,111].

Yet, an attempt has been made to analyse this error, by correcting the luminous intensity distribution, as if it were measured at a distance of 2m55. To do this, it has been assumed that the luminaire could be considered as a rectangular source with uniform luminance. We obtained new calculated illuminances which were about 3% below their value indicated in table 5.2 [105] : this cannot explain the total deviation observed in this table between calculated and measured values;

Table 5.2 : Comparison between measured and calculated illuminances. The illuminances have been determined (in lux) on 15 points belonging to the workplane (fig. 5.11).

	1 LUMINAIRE			2 LUMINAIRES		
Point	calculated values	measured values	deviations (%)	calculated values	measured values	deviations (%)
A	327	266	23	419	356	18
B	437	371	18	542	477	14
C	338	294	15	432	391	10
D	357	287	24	506	431	17
E	498	415	20	683	580	18
F	371	319	16	524	471	11
G	290	231	26	538	454	19
H	383	322	19	713	605	18
I	300	254	18	557	487	14
J	171	147	16	486	413	18
K	213	183	16	660	562	17
L	176	152	16	504	439	15
M	88	73	21	360	315	14
N	104	86	21	486	434	12
O	90	78	15	373	340	10
Average	276	232	19	519	450	15
Maximum			26			19

- also, dividing the luminaire into three point sources cannot explain the deviations observed : indeed, if the luminaires are discretized into 6 point sources, the calculated illuminances are not significantly modified (less than 1%);

- the discretization error has also been analysed : 83 facets (of about $1m^2$ each) have been used to solve this problem. If their size is further reduced, the calculated values are no longer modified. It must also be recalled that the approximation error is less than 10%;

- the illuminance-meter could have introduced a systematic error;

- the reflection factor under normal incidence could not correctly represent the reflection of the surfaces.

The first and the last explanations are the more plausible. In particular, an attempt of direct illuminance measurement under the luminaire number 1 has given 300 lux. The detector was placed just below the luminaire, at 2m55 : so, the intensity is $I = Ed^2 = 1951$ cd. If it is corrected to take into account the geometrical extent of the source (passing from 2m55 to 25m), the intensity becomes 2068 cd. Now, the corresponding intensity given by the manufacturer for a flux of 10800 lumens per luminaire is 2716 cd, i.e. a deviation of +31%.

This fast analysis shows that the systematic deviations observed can be explained by an error on the flux data. As we were not able to measure exactly the flux emitted by our luminaires, it was decided to compare the relative distributions of the illuminances on the workplane, in order to eliminate the systematic errors. So, the lamp fluxes have been corrected in the calculations, in such a way that the mean calculated and measured illuminances on the workplane were identical.

The results are shown in table 5.3 : the relative distribution of illuminances is now calculated with a mean deviation of only 2% , and a maximum error of 6%. This is a very good result if,it is compared with the approximation error specified by the user.

We had the opportunity to compare these results with four other softwares, during our common research with the I.N.R.S. of Nancy. The conclusion was that LUXCALC gave the more accurate relative illuminance distributions, i.e. the closest to the measured distributions. In particular, the leadership of LUXCALC was the more significant at point M, N and O of the workplane (fig.5.11), and for one luminaire switched on.

Table 5.3 : Comparison between the calculated and measured illuminances (lux) in the room of figure 5.10. The flux of luminaire number 1 has been reduced at 84.1% of its initial (without depreciation) value, and the luminaire number 2 at 89.7%.

	1 LUMINAIRE			2 LUMINAIRES		
Point	calculated values	measured values	deviations (%)	calculated values	measured values	deviations (%)
A	275	266	+3	357	356	+0
B	367	371	-1	461	477	-3
C	284	294	-3	368	391	-6
D	300	287	+5	434	431	+1
E	419	415	+1	585	580	+1
F	312	319	-2	449	471	-5
G	244	231	+6	467	454	+3
H	322	322	+0	618	605	+2
I	252	254	-1	483	487	-1
J	144	147	-2	426	413	+3
K	179	183	-2	580	562	+3
L	148	152	-3	443	439	+1
M	74	73	+1	318	315	+1
N	87	86	+1	430	434	-1
O	75	78	-4	330	340	-3
Average	232	232	2	450	450	2
Maximum			6			6

N.B. Average and maximum deviations are of course related to the absolute values

The table 5.4 gives the luminances calculated at several points in the room (the mesh is described in fig. 5.11). The fluxes of the luminaires have been corrected as explained above. It can be observed that there remains a systematic deviation of about 10% for the surface Y=3.5m, which is more important that the mean deviation detected for the illuminances (about 2%). However, the correspondence is satisfying, if it is considered that the luminances are directly affected by the modelization errors on the surfaces' reflection data.

Tableau 5.4 : Comparison between the calculated and measured luminances (cd/m^2) in the room of figure 5.10, on the mesh described in fig. 5.11. The flux of luminaire number 1 has been reduced at 84.1% of its initial (without depreciation) value, and the luminaire number 2 at 89.7%.

Surface Y = 3.5m				Surface X = 5m			
Point	calculated values	measured values	deviat. (%)	Point	calculated values	measured values	deviat. (%)
W1	44	40	10	V1	57	55	4
W2	59	56	5	V2	77	77	0
W3	63	59	7	V3	59	59	0
W4	62	60	3	V4	38	35	9
W5	55	53	4	V5	53	57	- 7
W6	28	23	22	V6	39	38	3
W7	42	37	14				
W8	42	35	20	Average	54	54	4
W9	46	42	10	Max.			9
W10	38	33	15				
				Ceiling	43	41	5
Average	48	44	11	Table	17	17	0
Maximum			22	Floor(Pt.I)	98	83	18

N.B. - Average and maximum deviations are of course related to the absolute values.
- The last three points are located at the centre of the ceiling, at the centre of the table, and at point I of the floor.

This example again illustrates the necessity to accurately characterize the luminous refelection of all materials in the lighted scene, not only to perform reliable simulations, but also to better investigate the origin of modelization errors.

Considering the luminances calculated in table 5.4, the law of reflection could be modified, and the influence of this modification on the calculated results could be analysed. This would allow to accept or reject the assumption, which states that the deviations are mainly due to modelization errors on the reflection properties.

Note that this is also valid for the modelization of the room geometry, the sources, or the obstructions : it is difficult to discuss about the comparison between calculated and measured results, if sufficiently reliable and realistic models are not available.

5.4. Application of the general model for light reflection in LUXCALC

5.4.1. Luminance factor calculation

The radiosity method described in this chapter can be applied for any expression of the luminance factor : this factor could be derived, either from measurements (see chapter 3), or from mathematical modelization (see chapter 4).

This last option is developed here. This is not the most simple way of proceeding, but the advantage is that the mathematical model can give the luminance factor for all angles of incidence (θ_1) and viewing (θ_2,ϕ).

Let us first recall the general model of reflection derived in the previous chapter :

$$\beta(\theta_1,\theta_2,\phi) = \alpha_s R^2_{(\theta_1,n)} \frac{2\pi\,\delta(\theta_2-\theta_1)\,\delta(\phi)}{\sin 2\theta_1} + \alpha_{sc} R^2_{(\delta_i,n)} \frac{C(\theta_1)\,C(\theta_2)}{\cos\theta_1 \cos\theta_2} \frac{1}{\cos^4\alpha} e^{-\frac{T^2}{4\sigma^2}\tan^2\alpha} + (1-\rho_{surf}(\theta_1))\,(1-\rho_{surf}(\theta_2))\,\rho_d \qquad (5.10)$$

$R^2_{(\delta_i,n)}$ is the Fresnel reflection factor, which is calculated for the angle of incidence δ_i and the refractive index "n". The angles δ_i and α are derived from the expressions (4.A12) and (4.29), respectively. $C(\theta)$ is a correction factor which has been introduced to take into account the shadowing effects (4.47), and $\rho_{surf}(\theta)$ is the surface reflection factor given by (4.54). "δ" represents the Dirac pulse.

The five parameters of the model are :
- the magnitude of the coherent surface contribution, α_s;
- the magnitude of the incoherent surface reflection, α_{sc};
- the magnitude of the volume reflection, ρ_d;

- the roughness parameter of the surface, $\left(\frac{T}{\sigma}\right)$;
- the refractive index, "n".

The model appears in the following sections of the LUXCALC program :

- the calculation of first-order reflections, i.e. the first term of (5.1) or the illuminance $E_{1r,i}$ in equation (5.4). This calculation requires the evaluation of $\beta(L,dS_k,dS_i)$;
- the calculation of higher order reflections (second term of (5.1)), and of the mutual exchange coefficients H_{ik} in equation (5.4). This calculation requires the evaluation of $\beta(diffus,dS_k,dS_i)$.

The evaluation of $\beta(L,dS_k,dS_i)$ raised several specific problems :

- the determination and memorization of the angles of incidence on the element dS_k, for each light source L. Two angles (θ_{dSk},ϕ_{dSk}) must be calculated to characterize the direction of the incident light ray (figure 5.13);

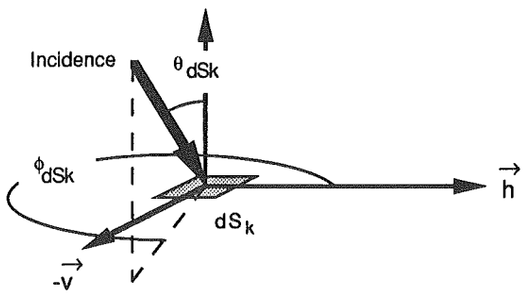

Figure 5.13 : Two angles (θ_{dSk},ϕ_{dSk}) must be calculated, to characterize the direction of the incident light ray.

- the determination of two viewing angles to characterize the direction of the reflected light ray from dS_k to dS_i . They are also defined, as indicated in figure 5.13;
- a particular routine must be conceived to calculate the coherent (specular) surface reflection contribution when $\alpha_s \neq 0$;
- another routine calculates the luminance factor, given the angular values provided by the main program, and the five parameters of the reflection model;
- finally, the total surface reflection factor ρ_{surf} must be calculated.

All these problems induce an increasing computing time, when non-lambertian surfaces are taken into account : this will be analysed in the following. For example, the last problem mentioned above would require the solution of a double integral (ρ_{surf}), each time the luminance factor must be evaluated.

To overcome this difficulty, it must be noted that the reflection factor ρ_{surf} only depends on one variable (the angle of incidence). Therefore, this factor can be tabulated, in 51 discrete values (i.e. for $\cos\theta = 0.02*j$, j=0,50). A linear interpolation on ($\cos\theta$) will lead to the reflection factor of any angle θ. The same method has been adopted for the luminance factor $\beta(diffus,\theta) = \rho(\theta)$: see eq.(5.6).

An important problem is also the calculation of the coherent surface reflection (for $\alpha_s \neq 0$). The luminance factor has been separated in two contributions, in the first term of equation (5.1) :

- the coherent term (α_s);
- the contribution of the two others terms (represented by α_{sc} and ρ_d).

The second contribution is calculated as explained in §5.3.3 for the lambertian reflection. The first contribution is determined by creating first-order image sources, for each pair (real source, specular facet). Each created image directly illuminates the receiving points, and these contributions are registered if the emitted light rays cross the corresponding specular facet (otherwise, the image source is an "imaginary" one).

This particular treatment of the coherent reflection is necessary, if we want to be sure to detect this contribution. Otherwise, this detection would be uncertain, because of the Dirac pulse in (5.10). The calculation of the mean illuminance due to first reflection $E_{1r,i}$ (5.4) is the following (for the coherent term only):

$$E_{1r,i} = \sum_{i \neq k=1}^{N} \frac{\alpha_{s\,k}}{S_i} \iint_{S_i} \left(\sum_{L_k'} R^2(\theta_{inc},n)\, E_{dir}(L_k',dS_i)\, \Delta(L_k',dS_i) \right) dS_i \qquad (5.11)$$

The quadruple integral in (5.4) becomes a double integral, which is solved by the Richardson extrapolation algorithm described above. In this expression, L_k' is the image of source L with respect to the facet number "k", and $R^2(\theta_{inc},n)$ is the Fresnel reflection factor of this facet, for an angle of incidence θ_{inc} determined by the specular light ray on S_k ($L \rightarrow S_k \rightarrow dS_i$). The function $\Delta(L_k',dS_i)$ vanishes, if L_k' is imaginary for dS_i. Otherwise, it is equal to 1.

The calculation of $\beta(diffus,dS_k,dS_i)$ does not raise specific problems, since this function has been tabulated. Therefore, the calculation of the second term of (5.1) and the coefficients H_{ik} (5.4) is performed in the same way as for the lambertian surfaces.

5.4.2. Consequences of the application of the general model of reflection

These consequences are illustrated by the following example. The illuminated room described in figure 5.10 has been modified as follows :

- the black curtain and the radiator have been included in the surface X=0;
- the luminaires are rotated by 180°, in order to directly illuminate the ceiling. They are suspended at 0.42m below the ceiling;
- the maximum approximation error is 20%.

The ceiling is first considered as a uniform diffusor (ρ=0.8). For the next simulations, it is characterized by a general luminance factor described by (5.10), with the following parameters : α_s=0, n=1.5, and $\left(\frac{T}{\sigma}\right)$ and α_{sc} are allowed to vary. The last parameter (ρ_d) is adjusted, such that the total reflection factor under normal incidence is fixed at 0.8, just like the lambertian ceiling. So, all these ceilings will lead to the same results in the measurement procedure described in §5.3.6.

The calculation results of LUXCALC are shown in table 5.5 : in particular, the deviations which are presented concern the illuminances calculated on the workplane, more precisely on the mesh described in figure 5.11.

First analysis : the computing times

A significant increase of the computing time is observed; it can be attributed to the following reasons :

- first of all, the calculations of the additional angles, and the procedure calls calculating the luminance factors;
- secondly, the luminance factor is not constant anymore, as it was for lambertian diffusers. Its dependence on the angles of incidence and viewing is sometimes so sharp, that the accuracy specified by the user is much more difficult to reach by the computer program.

Table 5.5 : Results of the program LUXCALC for the room illustrated in figure 5.10, and for several ceilings. The luminaires have been rotated to directly illuminate the ceiling.

Reflection of ceiling	Deviations (%) from the illuminances calculated for a lambertian ceiling. average	maximum	Computing time (sec.) on a Macintosh SE30
Lambert	0	0	882
$\left(\frac{T}{\sigma}\right)$=1; α_{sc}=0.1	0.2	0.3	2924
$\left(\frac{T}{\sigma}\right)$=1; α_{sc}=2.0	3.5	4.1	2719
$\left(\frac{T}{\sigma}\right)$=1; α_{sc}=2.9	5.5	6.2	2737
$\left(\frac{T}{\sigma}\right)$=2; α_{sc}=2.0	0.9	1.3	2930
$\left(\frac{T}{\sigma}\right)$=2; α_{sc}=5.25	4.3	5.0	2868
$\left(\frac{T}{\sigma}\right)$=5; α_{sc}=10^{-4}	0.0	0.0	2969
$\left(\frac{T}{\sigma}\right)$=5; α_{sc}=0.1	0.1	0.3	3003
$\left(\frac{T}{\sigma}\right)$=5; α_{sc}=2.0	0.5	0.8	2982
$\left(\frac{T}{\sigma}\right)$=5; α_{sc}=10.0	3.3	4.4	3159
$\left(\frac{T}{\sigma}\right)$=5; α_{sc}=12.4	4.1	5.2	3311
$\left(\frac{T}{\sigma}\right)$=10; α_{sc}=0.5	0.2	0.7	2998
$\left(\frac{T}{\sigma}\right)$=10; α_{sc}=2.0	0.4	0.7	3007
$\left(\frac{T}{\sigma}\right)$=10; α_{sc}=10.0	3.5	9.5	3403
$\left(\frac{T}{\sigma}\right)$=10; α_{sc}=25.0	7.9	11.9	3937

The first reason is illustrated by the execution with $\left(\frac{T}{\sigma}\right)=5$ and $\alpha_{sc}=10^{-4}$. The value of the luminance factor is approximately the same (within an accuracy of 10^{-4}) as the reflection factor of the lambertian ceiling. So, the increase of the computing time is here only due to the additional calculations of angles and luminance factors.

The second reason is illustrated by the increase of the computing time with α_{sc}, for $\left(\frac{T}{\sigma}\right)=10$. When α_{sc} is small enough, the luminance factor is close to the lambertian case, and the computing time is identical to the execution defined by $\left(\frac{T}{\sigma}\right)=5$ and $\alpha_{sc}=10^{-4}$. However, as α_{sc} increases, the angular dependence of the luminance factor becomes sharper, since the roughness parameter $\left(\frac{T}{\sigma}\right)$ indicates a very steep surface contribution. It is observed that the computing time is increased by 30% between the situations ($\alpha_{sc}=0.5$) and ($\alpha_{sc}=25$).

The opposite behaviour is observed for $\left(\frac{T}{\sigma}\right)=1$. Indeed, the modification of the surface reflection and its angular dependence implies a better accuracy of the calculated results. As a consequence, the computing time decreases when α_{sc} increases.

We must here introduce an additional comment to the conclusions drawn in a previous work [86] : the influence of extra angles and luminance factors calculations on the computing time can be more significant than the influence of the angular dependence of the luminance factor. In fact, this significance depends on the model adopted to represent light reflection.

Second analysis : the calculated illuminances and luminances

The deviations presented in table 5.5 suggest that the influence of the general model for light reflection on the illuminances of the working plane is rather weak : 10% maximum in the previous example. This conclusion is not surprising : indeed, the ceiling reflection does not exhibit any directional effect, since the main propagation to the working plane is along the vertical direction. Therefore, it is the reflection factor which is responsible for the flux exchanges, and this factor has been fixed at a constant value ($\rho=0.8$).

Greater deviations would be obtained, if the surface reflection contribution was more important. However, this contribution is limited by the physical constraint of a total reflection factor less than 1, for all possible angles of incidence. This implies that a maximum value of α_{sc} exists, for each value of the parameter $\left(\frac{T}{\sigma}\right)$: for example, for $\left(\frac{T}{\sigma}\right)$ = 10, this maximum value is

α_{sc} = 25, which corresponds to a surface reflection factor $\rho_{surf}(0°)=0.16$, and a volume reflection factor equal to (0.8-0.16=0.64).

The following calculation is an example of an asymmetrical situation, where the directional effect of the ceiling is significant. Consider once again the room of fig. 5.10, where only the luminaire number 1 has been switched on. The illuminances are calculated at 12 points of the vertical surface opposite to the luminaire (X=0). The reflection factor of the ceiling under normal incidence has been fixed to 0.5, whatever the luminance factor distribution.

Table 5.6 : Results of the program LUXCALC for the room illustrated in figure 5.10, and for several ceilings. Only luminaire number 1 is switched on and directly illuminates the ceiling ($\rho=0.5$). The deviations correspond to the illuminances calculated at 12 points of the surface (X=0).

Reflection of ceiling	Deviations (%) from the illuminances calculated for a lambertian ceiling. average	maximum	$\rho_{surf}(0°)$	ρ_d
Lambert	0	0	0.000	0.500
$\alpha_{sc}=0.1$	0.6	0.9	0.006	0.503
$\left(\frac{T}{\sigma}\right)=1$; $\alpha_{sc}=2.9$	21.8	30.0	0.174	0.614
$\left(\frac{T}{\sigma}\right)=2$; $\alpha_{sc}=5.25$	35.8	50.4	0.352	0.500
$\alpha_{sc}=0.1$	0.1	0.4	0.003	0.501
$\left(\frac{T}{\sigma}\right)=5$; $\alpha_{sc}=12.4$	26.5	51.0	0.312	0.479
$\left(\frac{T}{\sigma}\right)=10$; $\alpha_{sc}=25.0$	19.5	40.0	0.160	0.567

In this case, the deviations from the lambertian ceiling situation can reach 30 to 50% ! The maximum deviations are observed in the upper part of the surface X=0, where the specular effect

of the ceiling is the more important. In the lower part of the same surface, the deviations are close to 15% , i.e. the same magnitude as for the working plane.

The deviations between the luminances are directly related to the deviations between the illuminances presented in table 5.6, because the surface X=0 is uniformly diffusing.

About the luminances of the ceiling, it is obvious that the deviations from the lambertian case will reach very significant values, even if the ceiling illuminances are quite identical. The reason is that the luminances are directly proportional to the luminance factor, and that the deviations observed in chapter 4 between the general model (4.52) and the Lambert law can be directly transposed here. Of course, the position of the observer has also a significant influence.

Conclusion

The conclusion of this study is that the introduction of a general luminance factor (eq. 4.52 or 5.10) in the radiosity method (particularly in LUXCALC) has a significant influence on the results. The luminance distribution is obviously directly affected by the expression of the luminance factor, and any more realistic model than the Lambert law will improve the accuracy. It has also been shown in the previous example, that some illuminances are modified by a factor of 30% to 50%. However, this improvement also implies a significant increase of the computing time.

Chapter 6 : Conclusion

The first objective of this work was to acquire a better understanding of the spatial distribution of the reflected light, through experimental observation and measurements. The study has been carried out by (and for) lighting scientits, involved in lighting simulations, which implies the following :

- the measured quantity is a photometric one, i.e. the radiance (luminance) factor ;
- the study is not limited to usual materials, such as glass or perfectly conducting materials, which have already been fully characterized by physical researches. We were instead interested by other materials, such as concrete, wood, paper or keramics.

The measurements have brought additional information to the visual observation. For example, they can accurately characterize the increase of the reflected intensity around the specular direction, even for rough surfaces. They can also evaluate the influence of the angle of incidence of light, or the colour modification of the material, when the surface reflection contribution increases.

The measurements have also detected some phenomena which would be hardly seen at glance : for example, the decrease of the volume contribution at grazing incidence, or the retroreflection of the concrete block. These are significant effects, since their influence on the luminance factor is greater than the magnitude of the measurement errors.

Finally, the measurements have been used to establish and test the mathematical model of the luminance factor. On the one hand, they allowed the extension of theoretical results to take into account more complex realities and, on the other hand, they have been used extensively to determine the parameters of the model for several materials.

Therefore, this first experimental step was absolutely justified in our study, and it is intended to continue the experiments. Other materials will be measured. Moreover, measurements ouside the plane of incidence could be the source of new information, though we remain convinced that the most significant phenomena belong to this plane.

The continuation of the measurements will perhaps necessitate some transformations to the existing apparatus. Not only the automatization would be required for the comfort of the operator,

but also a better accuracy in the angular measurements : it has indeed been shown in chapter 3 that this improvement could significantly reduce the uncertainty on the luminance factor value, namely in the specular direction.

It must be pointed out that the photometric technology is particularly active in this field and that new more compact apparatus are now conceived. However, one of the advantages of our equipment is the possibility to measure big samples. This is particularly interesting in exterior lighting, when road surfaces' luminance factors have to be measured.

The second objective of this work was to develop a mathematical model for light reflection, which could be applied in lighting simulations. The photometric quantity to be modelized is the luminance factor. Our first intention was to characterize only the mixed reflection. It has been shown in chapter 4 that this objective has been extended, since the model can also take into account the regular reflection, the metallic reflection, or again some particular behaviours such as the retroreflection of concrete.

The development of the model has always been inspired by the idea that the model should be applied to the calculation of illuminances and luminances in a lighted scene. For example, this implied that the mathematical expression of the model would not be too complex, and that the computing time associated with its evaluation would be reasonable. It also implied that the number of parameters describing a material should be limited.

The model (4.52) which has been proposed in this work seems to be a satisfying compromise between all these requirements and an accurate modelization of the physical reality. The comparison, between the model and measurements performed for several materials, has shown that the mean deviations were often less than 5%. The number of parameters (five) is surely responsible for this good accuracy. As could be expected, the model (4.52) is much better than the Lambert law. But it is also significantly more accurate than the "three parameters models" (for example the Uetani model), mainly for the slightly rough surfaces.

The combination of theoretical and experimental studies has led to a satisfying model (4.52). The major drawback of this model, compared to the more simple ones, is the computing time. The analysis performed in chapter 5 has indeed shown that the influence of the model was significant, and the further improvements of the model will surely be assigned to the solution of this problem :

- either by the simplification of the mathematical expression of the model;
- or by the development of numerical methods to accelerate the calculation of the angles of incidence and viewing, and the luminance factor.

Is such an additional complexity necessary ? An answer to this question can be found in chapter 5. The influence of the general model for light reflection on calculations made by the finite element method is significant, not only on luminances calculations, but also on some illuminances values. Further investigations will try to illustrate this influence by in-situ measurements, and to demonstrate that the general model is significantly more accurate than the Lambert law. This has always been established in the fourth chapter, for the luminances of several samples, and it can be expected that this conclusion will always hold for luminances in a more complex situation. However, it is for the illuminances that the conclusions of this projected study will be interesting. It can be already stated that the experiments must be carefully prepared, in order to detect the deviations which can be attributed to light interreflections.

The improvement afforded by the general model in the description of light reflection by materials is sufficient to justify the development of such a model. The following fields can already be viewed as possible applications of the expression (4.52) : beyond lighting simulations which have already been thoroughly discussed in this work, these are the classification of materials with respect to light reflection, or the development of new more simple models for which the expression (4.52) would serve as a reference.

Finally, it is hoped that this work will contribute to a better knowledge in the field of light reflection by materials.

References

Physical properties of light reflection

[1] BORN, M. and WOLF, E., Principles of Optics, second (revised) edition, *Pergamon Press*, Oxford (1959);

[2] BOUSQUET, P., FLORY F. and ROCHE, P., Scattering from multilayer thin films : theory and experiment, *Jnl. Optical Soc. Amer.*, 71(9), 1981, pp. 1115-1123;

[3] CARNIGLIA, C.K., Scalar scattering theory for multilayer optical coatings, *Optical Engineering*, 18(2), 1979, pp.104-115;

[4] C.I.E. Publication n°17.4, Vocabulaire International de l'Eclairage, *Bureau Central de la C.E.I.*, Genève (1987);

[5] CROCE, P., Sur l'effet des couches très minces et des rugosités sur la réflexion, la transmission et la diffusion de la lumière par un dioptre, *J. Optics (Paris)*, 8(2), 1977, pp. 127-139; *J. Optics (Paris)*, 9(1), 1978, pp. 61-63; *J. Optics (Paris)*, 10(1), 1979, pp. 37-40; Sur la propagation d'une onde électromagnétique dans un milieu stratifié et diffusant, *J. Optics (Paris)*, 10(3), 1979, pp. 141-145;

[6] JENKINS, F.A. and WHITE, H.E., Fundamentals of Optics, third edition, *Mc Graw-Hill*, New York (1965);

[7] LEKNER, J., Theory of reflection, *Martinus Nijhoff Publishers*, Dordrecht (1987);

[8] ROMBAUTS, P., Phenomenology and characterisation of spatial distribution and reflection of light. Application to residential area lighting and reflector design, *Vrije Universiteit Brussel, Fakulteit der Toegepaste Wetenschappen*, Brussel (1992);

[9] SOMMERFELD, A., Optics, lectures on theoretical physics vol. IV, *Academic Press*, New York and London (1964);

[10] WORTHEY, J.A., The role of theory in lighting research and design, *Lighting Design & Applic.*, July 1991, pp. 15-17;

[11] YEH P., Optical waves in layered media, *Wiley*, New York (1988);

Measurement of light reflection

[12] C.I.E. and P.I.A.R.C. Joint technical report on Road Surfaces and Lighting, *Bureau Central de la C.I.E.*, Paris (1984);

[13] C.I.E. Publication n°15.2, Colorimetry, 2nd. edition, *Central Bureau of the C.I.E.*, Vienna (1988);

[14] C.I.E. Publication n°30.2, Calculation and measurement of luminance and illuminance in road lighting, *Bureau Central de la C.I.E.*, Paris (1982);

[15] C.I.E. Publication n°38, Radiometric and photometric characteristics of materials and their measurement, *Bureau Central de la C.I.E.*, Paris (1977);

[16] C.I.E. Publication n°44, Absolute methods for reflection measurements, *Bureau Central de la C.I.E.*, Paris (1979);

[17] C.I.E. Publication n°63, The spectroradiometric measurement of light sources, *Bureau Central de la C.I.E.*, Paris (1984);

[18] C.I.E. T.C. 2-20, Evaluation of the attribute of appearance called gloss, *C.I.E. Journal*, 5(2), 1986, pp. 42-51;

[19] CLARKE, F.J.J., GARFORTH, F.A. and PARRY, D., Goniophotometric and polarization properties of the common white diffuse reflection standards, *National Physical Laboratory Report Mom 13* , United Kingdom (1975);

[20] EMBRECHTS, J.J., Développement d'une nouvelle approche paramétrique du rendu des couleurs. Application à l'analyse et à la conception d'ambiances colorées, *Collection des Publications de la Faculté des Sciences Appliquées* n°116, Université de Liège (1988);

[21] EMBRECHTS, J.J., Mesure goniophotométrique de la réflexion spectrale d'un échantillon de matériau plan. Rapport interne, *Service d'Acoustique et d'Eclairage de l'Université de Liège*, Liège (1988);

[22] EMBRECHTS, J.J., Spectral radiance factors : Measurement by a gonioradiometric method, *Lighting Res. & Technol.*, 21(4), 1989, pp. 189-191;

[23] ERB, W., Requirements for reflection standards and the measurement of their reflection values, *Applied Optics*, 14(2), 1975, pp. 493-499;

[24] ERB, W., Computer-controlled gonioreflectometer for the measurement of spectral reflection characteristics, *Applied Optics*, 19(22), 1980, pp. 3789-3794;

[25] ERB, W., ZAI-QING, L. und NIKOLAUS, P., Super-Reflexion bei diffus reflektierenden Materialien, *Optik*, 71(2), 1985, pp. 80-88;

[26] ERB, W. and KRYSTEK, M., Reflection behaviour of the perfect reflecting diffuser under real conditions, *Optik*, 69(2), 1985, pp. 73-79;

[27] KOK, C.J. and MONARD, L.A.G., The ultraviolet and visible reflectance of building materials, C.I.E. Journal, 5(1), 1986, pp. 1-7;

[28] MATSUURA, K. and UETANI, Y., A separation measurement of boundary reflected and layer reflected components of the directional characteristics of building materials using a gonio-reflectometer with polarizers, *Proc. 6th Lux Europa Congress*, 2, Budapest, 1989, pp. 226-235;

[29] MORREN, L., Mesure absolue des facteurs de luminance et de réflexion, *Lux*, 45, 1967, pp. 3-8;

[30] MORREN, L., Quelques observations concernant la mesure de facteurs de réflexion et de transmission, *Lux*, 134, 1985, pp. 4-8;

[31] MURRAY-COLEMAN, J.F. and SMITH, A.M., The automated measurement of BRDFs and their application to luminaire modeling, *Jnl. of the I.E.S.N.A.*, 19(1), winter 1990, pp. 87-99;

[32] PHOTO-RESEARCH, Instruction manual for the Photo Research Spotmeter, Model UB and UBD (PR-1500), Chatsworth, California (1982);

[33] UETANI, Y., NAVVAB, M. and MATSUURA, K., Database of the bidirectional reflection of various materials for lighting calculations and computer graphics, *Proc. 7th Lux Europa Congress*, 2, Edinburgh, 1993, pp. 783-786;

[34] ZEISS, Spectrophotomètre PMQ II. Instructions d'emploi + Spectrophotomètre à réflexion diffuse (dispositif RA3);

Modelization of light reflection

[35] AGARWAL, G.S., Interaction of electromagnetic waves at rough dielectric surfaces, *Physical Review B*, 15(4), 1977, pp. 2371-2383;

[36] BAHAR, E. and RAJAN, G.G., Depolarization and scattering of electromagnetic waves by irregular boundaries for arbitrary incident and scatter angles full wave solutions, *I.E.E.E. Trans. Antennas Propag.*, AP-27, 1979, pp. 214-225;

[37] BAHAR, E. and FITZWATER, M.A., Depolarization and backscatter enhancement in light scattering from random rough surfaces : comparison of full-wave theory with experiment, *Jnl. Optical Soc. Amer. A*, 6(1), 1989, pp. 33-43;

[38] BECKMANN, P. and SPIZZICHINO, A., The scattering of electromagnetic waves from rough surfaces, *Macmillan*, New York (1963);

[39] CHANDLEY, P.J. and WELFORD, W.T., A re-formulation of some results of P. Beckmann for scattering from rough surfaces, *Optical and Quantum Electronics*, 7, 1975, pp. 393-397;

[40] DE BROGLIE, L., Problèmes de propagations guidées des ondes électromagnétiques, *Gauthier-Villars*, Paris (1941);

[41] EFTIMIU, C., Modified Wiener-Hermite expansion in rough-surface scattering, *Jnl. Optical Soc. Amer. A*, 6(10), 1989, pp. 1584-1594;

[42] EFTIMIU, C., Scattering by a rough dielectric interface : a modified Wiener-Hermite expansion approach, *Jnl. Optical Soc. Amer. A*, 7(5), 1990, pp. 875-884;

[43] ELSON, J.M., Infrared light scattering from surfaces covered with multiple dielectric overlayers, *Applied Optics*, 16(11), 1977, pp. 2872-2881;

[44] ELSON, J.M. and BENNETT, J.M., Relation between the angular dependence of scattering and the statistical properties of optical surfaces, *Jnl. Optical Soc. Amer.*, 69(1), 1979, pp. 31-47;

[45] ELSON, J.M., RAHN, J.P. and BENNETT, J.M., Light scattering from multilayer optics : comparison of theory and experiment, *Applied Optics*, 19(5), 1980, pp. 669-679;

[46] EMBRECHTS, J.J., Light scattering by rough surfaces : Electromagnetic model for lighting simulations, *Lighting Res. & Technol.*, 24(4), 1992, pp. 243-254;

[47] HORI, T., MATSUSHITA, N. and TAKAHASHI, S., Computer aided design method to predict luminous intensity distribution of luminaire, *J. Light & Vis. Env.*, 2(1), 1978, pp. 23-28;

[48] KRETSCHMANN, E. and KROGER, E., Reflection and transmission of light by a rough surface, including results for surface-plasmon effects, *Jnl. Optical Soc. Amer.*, 65(2), 1975, pp. 150-154;

[49] KROL, A., SHER, C.J. and KAO, Y.H., X-ray fluorescence of layered synthetic materials with interfacial roughness, *Phys. Review B*, 38(13), 1988, pp. 8579-8592;

[50] LEADER, J.C., Bidirectional scattering of electromagnetic waves from rough surfaces, *Jnl. Applied Phys.*, 42(12), 1971, pp. 4808-4816;

[51] LONLA, S.P., Détermination du diagramme de diffusion d'une surface rugueuse. Application de la méthode des rayons, *Mémoire de fin d'études, Faculté des Sciences Appliquées*, Université de Liège (1991);

[52] MINOUX, M., Programmation mathématique. Théorie et algorithmes. Tome 1, *Dunod*, Paris (1983);

[53] MOON, P. and SPENCER, D.E., An empirical representation of reflection from rough surfaces. Part I, *Jnl. of the I.E.S.N.A.*, 9(2), 1980, pp. 88-94;

[54] MOON, P. and SPENCER, D.E., An empirical representation of reflection from rough surfaces. Part II, *Jnl. of the I.E.S.N.A.*, 9(2), 1980, pp. 95-101;

[55] NIETO-VESPERINAS, M., Depolarization of electromagnetic waves scattered from slightly rough surfaces : a study by means of the extinction theorem, *Jnl. Optical Soc. Amer.*, 72(5), 1982, pp. 539-547;

[56] RICE, S.O., Reflection of electromagnetic waves from slightly rough surfaces, *Commun. Pure Appl. Math.*, 4, 1951, p. 351;

[57] SAILLARD, M. and MAYSTRE, D., Scattering from metallic and dielectric rough surfaces, *Jnl. Optical Soc. Amer. A*, 7(6), 1990, pp. 982-990;

[58] SOTO-CRESPO, J.M. and NIETO-VESPERINAS, M., Electromagnetic scattering from very rough random surfaces and deep reflection gratings, *Jnl. Optical Soc. Amer. A*, 6(3), 1989, pp. 367-384;

[59] SOTO-CRESPO, J.M. and NIETO-VESPERINAS, M., Scattering from slightly rough random surfaces : a detailed study on the validity of the small perturbation method, *Jnl. Optical Soc. Amer. A*, 7(7), 1990, pp. 1185-1201;

[60] TELLIER, P. et BOUATOUCH, K., Vers un modèle d'éclairement réaliste, *I.N.R.I.A., Rapport de Recherche n°1029*, Rennes, France (1989);

[61] THORSOS, E.I., The validity of the Kirchhoff approximation for rough surface scattering using a Gaussian roughness spectrum, *Jnl. Acoust. Soc. Amer.*, 83(1), 1988, pp. 78-92;

[62] THOUREL, L., Les antennes, *Dunod*, Paris (1956);

[63] TOIGO, F., MARVIN, A., CELLI, V. and HILL, N.R., Optical properties of rough surfaces : General theory and the small roughness limit, *Phys. Review B*, 15(12), 1977, pp. 5618-5626;

[64] UETANI, Y. and MATSUURA, K., A method of luminance calculation in an anisotropic diffuse reflecting interior, *Manuscript for the I.E.S.N.A. Annual Conference*, San Diego (1992);

[65] VIDAL, B. and VINCENT, P., Metallic multilayers for x rays using classical thin-film theory, *Applied Optics*, 23(11), 1984, pp. 1794-1801;

Calculation methods and lighting simulations

[66] ASHDOWN, I., Near-field photometry : a new approach, *Jnl. of the I.E.S.N.A.*, 22(1) , winter 1993, pp. 163-180 ;

[67] BALLMAN, T.L. and LEVIN, R.E., Illumination in partitioned spaces, *Jnl. of the I.E.S.N.A.*, 16(2), summer 1987, pp. 31-48;

[68] BENSE, R.H., Visulux II : 3D simulation of lighting effects, *Paper presented at C.I.E. Seminar on Computer Programs for Light and Lighting*, Central Bureau of the C.I.E., Vienna (1992);

[69] BOPP, R., Monte Carlo program for the calculation of tunnel road lighting, *Proc. 7th Lux Europa Congress*, 2, Edinburgh, 1993, pp. 812-816;

[70] BRACKETT, W.E., FINK, W.L. and PIERPOINT, W., Interior point-by-point calculations in obstructed spaces, *Jnl. of the I.E.S.N.A.*, 13(1), october 1983, pp. 14-25;

[71] BREKKE, B., A new generation computer program system for lighting planning, *Paper presented at C.I.E. Seminar on Computer Programs for Light and Lighting*, Central Bureau of the C.I.E., Vienna (1992);

[72] BRESCIANI, F., ROSSI, G. and VEZZADINI, L., Energetic simulation of light propagation in closed environments and roads, with different light sources and photorealistic representation, *Paper presented at C.I.E. Seminar on Computer Programs for Light and Lighting*, Central Bureau of the C.I.E., Vienna (1992);

[73] BRUSQUE, C., NGUYEN, V., CHARLOT, B. et LOUAGE, J., LISE : la synthèse d'images au service de l'Eclairage, *Bull. liaison Labo. Ponts et Chaussées*, Paris, 174, 1991, pp. 25-38;

[74] BRUSQUE, C., CARTA, V., NGUYEN, V. et LOUAGE, J., Qualification de LISE comme outil de simulation de la propagation de la lumière, *Bull. liaison Labo. Ponts et Chaussées*, Paris, 181, 1992, pp. 3-16;

[75] CARTER, D.J. and Mc EWAN, I., Obstructed spaces in interior lighting design : computer analysis, *Lighting Res. & Technol.*, 20(1), 1988, pp. 21-28;

[76] CHARLOT, B., Conception d'un logiciel de simulation de projets d'éclairage par synthèse d'images, Rapport de DEA IARFAG, Ecole Nationale des Ponts et Chaussées, Université de Paris VI (1989);

[77] C.I.E. Publication n°40, Calculs en Eclairage Intérieur. Méthode de base, *Bureau Central de la C.I.E.*, Paris (1978);

[78] DAHLQUIST, G. and BJORCK, A., Numerical methods, *Prentice Hall*, Englewood Cliffs, New Jersey (1974);

[79] DAVIS, R.G. and BERNECKER, C.A., An evaluation of computer graphic images of the lighted environment, *Jnl. of the I.E.S.N.A.*, 14(1), october 1984, pp. 493-514;

[80] DECLAYE, P., Application des méthodes de Monte-Carlo à la prévision des niveaux d'éclairement dans un espace clos, *Mémoire de fin d'études, Faculté des Sciences Appliquées*, Université de Liège (1988);

[81] DEHOFF, P., From averaged illuminance to 3D-luminance presentation : the wide range of computer aided interior lighting design, *Paper presented at C.I.E. Seminar on Computer Programs for Light and Lighting*, Central Bureau of the C.I.E., Vienna (1992);

[82] DI LAURA, D.L., On a new technique for interreflected component calculations, *Jnl. of the I.E.S.N.A.*, 9(1), october 1979, pp. 53-59;

[83] DI LAURA, D.L., On the simplification of radiative transfer calculations, *Jnl. of the I.E.S.N.A.*, 12(1), october 1982, pp. 12-16;

[84] EGGER, W., Influence of objects in rooms on illuminance and luminance distribution, *Jnl. of the I.E.S.N.A.*, 13(3), april 1984, pp. 308-313;

[85] EMBRECHTS, J.J., Une technique d'évaluation des niveaux d'éclairement faisant intervenir la réflexion semi-diffuse, *Lux*, 153, 1989, pp. 23-29;

[86] EMBRECHTS, J.J., Implementation of the finite element method for non-lambertian indoor surfaces, *Paper presented at C.I.E. Seminar on Computer Programs for Light and Lighting*, Central Bureau of the C.I.E., Vienna (1992);

[87] EMBRECHTS, J.J., Implementation of the finite element method for non-lambertian indoor surfaces, *Proc. 7th Lux Europa Congress*, 2, Edinburgh, 1993, pp. 750-753;

[88] FONTOYNONT, M., Genelux : a CAD software for natural and electric light computations, *Rapport du L.A.S.H.*, Ecole Nationale des Travaux Publics, Vaulx-en-Velin, France (1987);

[89] HOLMES, J.G., Photometry from the right distance, *Lighting Res. & Technol.*, 22(4), 1990, pp. 183-187;

[90] I.E.S. (Lighting design practice committee of the), Zonal-Cavity method of calculating and using coefficients of utilization, *Illuminating Engineering*, 59, may 1964, pp. 309-328;

[91] I.E.S. Lighting Handbook, Reference Volume, *Illuminating Engineering Society of North America*, New York (1984)

[92] JENSEN, J.J. and SORENSEN, K., Computer program for interior lighting, *Paper presented at C.I.E. Seminar on Computer Programs for Light and Lighting*, Central Bureau of the C.I.E., Vienna (1992);

[93] JONGEWAARD, M.P., Daylight calculations, measurements and visualization in non-empty rooms, *Proc. 7th Lux Europa Congress*, 1, Edinburgh, 1993, pp. 43-52;

[94] KAJIYAMA, H. and KODAIRA, S., An illuminance analysis in partitioned spaces using the Monte Carlo method, *Jnl. of the I.E.S.N.A.*, 18(2), summer 1989, pp. 93-108;

[95] LIGHTING TECHNOLOGIES, Lumen-Micro version 5, Boulder, Colorado (1990);

[96] LITTLEFAIR, P.J., Interreflection calculations : Improving convergence, *Lighting Res. & Technol.*, 23(4), 1991, pp. 175-177;

[97] Mc EWAN, I. and CARTER, D.J., Some approaches to the treatment of obstruction in interior lighting design, *Lighting Res. & Technol.*, 17(3), 1985, pp. 107-115;

[98] MILLER, N.J., NGAI, P.Y. and MILLER, D.D., The application of computer graphics in lighting design, *Jnl. of the I.E.S.N.A.*, 14(1), october 1984, pp. 6-26;

[99] MISTRICK, R.G., and DI LAURA, D.L., A new finite orthogonal transform applied to radiative transfer calculations, *Jnl. of the I.E.S.N.A.*, 16(2), summer 1987, pp. 115-128;

[100] MISTRICK, R.G., A priority based dual density finite element interreflected component calculation, *Jnl. of the I.E.S.N.A.*, 18(2), summer 1989, pp. 16-22;

[101] MISTRICK, R.G. and ENGLISH, C.R., A study of near-field indirect lighting calculation, *Jnl. of the I.E.S.N.A.*, 19(2), summer 1990, pp. 103-112;

[102] MITANCHEY, R., FONTOYNONT, M. and CHALLIER, R., Numerical simulation of the colour aspect of a luminous environment, *Proc. 7th Lux Europa Congress*, 2, Edinburgh, 1993, pp. 489-500;

[103] NBN L 14-002, Méthodes de prédétermination des éclairements, des luminances et des indices d'éblouissement en éclairage artificiel d'espaces clos, *Institut Belge de Normalisation*, Bruxelles (1975) + addendum 1 (1979);

[104] PABST, W., Radiative transfert calculation by Markov Statistics, *Jnl. of the I.E.S.N.A.*, 15(1), fall 1985, pp. 29-39;

[105] SALSI, S., BARLIER, A. et EMBRECHTS, J.J., Etude comparative de différentes techniques de simulation de l'éclairage de locaux industriels, *Rapport d'activités dans le cadre du programme d'actions intégrées Tournesol* (1992);

[106] SARAIJI, R.M.N. and MISTRICK, R.G., Calculation methods, error tendencies, and guidelines for finite element flux transfer, *Jnl. of the I.E.S.N.A.*, 21(1), winter 1992, pp. 92-102;

[107] SCHNEIDER, W., Computer integrated lighting architecture- New needs in standardization for the qualified assessing, *Paper presented at C.I.E. Seminar on Computer Programs for Light and Lighting*, Central Bureau of the C.I.E., Vienna (1992);

[108] SLATER, A.I., Illuminance distributions : Prediction for uniform and non-uniform lighting, *Lighting Res. & Technol.*, 21(4), 1989, pp. 133-158;

[109] SMITH, M., A new method of generating accurate color renderings of architectural spaces, *Jnl. of the I.E.S.N.A.*, 22(1), winter 1993, pp. 26-32;

[110] STANGER, D., Monte Carlo procedures in lighting design, *Jnl. of the I.E.S.N.A.*, 13(4), july 1984, pp. 368-371;

[111] STANNARD, S. and BRASS, J., Application distance photometry, *Jnl. of the I.E.S.N.A.*, 19(1), winter 1990, pp. 39-46;

[112] STOCKMAR, A., Basic concepts of computer aided lighting design, *Paper presented at C.I.E. Seminar on Computer Programs for Light and Lighting*, Central Bureau of the C.I.E., Vienna (1992);

[113] VAN BOMMEL, W. and DE MAN, M., Test model for computer programs used in interior lighting, *Proc. 7th Lux Europa Congress*, 1, Edinburgh, 1993, pp. 462-470;

[114] WARD, G.J. and RUBINSTEIN, F.M., A new technique for computer simulation of illuminated spaces, *Jnl. of the I.E.S.N.A.*, 17(1), winter 1988, pp. 80-91;

[115] WARD, G.J., Visualization, *Lighting Design & Applic.*, June 1990, pp. 4-5 and 14-20;

[116] ZHANG, J.X. and NGAI, P.Y., Lighting calculations in a multi-partitioned space, *Jnl. of the I.E.S.N.A.*, 20(1), winter 1991, pp. 32-43.

Imprimerie DEROUAUX ORDINA Editions
10, place Saint-Jacques – 4000 LIEGE
Tél. 32 41 23 12 53 – Fax 32 41 23 53 30